ARCHIVES OF ACOUSTICS
20, 4, 303–309 (1995)

NUMERIC ANALYSIS OF SODAR ECHO SIGNALS

J. FORTUNA

Department of Geodesy and Meteorology
Military University of Technology
(01-489 Warszawa)

The results of analysis based on the FFT with some methods of evaluating the power spectrum of sodar echo signals for investigating the vertical profiles of wind speed in lower atmosphere are discussed in the article. The best from the point of view of spreading of spectrum and computing time occurs to be the Goodman–Enochson–Otnes method (GEO) with frequency weight window. The results of applying the GEO method to evaluating the vertical profile of wind speed in lower atmosphere by means of MUT sodar are presented.

1. Introduction

The investigation of the lower layer of the atmosphere and the processes occurring there is the subject of interest for many scientists in various scientific fields and learning the structure of the lower layer and its main characteristic is the basic interest of the physics of the atmosphere. Applying conventional measurements equipment to investigation of the wind, temperature, humidity and turbulence in the lower layer of the atmosphere, along with advanced numeric methods of modelling led to great progress in analysis of physical phenomena in this part of the atmosphere. Simultaneously, in all those situations where direct measurement is problematic from technical point of view or impossible as far the measurement range is concerned, the detection methods become relevant.

From the teledetection methods the active acoustic sounding of the atmosphere by means of sodars seems to be particularly attractive, exceptionally for investigation of the wind vertical structure of the lower atmosphere [1, 2]. The necessity of processing the sodar echo signals in real time, relevant especially in detection of hazardous for aviation rapid changes of the wind speed and direction, made the constructors of the contemporary sodars choose the Fast Fourier Transformation (FFT) as the method for the analysis of the Doppler spectra [3].

The results of analysis based on the FFT method are shown below along with selected methods of determination of the momentary wind speed vertical structure in the lower atmosphere.

2. The methods of determination of the power spectra of echo signals

The main reason for determination of the power spectrum of a physical process is investigation of its frequency structure, which contains important information relevant to the basic features of the investigated physical structures. In the case of the wind structure of the lower atmosphere investigation by means of the sodar made by MUT (Military University of Technology) the power spectrum of echo signals was used to evaluate the Doppler shift of frequency of the echo signals in comparison with the emitted signals. However direct computing the power spectra of echo signals by means of Fast Fourier Transform may results in leak out the spectrum [4] or its negative values [5]. To determine the power spectrum of sodar echo signals the following was applied:

1. the Blackman–Tuckey's correlation function method using FFT and Hamming's window [6] — called the BT method,

2. Goodman–Enochson–Otnes method [7] — called GEO method.

The Hamming's window is a time window and Goodman–Enochson–Otnes' window is a frequency window. The analysis of sodar echo being the response of the investigated medium atmosphere boundary layer to probing by an acoustic wave, of 1.000 Hz frequency, was done. The received analog signal was scanned with the frequency of 5.120 Hz by means of 12-bit A–D converter. The receiving time was equal to about 5 seconds, which corresponded to 25.000 samples and sounding the layer 800 m thick. The power spectrum of sodar echo signal segments containing 1.024 and 2.048 samples was evaluated with the BT and GEO methods applied.

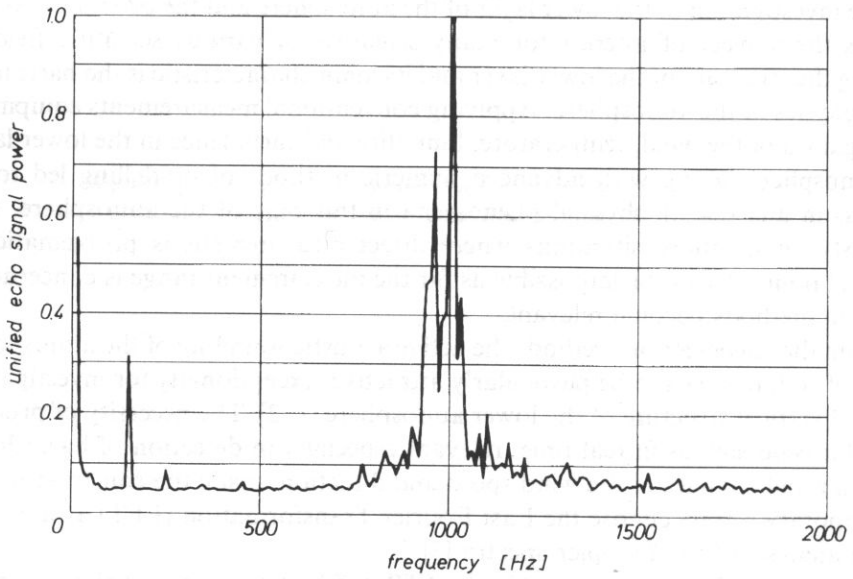

Fig. 1. The power spectrum of sodar echo signals evaluated by the Blackman–Tuckey method with Hamming window.

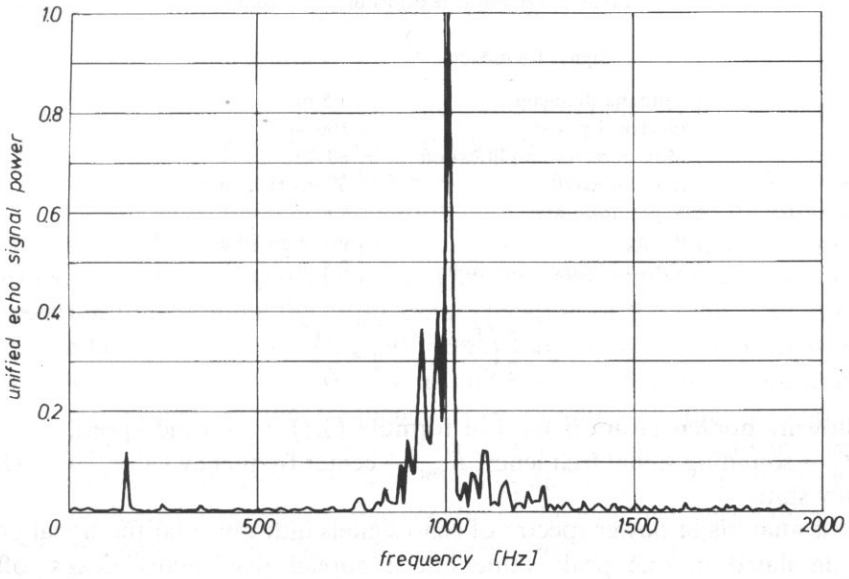

Fig. 2. The power spectrum of sodar echo signals evaluated by the direct method with Goodman–Enochson–Otnes window.

Figures 1 and 2 shows the power spectrum of sodar echo signal of one of the segments received with the BT and GEO methods applied, respectively. The comparison of Fig. 1 and Fig. 2 show that the power spectra in BT method are more spread than in the GEO one (in GEO method the echo signal power lies in narrower frequency range). These effects influence on the precision of wind speed evaluation. The BT method suffers higher level digital noises. Taking also into consideration the computing time when BT was used, the BT method was abandoned.

3. An application example of the Goodman–Enochson–Otnes method with balance method for evaluation of wind vertical profile in the lower atmosphere by means of sodar made by MUT

The Goodman–Enochson–Otnes' method was used for evaluation of wind vertical profile in the lower atmosphere during field investigation at the training area of Meterology Institute of MUT in May 1993. A monostatic Doppler sodar MUT was used [2]. The technical description of the sodar is given in Table 1. The atmosphere was sounded by the 1.000 Hz signal. The received echo signals, amplified and converted, were analysed according to the GEO method. The evaluated power spectra of the echo signal segments allow to estimate the Doppler shift Δf against the frequency of the sounding signals. The wind speed at an atmosphere level is evaluated from:

Table 1. Technical features of MUT sodar

Signal frequency	1 kHz (2 kHz)
Antenna diameter	1.5 m
Electrical power	100 W
Max. receiver amplification	80 dB
Impulse length	50 ms (100 ms)
Repetition time	8 s
Range	up to 1.000 m
Vertical range resolution	8.5 m (17 m)

$$v=\frac{c}{2}\left(\frac{f_{\text{mean}}-f_0}{f_0}\right)=\frac{c\Delta f}{2f_0} \tag{3.1}$$

The following nomenclature is used in formula (3.1): v — wind speed, c — sound speed, f_0 — sounding signal frequency, f_{mean} — center frequency value, Δf — Doppler frequency shift.

Precise analysis of power spectra of echo signals indicates that the signal power is not accumulated in one peak value but is spread over many peaks, often of comparable power. Figure 3 shows example fragment of power spectrum of echo signal as an illustration to the above mentioned phenomenon. The spreading of power spectra of received signals is mainly due to disturbing noises of various origins. The disturbing noises presence causes that the center frequency value f_{mean} of sodar echo signals, defined as the first moment of the signals power spectrum [6, 7], actually gives the center of gravity of the spectrum of signal and noise:

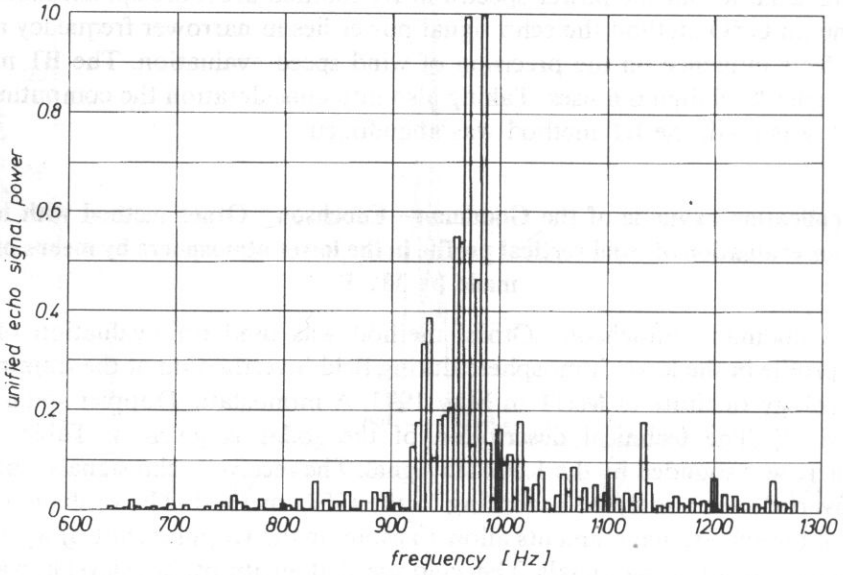

Fig. 3. Sector of the power spectrum of the echo signal of MUT sodar.

$$f_{s+n}=\frac{\int (G_s+G_n) f df}{\int (G_s+G_n)\, df} \tag{3.2}$$

where f_{s+n} — center frequency value of echo signal and noise, G_s — signal power, G_n — noise power, f — the sounding signal frequency.

For precise evaluating of the wind speed it is necessary to precisely evaluate the Doppler frequency shift. Such an evaluation may be accomplished by application of the balance method [7]. The procedure is carried out in two stages with successive improvements in accuracy and precision. The first stage consist of search over the entire spectrum to determine the approximate location of the echo. This is done by balancing method whereby the entire spectrum is scanned by fixed moving window of width Δf_B, devided into two subwindow of $\Delta f_B/2$ width. The initial position of the window is established by the frequency corresponding to the spectral line of maximum power in the segment. The window is shifted along the frequency axis. The power contained in each of the two windows, $G_{l,i}$ and $G_{p,i}$ respectively, is measured the echo is considered acquired for that locatio of the windows where the difference reaches the minimum. Then the ratio between such levels and the average level obtained in any other location is calculated.

$$|\Delta G_i| = |G_{l,i}-G_{r,i}| \tag{3.3}$$

Here the following abbreviations are used: ΔG_i — difference between the right and left sub windows, G_l — power in the left sub window, G_r — power in the right sub window.

The second stage of the procedure is determination of the "center" frequency f_{mean}, and, consequently, of the radial wind is obtained. The central frequency value is defined by the first moment of spectrum (according to GEO method):

$$f_{\text{mean}}=\frac{\sum_{0}^{\Delta f_B} G_i f_i}{\sum_{0}^{\Delta f_B} G_i}, \tag{3.4}$$

where f_{mean} — center frequency value of the power spectrum of the echo signal, Δf_B — window width, G_i — spectral line power of the spectrum at f_1 frequency, f_i — frequency of i-spectral line in window ΔF_B.

Figure 4 shows the example of the difference spectra of the power evaluated in left and right subwindow when the power spectrum of echo signal is scanned according to the balance method. The minimum of the difference as shown in Fig. 4 defines precisely the center frequency value f_{mean} of the echo signal. The GEO method with balance method was applied to estimation of the wind speed vertical profile in lower atmosphere by means of MUT sodar. Figure 5 shows examples of vertical profiles of horizontal components of wind speed evaluated for equal window width 80 Hz in balance method in various lengths of the analysed sequence.

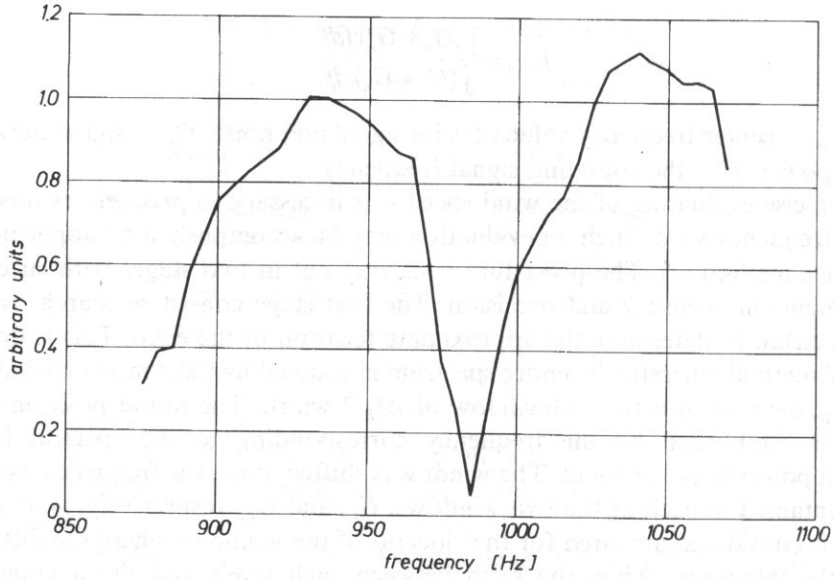

Fig. 4. The power difference between left and right windows for power spectrum of signal analysed by the bvalance method.

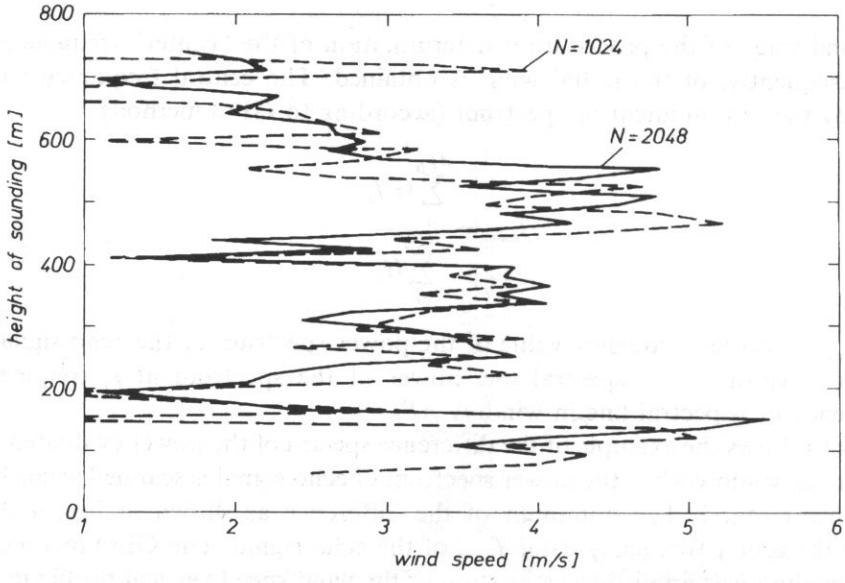

Fig. 5. Vertical changes of the momentary horizontal component of the wind speed evaluated by the balance method with 80 Hz window for both profiles; solid lines $N=1.024$ samples, dashed lines $N=2.048$ samples.

The window width was required to take into consideration all relevant peak values of the power spectrum in the sequence.

Figure 5 shows the differences of two vertical profiles of horizontal component of wind speed caused by different length of analysed measurement segments. For a segment 1.024 samples long the Doppler frequency shift origins from the atmosphere layer 64 m thick; for the 2.048 samples long segment the thickness is 128 m. It may result in relevant differences of evaluated wind speeds at a level because of mutual compensation of negative and positive Doppler frequency shifts caused by air movement in various directions in the same layer. The greater length of the segment involves greater averaging range and, consequently, reduction of short period wind pulsations.

The vertical profiles of wind speed changes shown on Fig. 5 are characteristic for wind speed profiles in lower atmosphere with developed convection.

4. Conclusion

Based on the analysis the following may be concluded:

1. The tests performed enabled the initial estimation of the application range and effectiveness of the proposed method of numeric sodar echo signal conversion for evaluation of wind speed vertical profile in lower atmosphere.

2. The evaluated Goodman–Enochson–Otnes method combined with the balance method proved to be effective for real time evaluation of wind speed at a certain level.

References

[1] J. FORTUNA and E. KOZACZKA, *Review of acoustical methods of probing the atmospheric boundary layer*, Archives of Acoustics, **17**, 453–510 (1992).

[2] J. FORTUNA and S. PIETREK, *Pomiar profilu średniej prędkości wiatru w dolnej atmosferze przy pomocy sodaru dopplerowskiego*, (in Polish) Biul. WAT, **5**, 95–104 (1992).

[3] D.H. LENSCHOW, *Probing the atmospheric boundary layer*, Am. Meteorol. Soc., Boston Mass 1986.

[4] A.V. OPPENHAIM and R.W. SCHAFER, *Cyfrowe przetwarzanie sygnałów*, (in Polish), Wyd. Kom. Łączn., Warszawa 1973.

[5] R.K. OTNES and L. ENOCHSON, *Analiza numerycznych szeregów czasowych* (in Polish), WNT, Warszawa 1973.

[6] D. SRMANS and B. BUNGORNER, *Numerical comparison of mean frequency estimators*, J. Appl. Meteorol., **14**, 991–1003 (1975).

[7] G. MASTRANTONIO and G. FIOCCO, *Accuracy of wind velocity determinations with Doppler sodars*, J. Appl. Meteorol., **21**, 823–830 (1982).

ARCHIVES OF ACOUSTICS
20, 4, 311–326 (1995)

ACOUSTIC MODELLING OF SURFACE SOURCES. PART I. PISTON MODEL, DISCRETIZING ERROR, AXISYMMETRICAL PROBLEM

A. BRAŃSKI

Institute of Technology
Pedagogical College
(33-310 Rzeszów, ul. Rejtana 16a)

The paper discusses the application of irregular boundary elements in BEM method. These elements were proposed in order to reduce the number of the elements in acoustical model of surface source. The boundaries of irregular elements were introduced by optimizing a mean square distance between exact directivity function and approximation one. The constant vibration velocity on each element was calculated employing the definition of an average function value. For simplicity as an example radiation axisymmetric problem governed by Helmholtz–Rayleigh integral was considered. Examples are shown that applying irregular discretization better model may be obtained.

The list of symbols

a, b — internal and external radius of surface S_1,
$J_0(x)$ — Bessel function of the first kind and zeroth order,
k — dimensioness wave number,
G — fundamental solution to the Helmholtz equation in the space E_3,
S_1 — vibrating surface (driving surface),
S_0 — baffle board (baffle),
v — vibration velocity of the driving surface,
Φ — velocity potential,
ρ, ϕ — polar coordinates.

1. Introduction

Boundary Element Method (BEM) is now a method frequently applied to solve the boundary value problem in regions with irregular surfaces [10]. This method is also widely applied to the problems of sound radiation by a sources with a finite baffle (source = vibrating surface + baffle), or sound diffraction on irregular surfaces [8, 11].

The mathematical model describing the physical model both of those problems includes, among others, boundary integral equation (BIE). There is a short review of BIE applied to describe harmonic acoustic phenomena in time given in [6].

In the problem of sound radiation by a source with a finite baffle the solution is given by the Helmholtz–Huygens integral, where the acoustic pressure acting on the surface of the source, as well as the vibration velocity of the vibrating surface, are unknown. Both acoustic parameters are coupled with each other by a BIE. The vibration velocity in selected points of the source can be determined experimentally, whereas the acoustic pressure is the solution of BIE. Practically, the application of numerical methods is the only possible way to solve these equations. Then, after the discretization, the integral equation is replaced by a system of algebraic equations.

The number of unknowns and constans in the system of equations is proportional to the number of discrete elements. Too many discrete elements complicate the physical model causing it's mathematical equations to be difficult in solving. Therefore it is evident that the elaboration of a model having the minimum number of elements and giving a good result (an optimal model) should be aimed at. The purpose of this paper is to work out a model with minimal number of the discrete elements which ensures the theoretical predictions to fit in with experimental observations and measurements.

The discretization including source geometry and acoustic parameters should be the first step in modelling.

In the examples of radiation and diffraction problems analysed and published so far a constant value of acoustic parameters on a source of an arbitrary geometry was assumed. Then, above all, the fundamental discretization is imposed by the source geometry (e.g., the boundaries). An additional regular discretization, if needed, is carried out between the lines of the fundamental discretization. The division to smaller elements is carried out until a good model is approached. The model obtained using this method, however, includes too many elements.

In this paper, addition irregular discretization was proposed in order to reduce the number of model elements. In the literature concerning sound radiation and diffraction, any additional irregular discretization of the source (any optimal model problem) has not been discussed yet.

According to the publication [5], it appears that the regular discretization and all irregular ones do not have any theoretical base.

Systematization of the difficulties appearing in source modelling problems (including discretization) and providing the rules of finding their solutions is taken up in the publication series Acoustic Modelling of Surface Source. This paper is the first one in this series.

The irregular discretization problem is examined basing on the example of a plane source where the vibration velocity function is not constant. The problem may be simplified due to the fact that the discretization of the source geometry is no longer needed and only the vibration velocity has to be discretized. The mathematical description is also simplified. This case is not described by Helmholz–Huygens integral with BIE but only by Helmoholz–Rayleigh integral.

In general, plane surface source modelling is carried out in the following stages:

1 — the vibrating surface is discretized into $j=1, 2,...,J$ elements;

2 — vibration velocity points (i-points) are selected on each element, $i=1, 2,...,I$;

3 — basing on the measured discrete values of the vibration velocity the vibration velocity on each element is evaluated in one of the three ways:

3.1 — as the arithmetic mean of vibration velocity values measured in a large number of the i-points. Then it is assumed that every point of the given element is vibrating with the arithmetic mean vibration velocity. It is assumed, therefore, that the element vibrates in the same way as a piston. A set of all pistons generates a piston model of the source (PM^m). It has to be observed that the measurement of the vibration velocity values in larger number of i-points will not affect significantly to the value of the average vibration velocity. The quality of the model created in this way results from only the discretization error, i.e. the error resulted from the insufficient large number of i-points is not be included in the model.

3.2. — as the arithmetic mean of the values of the vibration velocity measured in the finite number of i-points.
Similarly as in item 3.1., a piston model (PM^a) is considered. The quality of this model is caused by the discretization error as well as by the insufficiently large number of the i-points.

3.3. — an appropriate shape of vibration velocity function is reproduced making use of interpolation functions. The source elements with such built vibration velocity functions constitute so called the interpolation model (IM).

For the assumed vibration velocity function, the convergence of the model with the source can be analysed. It can be done by examining the acoustic fields calculated from the Helmholz–Rayleigh integral and from "discrete" form of this integral.

In acoustic the divergence of the model with the exact one can be defined, for example, by the distance between their directivity functions (DFs) i.e.:

1 — an absolute distance;

2 — a relative distance;

3 — a mean square distance.

Applying the second or the third option and the irregular discretization a minimal relative or mean square distance is sought for the given number of elements. The problems outlined above belong to the optimization problems [12]. Therefore, the source model obtained as a solution of these problems is called the optimal model.

In this paper, a plane axisymmetric source was considered where the vibration velocity function is axially symmetrical, the source axis (the z-axis on Fig. 1) being the axis of symmetry of the velocity function. A line of the source is the results of a cross section of such source made by a perpendicular plane. The discretization of the source reduces to the discretization of the line of the vibration velocity function. A vibration velocity function without nodes was assumed on the vibrating surface. The value of the constant vibration velocity was calculated as the average value of the vibration velocity function (see item 3.1). Applying the irregular discretization, the minimal number of elements was looked for by the analysis of the absolute distance between the exact DF and DF of the model.

2. Acoustic field of an axisymmetric source

The acoustic field of a circular vibrating surface located in an infinite and rigid baffle is calculated using Hyugens–Raleigh integral [9]

$$\Phi_{MN}=\frac{1}{2\pi}\int_S v_{MN}(\rho,\phi)G(r)dS, \tag{2.1}$$

where in polar coordinates

$$dS=\rho\,d\rho\,d\phi, \tag{2.2}$$

$$G(r)=\frac{\exp[-ikr(\rho,\phi)]}{r(\rho,\phi)}, \tag{2.3}$$

Vibration velocity of an axisymmetric source will be denoted by $v_{0N}(\rho)$. Such source radiates an axisymmetric acoustic field, constant for each constant angle ϕ_P and ρ_P. This field can be considered in a plane crossing the source axis of symmetry and described by angle $\phi_P=\text{const}$. Acoustic field of the axisymmetric problem is described by formula (1) for $M=0$ and for e.g. $\phi_P=0$, that is

$$\Phi_{0N}=\frac{1}{2\pi}\int_\rho v_{0N}(\rho)\left[\int_0^{2\pi} G(r)d\phi\right]\rho\,d\rho. \tag{2.4}$$

It is possible to calculate analytically the integral inside the square bracket. Thus the evaluation of the axisymmetric field reduces to calculation of the integral (2.4) only

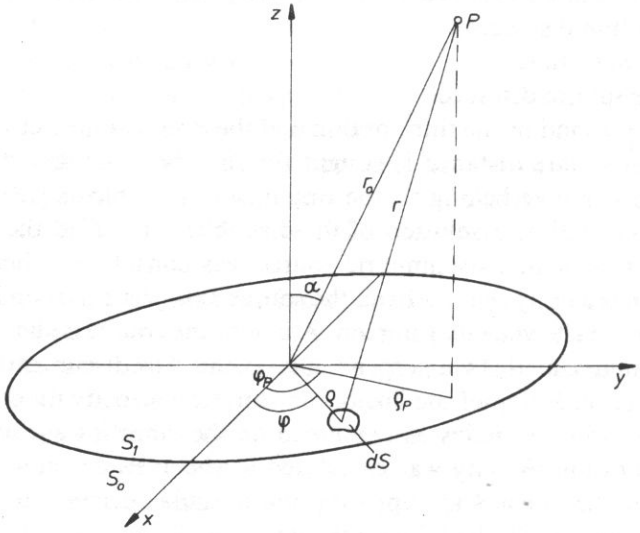

Fig. 1. The geometry of the problem.

over the source cross section. However the calculation of the integral requires the separation of integration variables ρ, ϕ by expanding the integrand in a series of special functions [7]. To calculate the integral in bracket it is convenient to apply the numeric integration.

Formula (2.4) is valid for any distance of point P from the source. But only the far field was considered in the present publication. In the far field the Fraunhofer approximation is applied to formula (2.4), Fig. 1. In the far field:

$$\frac{1}{r} \cong \frac{1}{r_0}, \quad r \cong r_0 - \rho\cos(\rho, r_0) = r_0 - \sin\alpha\cos(\phi - \phi_P). \tag{2.5}$$

Inserting (2.5) into (2.3) and then to (2.4) one gets

$$\Phi_{0N}(a) = C_0 Q_{0N}(\alpha), \tag{2.6}$$

where

$$C_0 = \frac{\exp(-ikr_0)}{r_0}, \tag{2.7}$$

$$Q_{0N}(\alpha) = 2\pi \int_L v_{0N}(\rho) \left[\int_0^{2\pi} \exp(ik\rho\sin\alpha\cos\phi) d\phi \right] \rho\, d\rho. \tag{2.8}$$

The integral in the square bracket is given by the following formula [7]

$$\int_0^{2\pi} \exp(ik\rho\sin\alpha\cos\phi) d\phi = 2\pi J_0(k\rho\sin\alpha). \tag{2.9}$$

Therefore,

$$Q_{0N}(\alpha) = \int_\rho v_{0N}(\rho) J_0(k\rho\sin\alpha)\rho\, d\rho \tag{2.10}$$

Formula (2.6) expresses the acoustic potential in the far field and is the starting point for the calculation of the cross section of the DF.

The DF is defined as a ratio of a field radiated in any direction to the field (2.7) radiated by a point source located in the center of the coordinate system (2.7). Therefore, the DF is given by formula (2.10)

3. Acoustic field of the piston model

3.1. The average value of the vibration velocity function

A constant vibration velocity on j-element was calculated employing the definition of average function value which, in polar coordinates, is given by the following formula:

$$v_j^m = \frac{1}{L_j} \int_{G_1}^{G_2} v_{0N}(\rho)\, d\rho, \tag{3.1}$$

where G_1, G_2 are boundaries of the discrete j-element and

$$L_j = G_2 - G_1. \tag{3.2}$$

This formula should be considered as the arithmetic mean of vibration velocity calculated from the velocities measured in large number of i-points on the vibrating surface (see "Introduction", item 3.1).

If the discretization is irregular the boundaries G_1, G_2 of the j-element are chosen arbitrary. However, if any of the j-elements (or the whole vibrating surface) having the boundaries G_1, G_2, is divided into $j=1, 2,...,J$ smaller elements equal to each other than the new boundaries are given by formula

$$\begin{aligned} g_1 &= G_1 + (j-1)(G_2 - G_1)/J, \\ g_2 &= G_1 + j(G_2 - G_1)/J. \end{aligned} \tag{3.3}$$

The formula for the DF of the considered model is obtained by inserting formula (3.1) into (2.10). In this way one gets,

$$Q_{0N}^m(\alpha) = \sum_{j=1}^{J} v_j^m \int_{\rho_j} J_0(k\rho \sin\alpha)\rho\, d\rho. \tag{3.4}$$

If formula (3.1) is inserted into formula (2.4) then a "discrete" form of Helmholz–Rayleigh integral is obtained for both the axisymmetric as well as the far field problem.

4. Numerical calculations

A piston model was analysed to establish dependence on:

- vibration frequency,
- shape of the vibration velocity function,
- place of the vibrating surface within the baffle.

The sinus function was chosen as the vibration velocity function. Three axisymmetric sources were considered with axes:

- crossing the maximum of the sinus function (Fig. 2a)
- crossing the zero point of the sinus function (Fig. 2b)

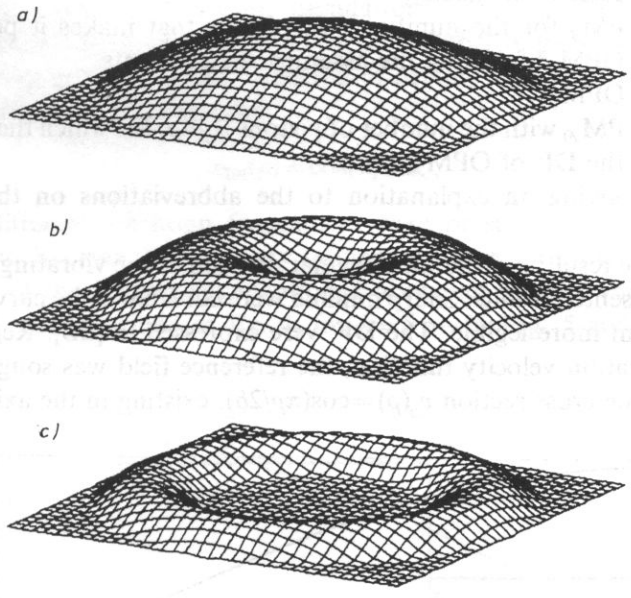

Fig. 2. The shape of the vibration velocity functions.

• outlying the sinus function (Fig. 2c), in this case a ring shaped source is obtained.

It should be noted that sinus is involved in the free vibration modes of vibrating plates and membranes. The discretization method given in this publication can be therefore applied to the model of vibrating surfaces of this kind.

The piston model with the DF fulfilling the criterion of concidence with the exact directivity was sought in two ways:

• by increasing discretization,

• for a fixed discretization the sizes of some pistons were changed.

The following symbols were introduced:

PM_J — a piston model composed of J — regular pistons,

OPM_J — an optimal piston model composed of J — irregular pistons.

While searching OPM_J numerically the boundaries between the pistons were changed with 0.01 step. Decreasing the step requires long calculations. For the practical purposes it was recognized as the OPM_J gives approximate DF (by shape and value) to the exact DF has minimal number of pistons. The difference between shorp minima of the exact DF and approximation one may be described by an angle $\Delta\alpha$ while the positions of both patterns maxima are approximately described by the values ΔD_{0N} ($\Delta\alpha \cong 0.025$ [rad] $\cong 1.43°$, $\Delta D_{0n}(\alpha) \cong 2$ [dB] were assumed).

The results of the calculations are presented in figures that present:

1 — the cross section of the vibrating surface,

2 — the plots for the following DF (or their fragments):

2.1. — calcualted exactly,
2.2. — PM_J for the number J of pistons that makes it possible to find OPM_J[a] fulfilling the assumed requirements,
2.3. — OPM_J,
2.4. — PM_{J0} with the number of pistons $J_0 > J$, for which the DF is close to the DF of OPM_{J0}.

3 — a table giving an explanation to the abbreviations on the section and diagrams.

The advantage resulting from the irregular division of the vibrating surface can be seen from the presented results. Sharp minima were cut from some curves to make the remainder of them more legible. The DF were expressed in [dB]. Regardless of the shape of the vibration velocity function, the reference field was sought as constant value field with the cross section $v_0(\rho)=\cos(\pi\rho/2b)$, existing in the axis of symmetry (z-axis).

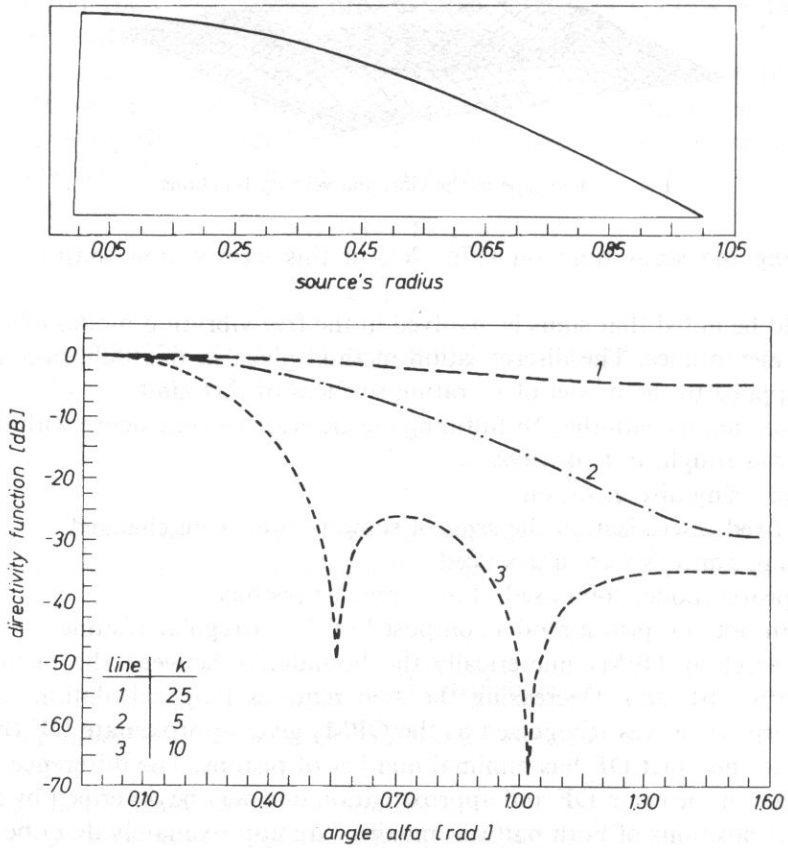

Fig. 3. The influence of the vibration frequency on the directivity functions for the source vibrating with the velocity $v_{0N}(\rho)=\cos(\pi\rho/2b)$: curve 1 — $k=2.5$ ($v \cong 130$ Hz), curve 2 — $k=5$ ($v \cong 260$ Hz), curve 3 — $k=10$ ($v \cong 520$ Hz), $\alpha \in \langle 0,\pi/2\rangle$.

In the first group of numerical calculations the influence of the vibration frequency (expressed by wave number k) on the number of pistons in the model was considered. It was assumed a fixed position of driving surface in the baffle and the following vibration velocity function

$$v_{0N}(\rho)=\cos(\pi\rho/2b), \tag{4.1}$$

The DF for different vibration frequencies were presented in Fig. 3. From this figure it follows that vibration velocity influences strongly on the shape of the DF. Then for each of the frequencies mentioned above an optimal model was sought. DF for $k=2.5$ was presented in Fg. 4, for $k=5$ — in Fig. 5 and for $k=10$ — in Fig. 6.

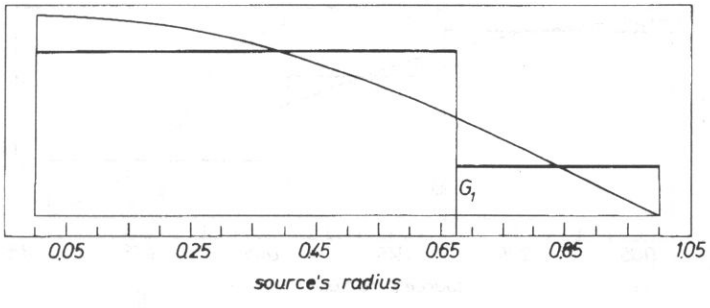

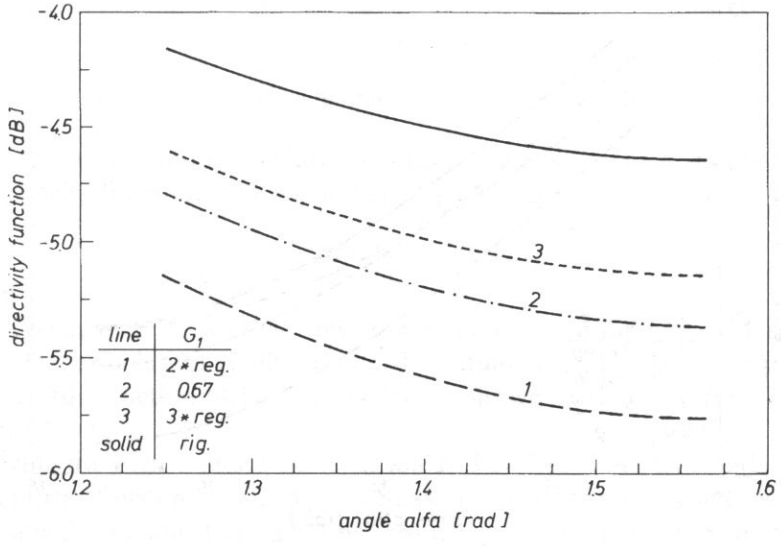

Fig. 4. The directivity functions for $k=2.5$, $v_{0N}=\cos(\pi\rho/2b)$

The figures show that the optimal model was obtained for different number of pistons depends on the frequency. For $k=2.5$ the optimal model has two pistons, for $k=5$ — three pistons, for $k=10$ — four pistons.

It has been shown that for the same number J of pistons OPM_J gives far better results than PM_J. The divergence between these models can be better observed for higher frequencies. By the model optimization it is possible to get DF quite similar to DF of PM_{J0} for less number of pistons. The number of pistons in PM_{J0} depends also on frequency.

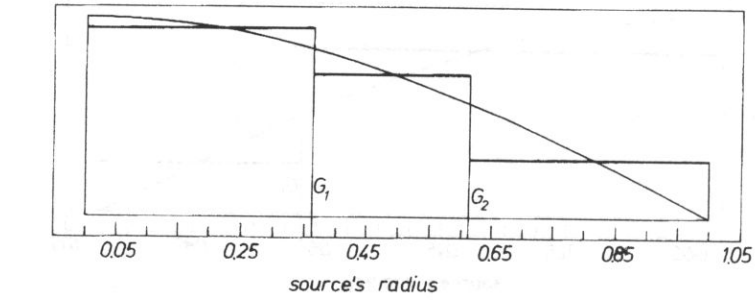

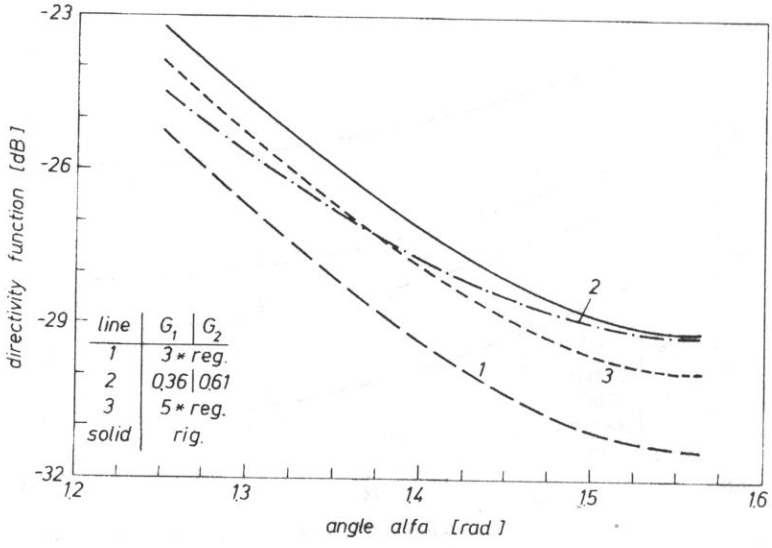

Fig. 5. The directivity functions for $k=5$, $v_{0N}=\cos(\pi\rho/2b)$.

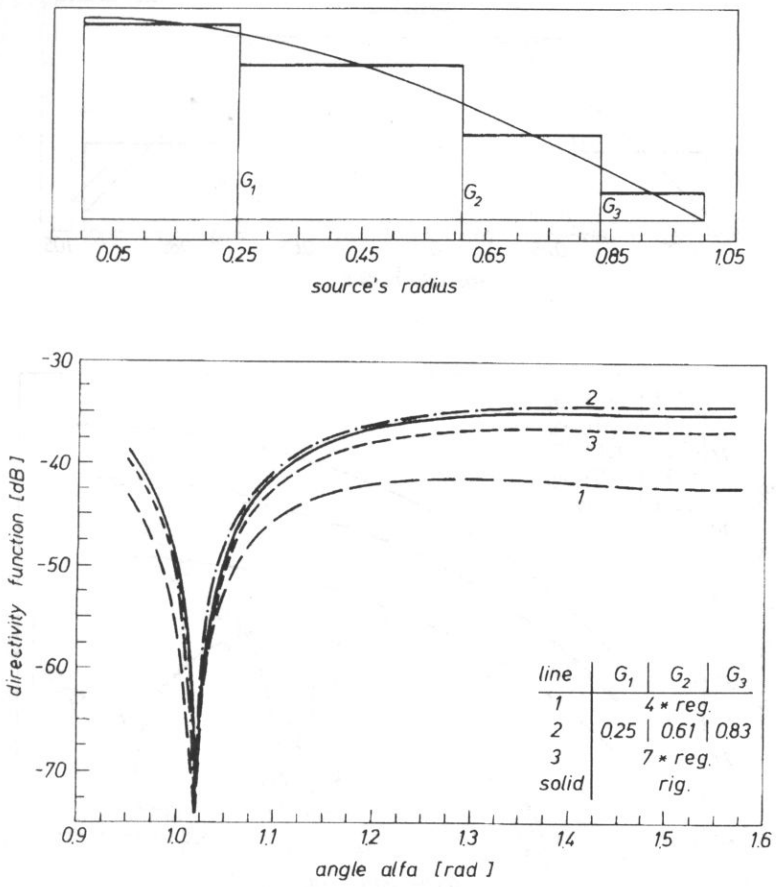

Fig. 6. The directivity functions for $k=10$, $v_{0N}=\cos(\pi\rho/2b)$.

II. The second group of calculations concerns the influence of the shape of the vibration velocity function on the number of pistons in the model. The function

$$v_{0N}(\rho)=\sin(\pi\rho/2b), \tag{4.2}$$

was chosen.

It should perhaps be noted that this is a symmetrical function with respect its maximum. The calculation results obtained for function (4.2) were compared with that obtained for function (4.1). The results are shown in Fig. 7 — for $k=5$ and in Fig. 8 — for $k=10$.

Comparing the Figs. 5 and 7 and afterwards the Figs. 6 and 8 it can be observed that the number of pistons in OPM_J as well as in PM_J does not depend on the shape of the examined function. For the same frequency, however, the dimensions of the pistons are different for different function shapes. In this case the number of pistons also depends on the vibration frequency (Fig. 7 and 8).

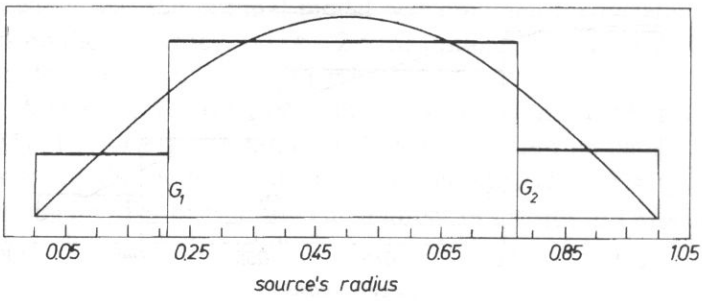

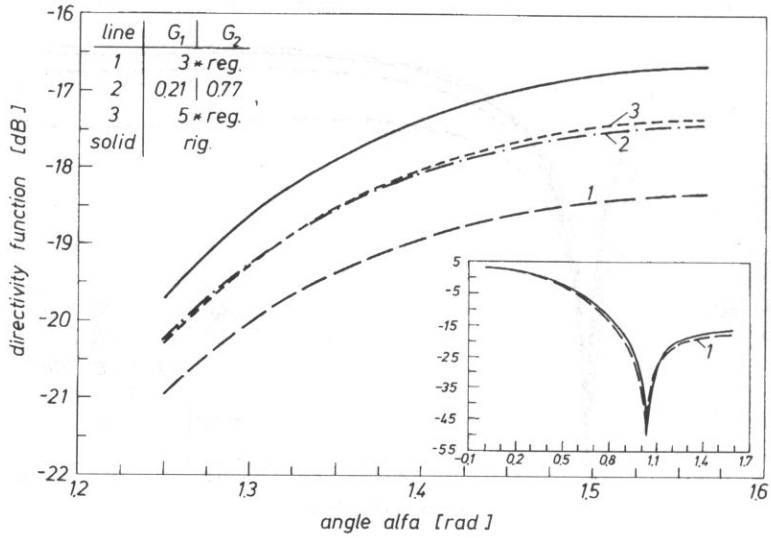

Fig. 7. The directivity functions for $k=5$, $v_{0N}=\sin(\pi\rho/b)$

III. The last group of calculations concerns the influence of the position of the vibrating surface in the baffle on the number and dimensions of the elements. The function

$$v_{0N}(\rho)=\sin(\pi(\rho-a)/(b-a)), \tag{4.3}$$

as vibration velocity was chosen. The source having such vibration velocity is a ring. Its internal and external radii were assumed to be $a=1$ and $b=2$, respectively. The calculation results were shown in Fig. 9 for $k=5$ and in Fig. 10 for $k=10$. The figures show that for the chosen position of the ring the number of pistons increases with increasing frequency.

It may be observed, comparing Figs. 7 with 9 and next with the Figs. 8 and 10, that the boundaries of the pistons in OPM_J depend on the position of the ring with respect

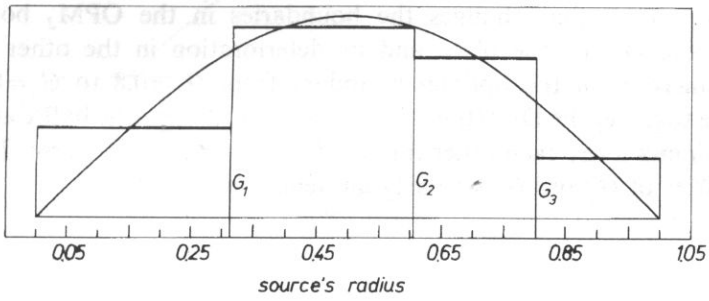

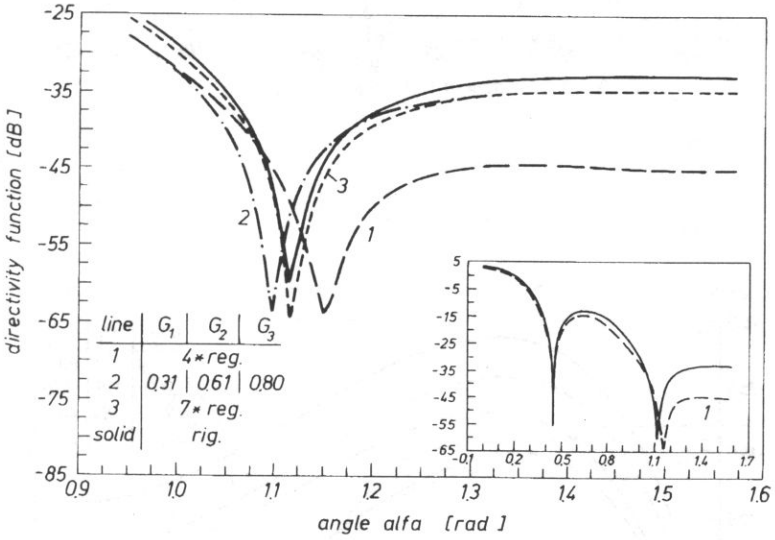

Fig. 8. The directivity functions for $k=10$, $v_{0N}=\sin(\pi\rho/b)$.

to the source axis. It turns out that the number of pistons also depends on the ring position. E.g. $\mathrm{OPM}_{J=4}$ fulfilling the assumed requirements has not been found for $a=4$, $b=5$. Any OPM_J for $J>4$ has not been sought because of the fact that such a consideration is rather tedious.

The influence of the changes the boundaries of $\mathrm{OPM}_{J=4}$ on the shape of DF was presented for function (4.3) for $k=10$. For fixed G_1 and G_2 boundary G_3 was changed with the step 0.01. The results are presented in Fig. 11.

That figure shows that changes the boundaries in the OPM_J both the improvement of the DF in one place and its deterioration in the other place. For example, the increase of the optimal boundary from $G_3=0.8$ to $G_3=0.81$ makes approach close together the DFs (the solid line and line 2) near the baffle at the cost of pushing the minima away each other for $G_3=0.79$, the result is inverse. The changes in the boundaries of G_1 and G_2 similarly influence on the DF.

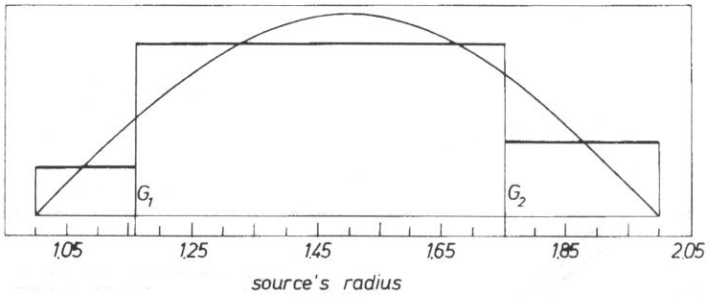

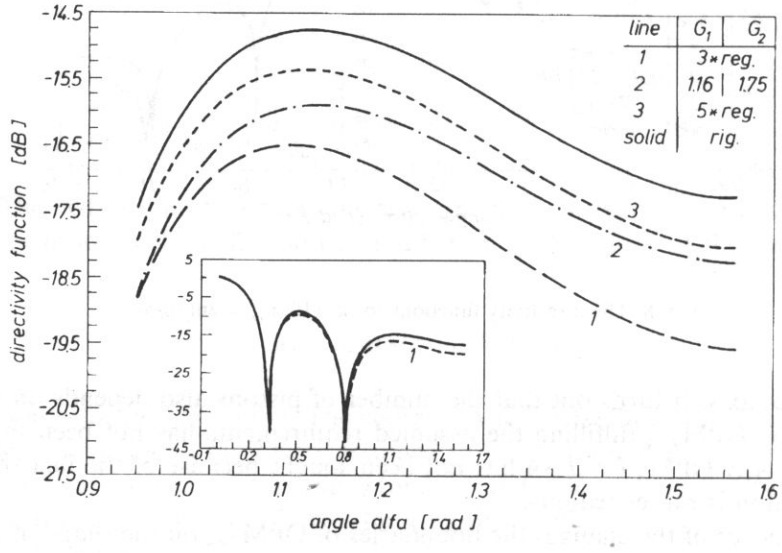

Fig. 9. The directivity functions for $k=5$, $a=1$, $b=2$, $v_{0N}(\rho)=\sin(\pi(\rho-a)/(b-a))$.

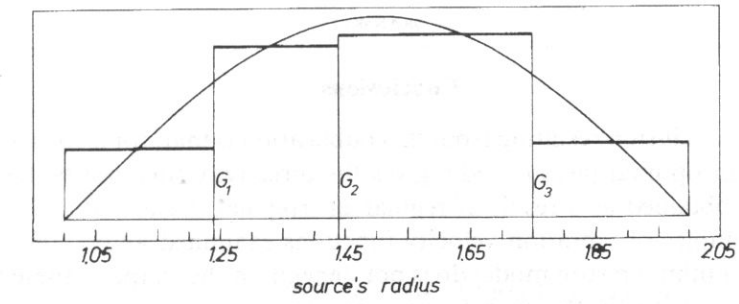

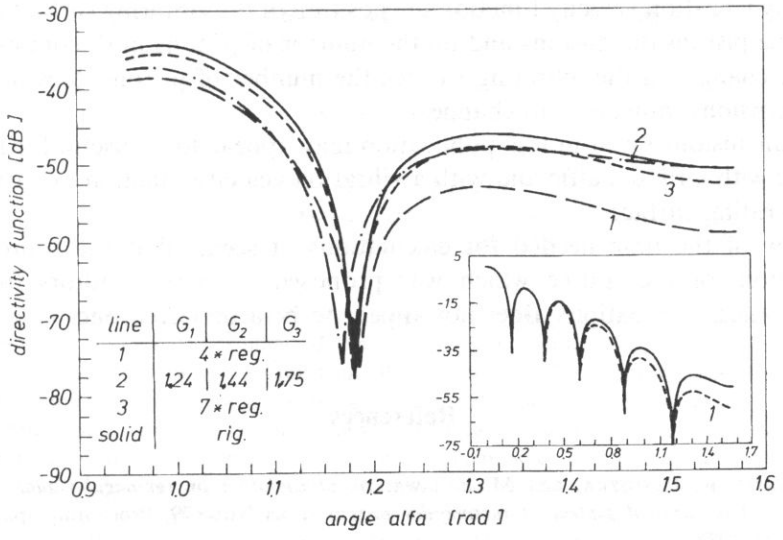

Fig. 10. The directivity functions for $k=10$, $a=1$, $b=2$, $v_{0N}=\sin(\pi(\rho-a)/(b-a))$.

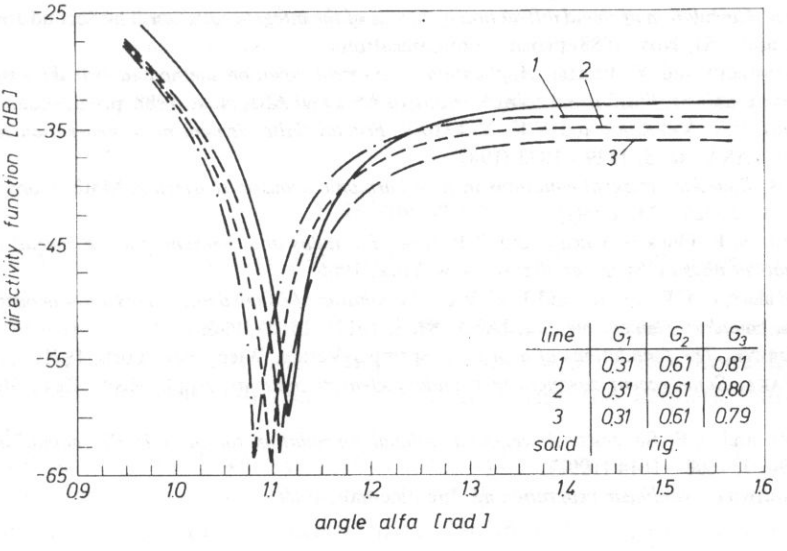

Fig. 11. The influence of the boundary changes in the optimal piston model on the directivity functions for $k=10$, $v_{0N}=\sin(\pi\rho/b)$.

Conclusions

A general conclusion resulting from this publication is that, for a constant number of elements, an optimal piston model gives the directivity function better than any piston model obtained as a result of regular or irregular discretization.

In the examples of vibration velocity functions examined above, the number of pistons in the optimal piston model does not depend on the shape of these functions. The piston boundaries in the model, however, varies.

For any vibration velocity function the position of the vibrating surface influences on both the pistons dimensions and on the number of pistons in the optimal model. For slight changes in the vibrating surface the number of pistons does not change. Their dimensions, however, do change.

The conclusions given in this publication may appear to be useful for modelling the source with a finite baffle and with a vibration velocity function of varying form on the vibrating surface.

In view of the time needed for calculations, it seems that the source regular discretization, of the source which was proposed by many authors for solving boundary integral equations, does not appear to be a preferred one.

References

[1] A. BRAŃSKI, R. PANUSZKA, and M. ZABAWA, *Iound radiation by rectangular plate represented by a model in form of system of rectangular pistons*, Inter-Noise'79, Proceedings pages 53–56, Warszawa, 1979.

[2] A. BRAŃSKI, *Acoustical model of the plates* (in Polish), WSP, Rzeszów, 1991.

[3] Y. FURUE, *Calculation of sound diffraction by means of the integral equation*, The Second Joint Meeting of ASA and ASJ, Nov. 1988, private communication.

[4] Y. HORINOUCHI and Y. FURUE, *Application of integral equation method to two dimensional sound diffraction problems*, The Second Joint Meeting of ASA and ASJ, Nov., 1988, private communication.

[5] J.H. JENG, V.V. VARADAN and V.K. VARADAN, *Fractal finite element mesh generation for vibration problems*, JASA, **82**, 5, 1829–1833 (1987).

[6] R. KRESS, *Boundary integral equations in time-harmonic acoustic scattering*, Math. Comput. Modelling, **15**, 3–5, 229–243 (1991).

[7] W. MAGNUS, F. OBERHETTINGER and R.P. SONI, *Formulas and theorems for the special functions of mathematical physics*, Springer-Verlag, New York, 1966.

[8] A.F. SEYBERT, C.Y.R. CHENG and T.W. WU, *The solution of coupled interior/exterior acoustic problems using the boundary element method*, JASA, **88**, 3, 1612–1618 (1990).

[9] E. SKUDRZYK, *The foundations of acoustics*, Springer-Verlag, Wien, New York, 1971.

[10] M. TANAKA, *Some recent advances in boundary element methods*, Appl. Mech. Rev., **36**, 627–634 (1983).

[11] T.W. WU and A.F. SEYBERT, *A weighted residual formulation for the CHIEF method in acoustics*, JASA, **90**, 3, 1608–1614 (1991).

[12] W.I. ZANGWILL, *Nonlinear programming*, Prentice-hall, 1969.

ARCHIVES OF ACOUSTICS
20, 4, 327–345 (1995)

ACOUSTIC MODELLING OF SURFACE SOURCES PART II. PISTON MODEL, ASYMMETRICAL FUNCTION OF VIBRATION VELOCITY, DISCRETIZING ERROR, AXISYMMETRICAL PROBLEM

A. BRAŃSKI

Institute of Technology
Pedagogical College
35-310 Rzeszów, ul. Rejtana 16a

In the paper, by applying irregular discretization of the axisymmetrical plane source, an optimal piston model was obtained. An asymmetrical function of the vibration velocity, with regard to its zeros was assumed on vibrating surface. The vibration velocity of the single piston was calculated as an integral mean value of the vibration velocity of the vibrating surface. Then the model of the source consists of an array of driving pistons. In order to select the optimal position of the boundary between the pistons, the measure of the divergence/convergence between directivity function of the model and exact was analysed. The least squares distance and uniform distance were taken as a measure of deviation of the directivity function of the model from the exact one. Numerical calculations showed that the irregular discretization gives particularly good results for asymmetrical function of vibration velocity. It was also proved that the least squares distance is a better measure of directivity functions of the model and exact one the uniform distance. Its variation, as a function of vibration velocity or position of the vibrating surface in the baffle or nondimensional wave number, is more regular than the variation of uniform distance.

1. Introduction

Modelling acoustical source with arbitrary geometry is the subject of a lot of articles, e.g. paper [5]; see also Refs. given in [5]. Mathematical model of such sources contains, among other things, boundary integral equations (BIE). Boundary element method (BEM) is applied to solve BIE. The first step of the modelling is discretization. Both geometry surface of the source and the acoustic variables are discretized.

In literature cited in [5], sources with arbitrary geometry were considered, however constant, acoustic variables were assumed on the whole surface. In these papers, planar elements of the surface were utilized, and in addition, the acoustic variables were represented by the constant value on each element. In such case, discretization applies mainly to geometry. Primary discretization is imposed by the singularities of

the surface, e.g. sharp edges. More refined model may be obtained if the elements of primary discretization are discretized again [4, 5, 6].

In paper [3] a planar source was examined, but vibration velocity function not constant was assumed. In this instance, vibration velocity is discretized, but not the surface of the source. Furthermore, in Ref. [3], general rules of primary discretization of vibration velocity with nodal lines were given. In Ref. [3] as in Refs. mentioned above, the secondary regular discretization was applied to improve the quality of the model. As expected, if the number of regular elements was increased very good piston model was obtained. However, it contains too many elements. Using too many elements is a burden to the user and is also not computationally efficient.

In order to partially remedy the difficulty, irregular discretization was suggested, Ref. [2]. As an example, planar axisymmetrical source was considered which creates axisymmetrical surface of the vibration velocity. Therefore, due to the symmetry of the surface, only its cross section line has to be discretized. As it was pointed out in Ref. [2], the irregular discretization gave a good irregular model which contained not so many elements as the regular model. The irregular model which contained the minimum number of the elements and whose acoustical field fulfilled the assumed boundary convergence to the exact acoustical field was called optimal model.

In Ref. 2, sinus function was chosen as the function of vibration velocity. This function has the maximum halfway along the distance between zero points, i.e. it is symmetric to its maximum. The absolute distance (in dB) was assumed as the measure of the convergence.

In this paper, a planar axisymmetrical source was considered. But the shape of the vibration velocity is not symmetric to its maximum. Two new measures of the convergence were taken into account, namely (1) the least squares distance and (2) uniform distance nondimensional between exact directivity function and the directivity of the model.

In the paper two problems were solved. First, the influence of asymmetry of the vibration velocity, frequency of the vibration, place of the vibrating surface in the plane baffle on the optimal piston was found. Secondly, it was pointed out that, generally, the least square distance is a better measure of convergence between directivity functions than the uniform one.

2. Acoustic field of the axisymmetric (AS) source

In this and the next section, an outline of the theory is presented upon which the calculations are based. A detailed treatment of the theory can be found in Ref. [2].

The acoustic field of the vibrating surface placed in an infinite plane and rigid baffle is given by Huygens–Rayleigh integral. Assuming fully AS source (i.e. both the source shape and acoustic variables are independent of the angle of revolution of the source), an acoustic field is AS too, and Huygens–Rayleigh integral takes the form [2]

$$\Phi_{0N}=\frac{1}{2\pi}\int_{\rho} v_{0N}(\rho)\left[\int_{0}^{2\pi} G(r)\,\mathrm{d}\phi\right]\rho\mathrm{d}\rho, \tag{2.1}$$

where

$$G(r)=\frac{\exp[-\mathrm{ikr}(\rho,\phi)]}{r(\rho,\phi)}, \tag{2.2}$$

$$v_{0N}(\rho)=C_1\sin(\pi\rho)\exp(-C_2\rho), \tag{2.3}$$

k — nondimensional wave number, $v_{0N}(\rho)$ — vibration velocity of the driving surface asymmetrical to its maximum, C_1, C_2 — coefficients, they have been selected to fulfil the assumed asymmetry of the $v_{0N}(\rho)$. General geometry of the radiation problem is given by Fig. 1.

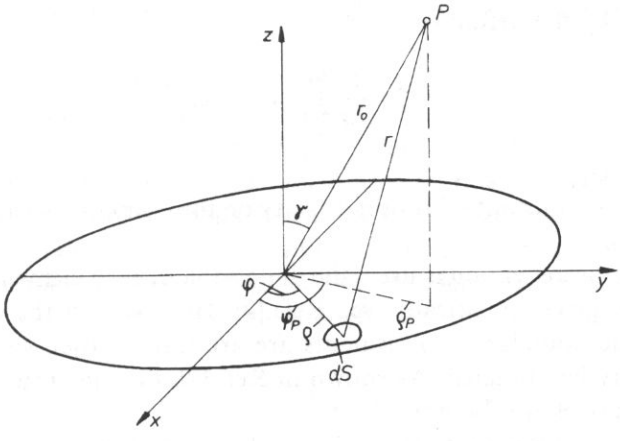

Fig. 1. Nomenclature for a radiation problem.

In the far distance away from the source, the Fraunhofer approximation is applied (Ref. [2]).

$$\frac{1}{r}\cong\frac{1}{r_0}, \qquad r\cong r_0-\rho\cos(\rho,r_0)=r_0-\rho\sin\gamma\cos(\phi-\phi_P). \tag{2.4}$$

Substituting Eq. (2.4) into Eq. (2.1) we obtain

$$\Phi_{0N}(\gamma)=C_0 Q_{0N}(\gamma), \tag{2.5}$$

where

$$C_0=\frac{\exp(-\mathrm{ikr}_0)}{r_0}, \tag{2.6}$$

$$Q_{0N}(\gamma)=\int_{\rho} v_{0N}(\rho)\,J_0(\mathrm{k}\rho\sin\gamma)\rho\,\mathrm{d}\rho, \tag{2.7}$$

$J_0(x)$ — Bessel function of the first kind and zeroth order.

In a great distance from the source, the directivity function is usually analyzed. To obtain directivity function the acoustic field Eq. (2.5) may be normalized by the acoustic field Eq. (2.6), generated by the point source set in the origin of the coordinates. Then, under these circumstances, the directivity function is given by (2.3).

3. Acoustic field of the piston model

The mean vibration velocity

The constant vibration velocity on j-element as the mean velocity — v_j^m over the driving surface of the source has been calculated. If AS case is considered, the mean velocity is given by the definition

$$v_j^m = \frac{1}{L_j} \int_{G_{\rho 1}}^{G_{\rho 2}} v_{0N}(\rho)\, \mathrm{d}\rho, \tag{3.1}$$

where $L_j = G_{\rho 2} - G_{\rho 1}$.

The model with the constant vibration velocity on the elements of the surface is called the piston model.

If the regular discretization is used, the dimension of each element is the same and $G_{\rho 1}$, $G_{\rho 2}$ may be given analitically, see Ref. [2]. However, in the case of irregular discretization, the boundaries of elements are arbitrary chosen so that an optimal piston model may be obtained. As shown in Ref. [2], the dimensions of elements in optimal piston model are different.

If Eq. (2.6) is substituted into Eq. (2.7), the directivity function of the piston model is obtained

$$Q_{0N}^m(\gamma) = \sum_{j=1}^{J} v_j^m \int_{\rho_j} J_0(\mathrm{k}\rho \sin\gamma)\rho\, \mathrm{d}\rho. \tag{3.2}$$

4. Verification of the model

The quality of the piston model may be improved in two ways if:

1 — the discretization is increased,

2 — assuming that the number of pistons is constant the dimensions of the pistons are changed.

To simplify the notation, the following labels are introduced:

M_r — regular piston model,

M_i — irregular piston model.

First of them consists of J equal elements and the second contains J different elements.

To analyse the position of directivity functions in relation to each other (convergence/divergence of the directivity functions) optimal methods may be used.

Then, the optimal model ought to be built. The main problem of optimalization is the minimization or the maximization of some function subjected to some constraints. The function whose the least or the greatest value is being sought is called an objective function and the collection of the values of the variables at which the least value is attained defines the optimal solution.

To simplify an optimalization analysis, two element model ($J=2$) is chosen. Assume that the constraints are given by

$$r_\alpha - G_1 \geqslant 0, \quad G_1 \geqslant 0, \tag{4.1}$$

where

$$G_1 = G.$$

It is required to choose among the set of G such G that would minimize the objective function.

The objective function may be:

- least squares distance between $Q_{0N}(\gamma)$ and $Q_{0N}^m(\gamma,G)$ or
- uniform distance among the points of $Q_{0N}(\gamma)$ and $Q_{0N}^m(\gamma,G)$.

The directivity function $Q_{0N}^m(\gamma,G)$ is a function of G, Eqs. (3.1) and (3.2), in which G appears in boundaries of integrals. Then, the optimalization belongs to nonlinear optimalization. Applying one of the methods of solving nonlinear optimization model (Ref. [7]), an optimal solution is obtained. The model which is connected with an optimal solution may be called optimal model.

4.1. Least squares distance between directivity functions

Optimalization of least squares distance is closely related to the least squares method [1].

It is necessary to approximate the function $Q_{0N}(\gamma)$, i.e. the exact directivity function, with the function $Q_{0N}^m(\gamma,G)$, i.e. the directivity function of the model. An approximate function $Q_{0N}^m(\gamma,G)$ may be written

$$Q_{0N}^m(\gamma,G) = \sum_{j=1}^{J} v_j^m(G) f_j(\gamma,G),$$

where the base functions are

$$f_j(\gamma,G) = \int_{\rho_j} J_0(k\rho \sin\gamma)\rho \mathrm{d}\rho.$$

The number

$$d_l(Q_{0N}, Q_{0N}^m) = d_l(G) = \left\{ \int_0^{\pi/2} [Q_{0N}(\gamma) - Q_{0N}^m(\gamma,G)]^2 \mathrm{d}\gamma \right\}^{1/2}, \tag{4.4}$$

is called the least squares distance between functions $Q_{0N}(\gamma)$ and $Q_{0N}^m(\gamma,G)$.

The main problem of the least mean method is to find such a function $Q_{0N}^{m}(\gamma,G)$ so that the least squares distance ought to be minimal. Thus, the main aim is to find the function Q_{0N}^{m}, (γ, G).

In fact, suitable coefficients $v_j^m(G)$ are looked for. This means that suitable vibration velocity on the elements are looked for. Analysing the least squares distance $d_l(G)$ between directivity functions, the acoustical field of the model is investigated directly, however the vibration velocity on the elements of the model is investigated indirectly.

The problem mentioned above may be solved as optimalization problem, i.e. the minimum of the $d_l(G)$ is searched without regard to function $Q_{0N}^{m}(\gamma,G)$. As a result, an optimal model is obtained which is the best approximation of the source in terms of the least squares distance between directivity functions.

4.2. Uniform distance between directivity functions

Optimalization of the model may be carried out if the uniform distance between directivity function as an objective function is chosen. The objective function is the distance $d_u(\gamma,G)$ between some point $A_0(x_0,y_0)$ of one directivity function and the straight line which passes through neighbouring points $A_1(x_1,y_1)$, $A_2(x_2,y_2)$ of the other directivity function, Fig. 2. The distance $d_u(\gamma,G)$ may be accepted as the measure

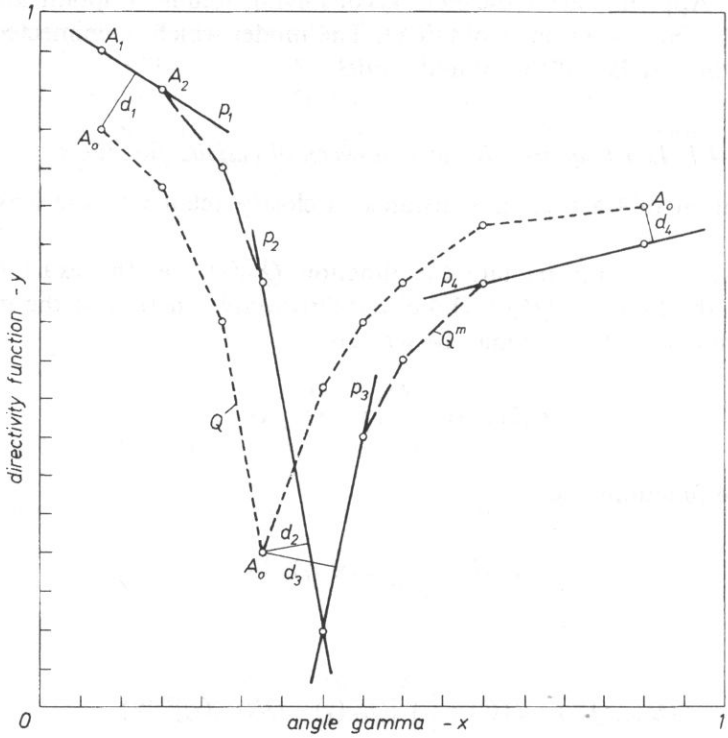

Fig. 2. Uniform distance d_u between the lines as a function of angle gamma.

of the distance between directivity functions at point A_0. Let point B be a projection on the straight line A_1A_2 of the $A_0(x_0, y_0)$. This measure will be the best if the projection of B is the midpoint between points A_1, A_2. The distance $d_u(\gamma,G)$ can be expressed in terms of the coordinates of the points A_0, A_1, A_2 by the formula

$$d_u(\gamma,G)=\frac{a_1x_0+a_2y_0+a_3}{\sqrt{a_1^2+a_2^2}}, \tag{4.5}$$

where

$$a_1=y_1-y_2, \quad a_2=x_2-x_1, \quad a_3=x_1y_2-y_1x_2.$$

It should be noted, that if the acoustical field of AS source is analyzed, the acoustical pressure [Pa] or the directivity function [dB] are displayed along the axis of abscissa. Therefore, the concept of the distance between directivity functions introduced above is meaningless for two reasons. First, a unit of the distance $d_u(\gamma,G)$ has no physical sense. Second, because of the different scales of the axis the influence of the values of ordinates and abscissas on the value of the distance $d_u(\gamma,G)$ will be different. This difference is particularly visible if the directivity functions are given in dB scales considered.

In order to overcome these difficulties the directivity functions ought to be written in normalized coordinates. These coordinates are nondimensional and they are transformed so that they may take values $\langle 0, 1\rangle$.

For the directivity functions of which the ordinates and abcissas vary between 0 and 1 the nonlinear programming methods point out the boundary G of optimal two-piston model (M_0, $J=2$).

Applying nonlinear programming methods to such complicated function as (4.4) or (4.5) is very difficult [7]. It is convenient to calculate the value of objective function for the discrete values of G_v and next to chose that G for which the function possesses a minimum.

If the least squares distance is the objective function, then for the set of G_v, the set of values $d_{l,v}$ is calculated; the minimal value $d_{l,\min}$ points out the boundary $G_{0,l}$ of the optimal model.

By using the uniform distance as an objective functions the searching for the boundary G_{0u} of optimal model overlooking nonlinear programming method is fairly difficult. It can be done by using the following approach described below. For the constant G_v a finite number of μ points $A_0(\gamma_\mu)$ of the directivity function Q_{0N} is determined. For each point $A_0(\gamma_\mu)$ the distance $d_u(\gamma_\mu,G_v)=d_{u,v}(\gamma_\mu)$ from the directivity function $Q_{0N}^m(\gamma,G_v)$ is searched. In this way the set of values $d_{u,v}(\gamma_\mu)$ is obtained from which the maximum of $d_{u,m}$ suitable to G_v ought to be chosen. This procedure outlined above ought to be repeated for the set of G_v. From the set of $d_{u,m}$ the maximum value of $d_{u,\min}$ is chosen which is pointing out G_{ou} of the optimal model. Using the uniform distance as a measure of divergence of the acoustic field has such an advantage that for constant G_v it is possible to investigate $d_{u,v}(\gamma_\mu)$ as a function of the angle γ.

It is obvious that for separate values of G_v, regions of three dimensions space described by angle γ_μ can be found where the divergence of directivity functions is the biggest. As shown in Fig. 2 the biggest divergence is at minimum or maximum and it is equal $d_{u,m}=d_3>d_1>d_2>d_4$. It is not necessary to investigate $d_{u,v}(\gamma_\mu)$ the full interval of the angle γ. Only maxima or minima of the directivity functions pointed out $d_{u,v}(\gamma_\mu)$. The jump of discontinuity from d_2 to d_3 should be noted.

5. Numerical calculations

The numerical calculations were performed to solve two basic problems: 1 — to establish the influence of the asymmetry of the vibration velocity function, frequency of vibration and the place of driving surface in the baffle on the optimal model, 2 — to point out a better method of investigation of the convergence (divergence) between directivity function of the model and exact one. Furthermore it was shown, assuming asymmetrical function of vibration velocity, that the irregular piston model gives a better result then the regular one if the number of elements in the both models is the same. To simplify the numerical calculations a two-elements model was considered, i.e. $J=2$. Further in the paper, to simplify the notation, the subscript J has been dropped out.

The aim of the first calculation is to show which measures of divergence should be optimized to obtain a better optimal model. These calculations consist of three steps marked **I.1**, **I.2**, **I.3**.

I.1. For fixed position of the vibrating surface in a baffle, $a=0$, $b=1$ and $k=2.5$, the place of maximum of the vibration velocity $v_{\max}\rho_c$, was changed. For $\rho_c=\{.3, .4, .5, .6, .7\}$ the detailed results were presented in Figs. 3, 4, 5, 6, 7 respectively.

Each figure consists of part A and B.

Part A presents:

1 — a picture of vibrating surface,

2 — plots:

— least squares distance $d_{i,v}$

— uniform distance $d_{u,v}$

— table which explains the symbols.

Part B presents:

1 — cross-section of vibrating surface and M_{ol} which is obtained as a result of optimalization of d_l,

2 — directivity functions:

— exact (solid line),

— of the model M_r,

— of the model M_{ol},

— of the model M_{ou} which is obtained as a result of optimalization of d_u,

— table which explains the symbols.

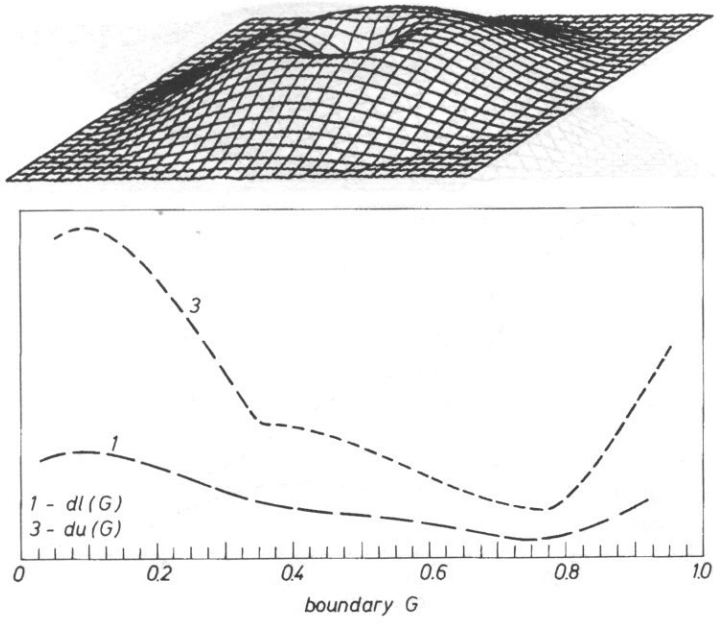

Fig. 3A. Picture of the vibrating surface, $\rho_c = 3$. Plots of the mean square distance $d_{l,v}$ and relative distance $d_{u,v}$ $a=0$, $k=2.5$.

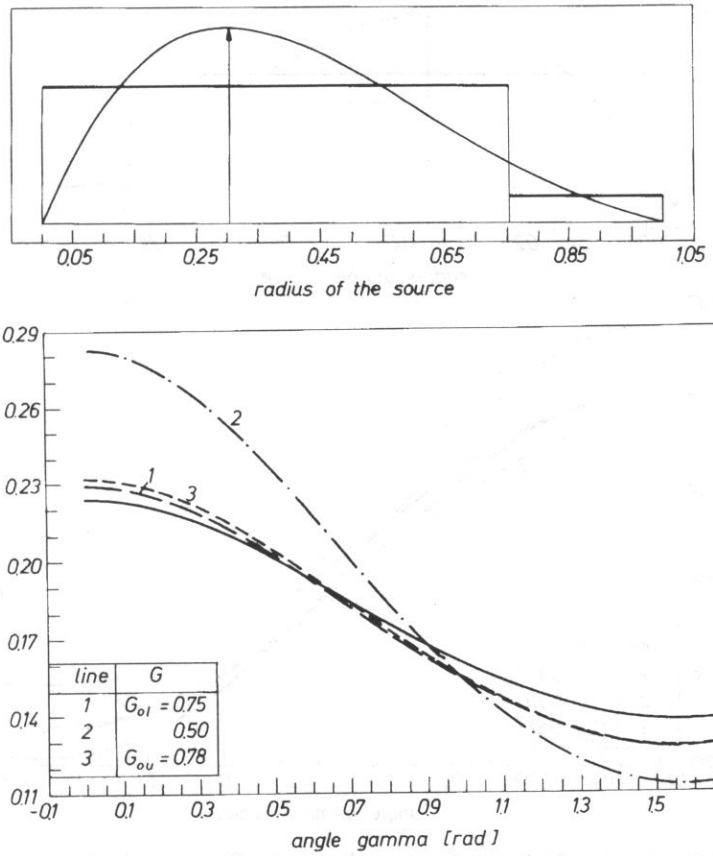

Fig. 3B. Cross-section of the vibrating surface ($\rho_c = 3$) and M_{ol}. Directivity functions of the source M_{ol}, M_r and M_{ou}; $a=0$, $k=2.5$.

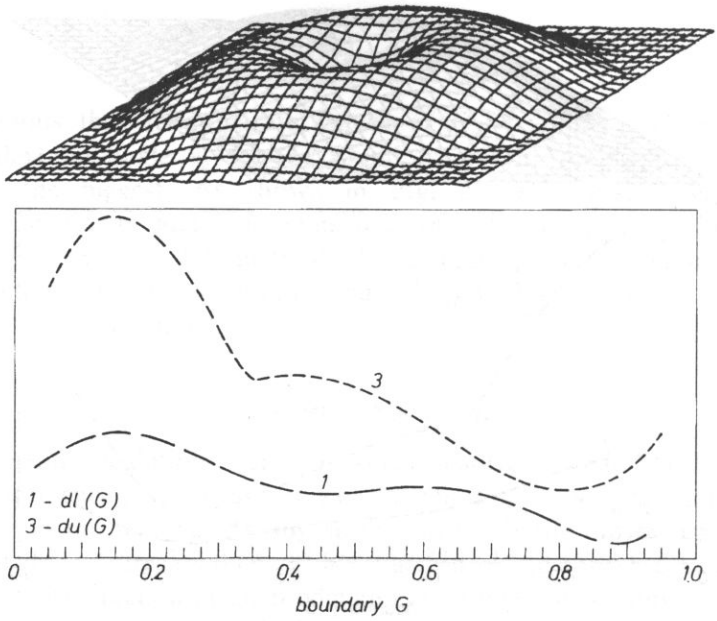

Fig. 4A. Picture of the vibrating surface $\rho_c = .4$. Plots of the mean square distance $d_{l,v}$ and relative distance $d_{u,v}$, $a=0$, $k=2.5$.

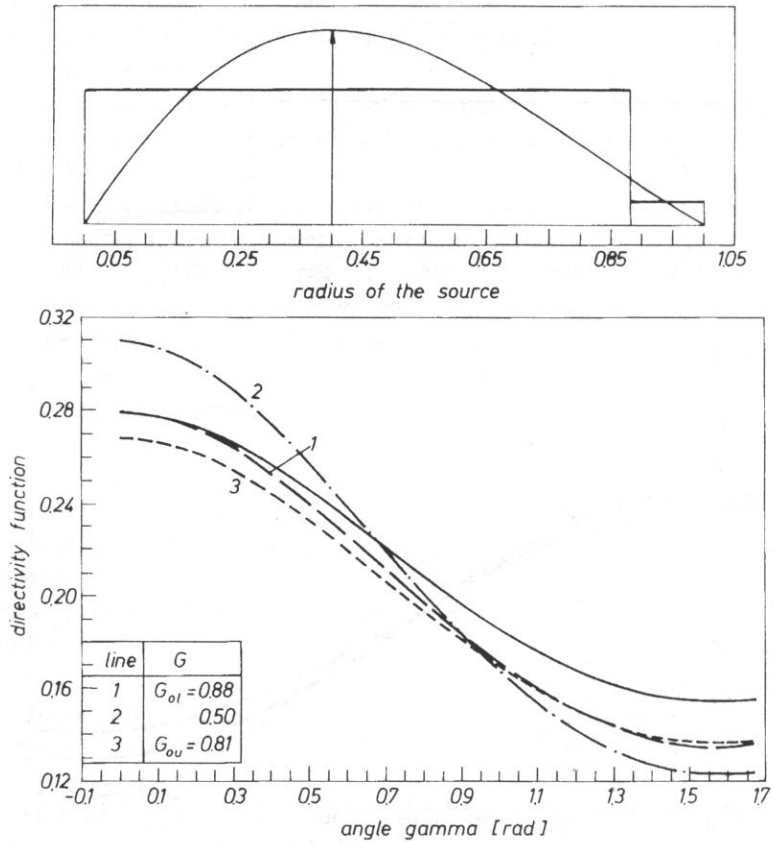

Fig. 4B. Cross-sections of the vibrating surface ($\rho_c = .4$) and M_{ol}. Directivity functions of the source, M_{ol}, M_r and M_{ou}; $a=0$, $k=2.5$

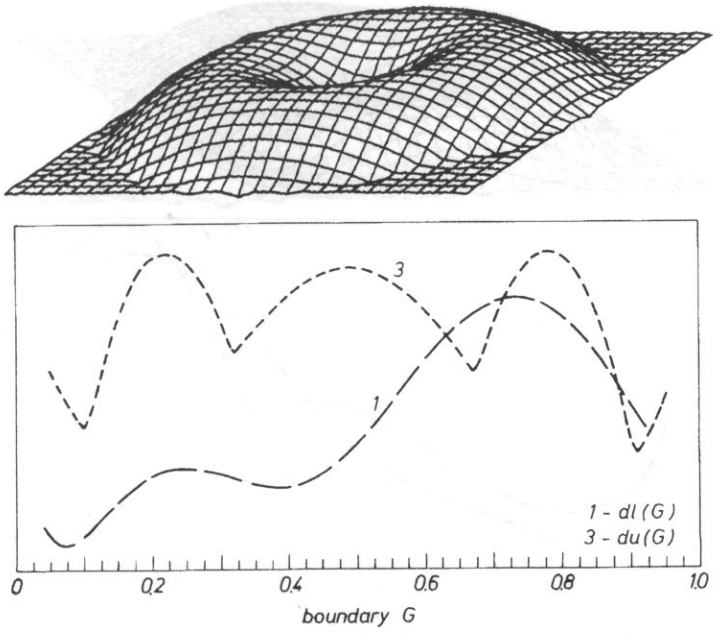

Fig. 5A. Picture of the vibrating surface $\rho_c = .5$. Plots of the mean square distance $d_{l,v}$ and relative distance $d_{u,v}$, $a=0$, $k=2.5$.

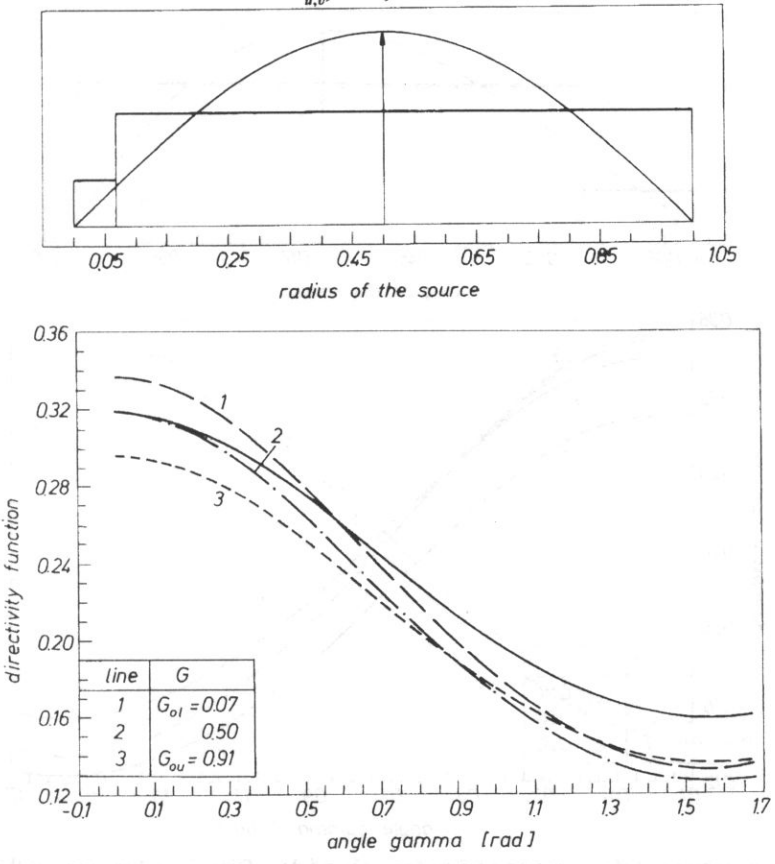

Fig. 5B. Cross-sections of the vibrating surface ($\rho_c = .5$) and M_{ol}. Directivity functions of the source, M_{ol}, M_r and M_{ou}; $a=0$, $k=2.5$.

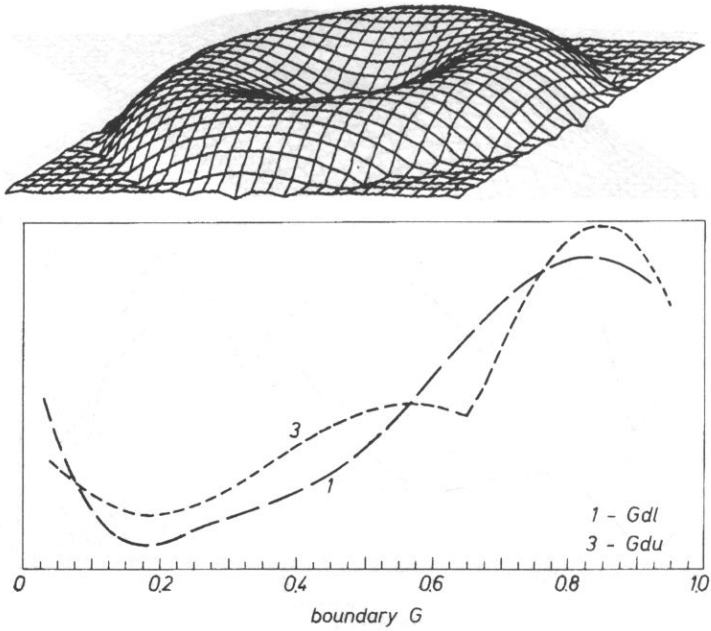

Fig. 6A. Picture of the vibrating surface $\rho_c = .6$. Plots of the mean square distance $d_{l,v}$ and relative distance $d_{u,v}$, $a=0$, $k=2.5$.

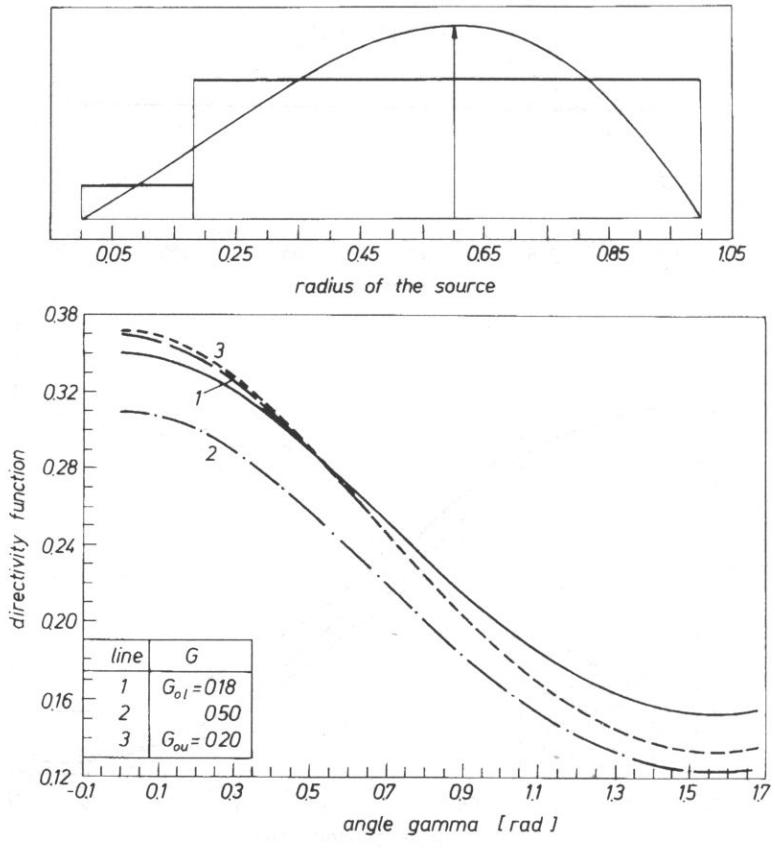

Fig. 6B. Cross-sections of the vibrating surface ($\rho_c = .6$) and M_{ol}. Directivity functions of the source, M_{ol}, M_r and M_{ou}; $a=0$, $k=2.5$.

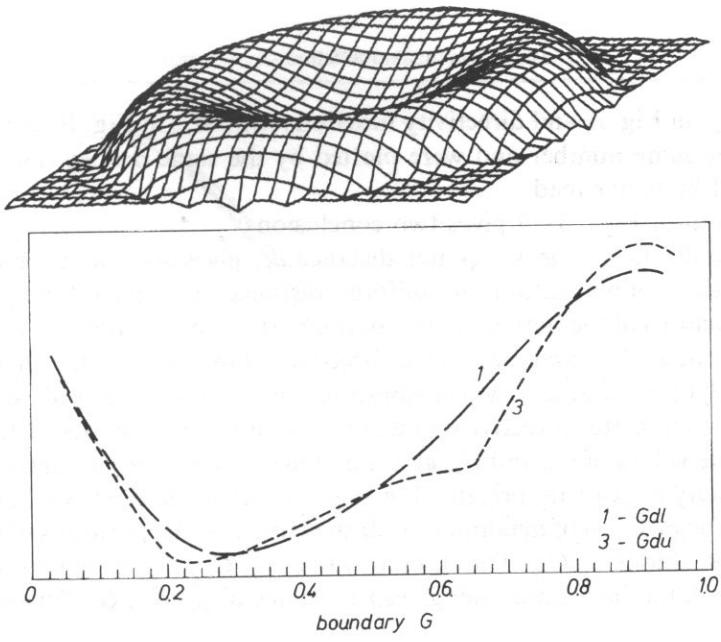

Fig. 7A. Picture of the vibrating surface $\rho_c = .7$. Plots of the mean square distance $d_{l,v}$ and relative distance $d_{u,v}$, $a = 0$, $k = 2.5$.

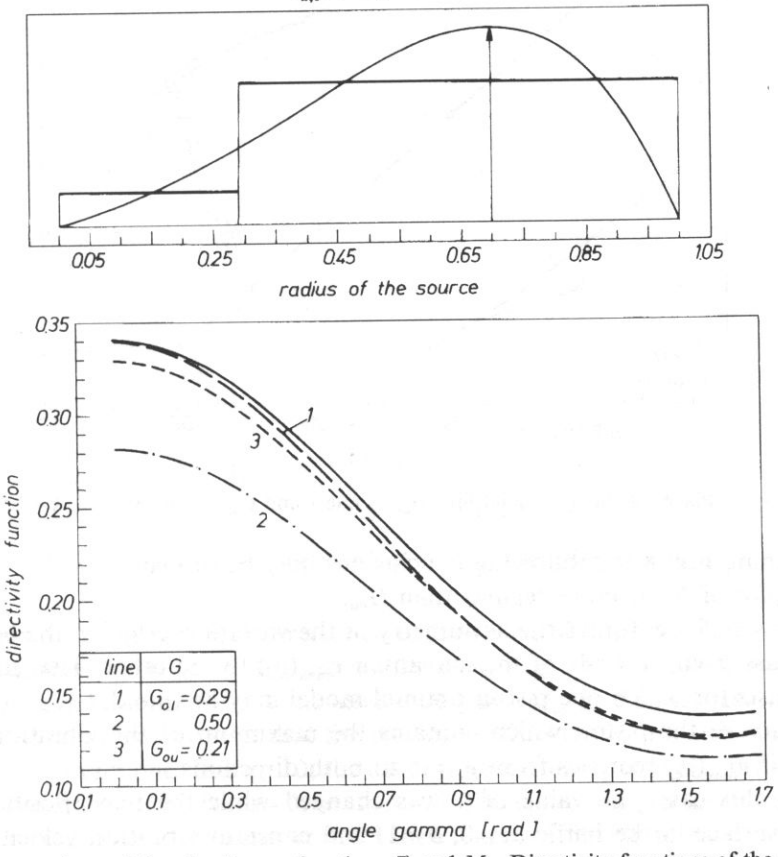

Fig. 7B. Cross-sections of the vibrating surface ($\rho_c = .7$) and M_{ol}. Directivity functions of the source, M_{ol}, M_r and M_{ou}; $a = 0$, $k = 2.5$.

Curves $d_{l,v}$, $d_{u,v}$ in Fig. A and directivity functions M_{ol}, M_{ou} in Fig. B respectively are marked by the same number and were plotted by the same dashed line so that the figures should be better read.

Examination of Figs. 3–7 gives two conclusions:

1 — optimalization of least squares distance $d_{l,v}$ gives somewhat better optimal model than the optimalization of uniform distance d_u. The difference between directivity functions of the both models is particularly seen near the axis of the source.

2 — both models, M_{ol} and M_{ou}, give directivity functions better than M_r. The exception is M_r of the source of which vibrating velocity is symmetrical, see Fig. 5 line 2, and which gives better directivity function but only near the axis of the source.

The discrete values of G_{ol} and G_{ou} as a function of the position of maximum of the vibration velocity $v_{\max}(\rho_c)$ are presented in Fig. 8 where $a=0$, $b=1$, $k=2.5$. The solid line indicates the position of maximum ρ_c, dashed line 1 — the positions of G_{ol}, dashed line 3 — the positions of G_{ou}. The discrete values ρ_c, G_{ol}, G_{ou} were marked by light points. In Fig. 8 the horizontal line gives the values of ρ_c, G_{ol}, G_{ou} for one source.

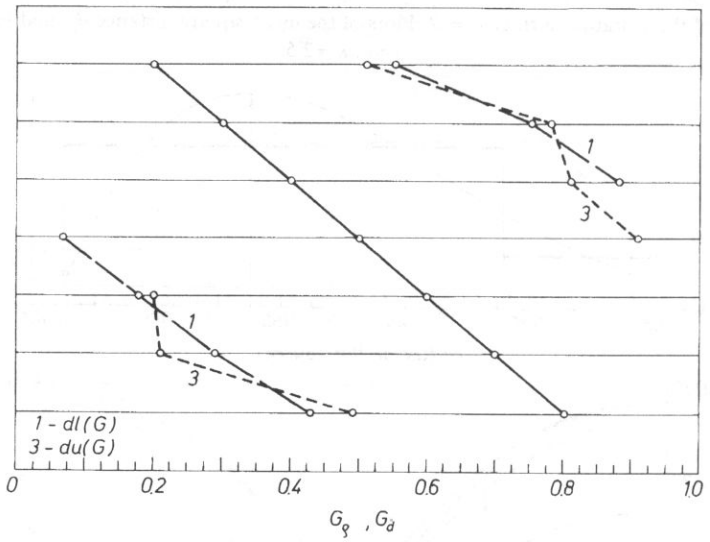

Fig. 8. Places of the ρ_c — solid line, G_{ol} — line 1 and G_{ou} — line 3; $a=0$, $k=2.5$.

Examining Fig. 8 the following conclusions may be drawn:

- the plot of G_{ol} is more regular than G_{ou},
- near $\rho_c \simeq .5$, i.e. for a little asymmetry of the vibration velocity, the boundaries G_{ol}, G_{ou} pass from one side of the maximum $v_{\max}(\rho_c)$ to the other. That means that such ρ_c exists for which one-piston optimal model may be found.
- surface of the piston which contains the maximum of the vibration velocity decreases if $v_{\max}(\rho_c)$ removes from $\rho_c=.5$ to both directions.

I.2. In this case, the value of k was changed while the fixed position of the vibrating surface in the baffle ($a=0$, $b=1$) and constant vibration velocity ($\rho_c=.3$)

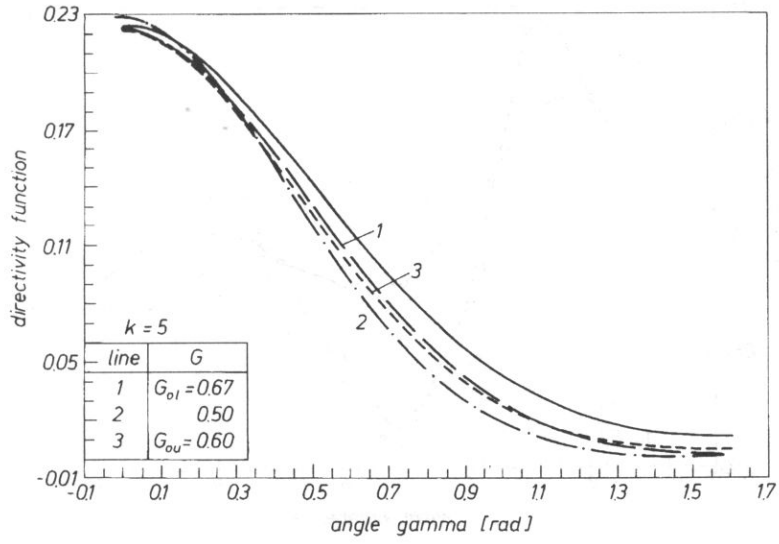

Fig. 9A. Directivity functions of the source, M_{ol}, M_r and M_{ou}; $k=5$, $a=0$, $b=1$, $\rho_c=.3$.

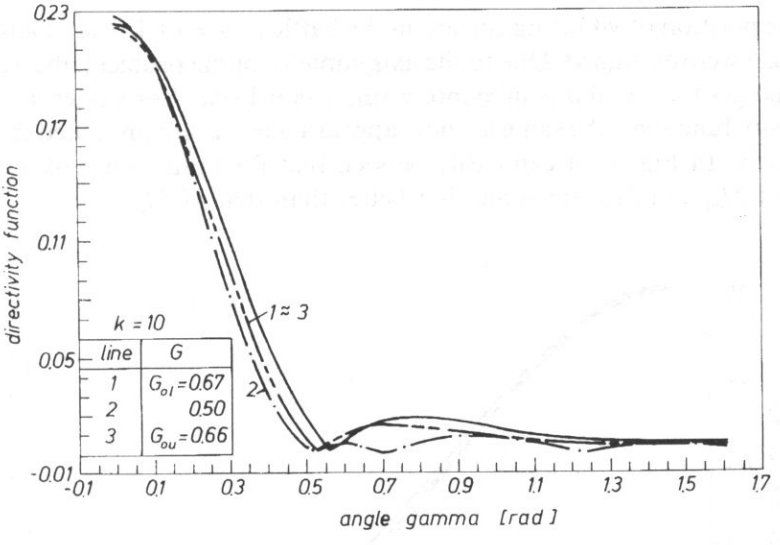

Fig. 9B. Directivity functions of the source, M_{ol}, M_r and M_{ou}; $k=10$, $a=0$, $b=1$, $\rho_c=.3$.

were assumed. The analytical directivity function (solid line) and next directivity functions of the M_r, M_{ol} and M_{ou} are displayed in Fig. 9A, B for discrete values of $k=5$, 10. As can be seen in Fig. 9 the models M_{ol} and M_{ou} give better results than M_r. In Fig. 9B, it can easily be seen that the plot of the directivity function of M_u is even other than the exact one. In Fig. 10, the discrete values of G_{ol} and G_{ou} as functions of wave number k are shown for $a=0$, $b=1$, $\rho_c=3$. The curve of G_{ol} is more regular than the curve of G_{ou}. For wave number $k>7$ these curves coincide to each other.

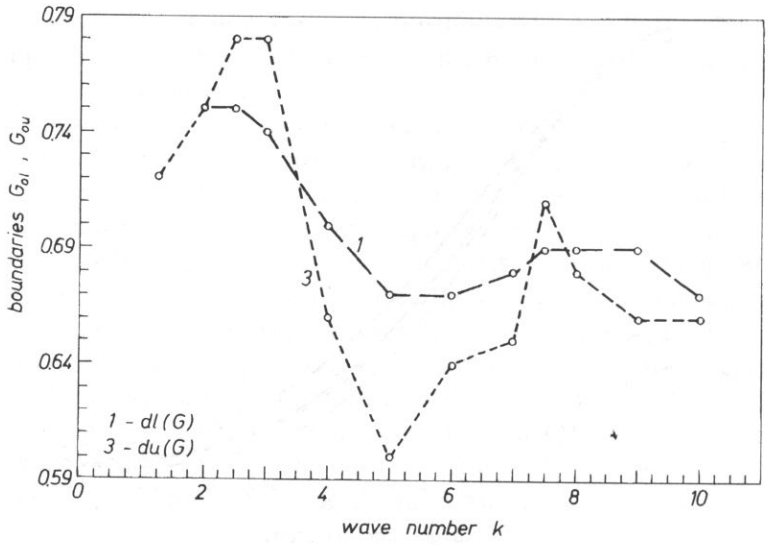

Fig. 10. Values of G_{ol} and G_{ou} as a function of wave number k; $a=0$, $\rho_c=.3$.

I.3. The position of vibrating surface in the baffle a ($b=a+1$) was changed where $\rho_c=3$, $k=2.5$ were asssumed. Due to the axisymmetry of the problem, the assumption of $a>0$ changes the circular source into a ring-shaped one. For values $a=\{0.5, 1.0\}$ the directivity functions, the same as these appearing in **I.2**, are presented in Fig. 11A, B respectively. In Fig. 11 it can easily be seen that for both values of a directivity functions of M_{ol} and M_{ou} are somewhat better than that of M_r.

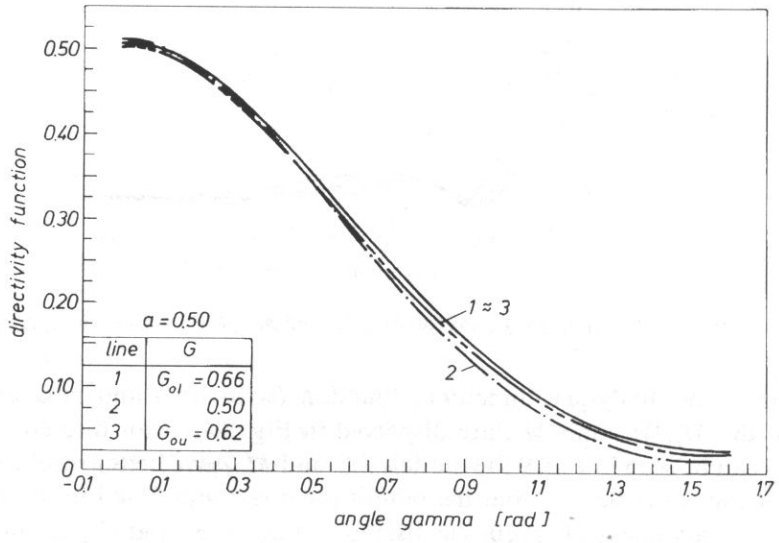

Fig. 11A. Directivity functions of the source, M_{ol}, M_r and M_{ou}; $a=.5$, $\rho_c=.3$, $k=2.5$.

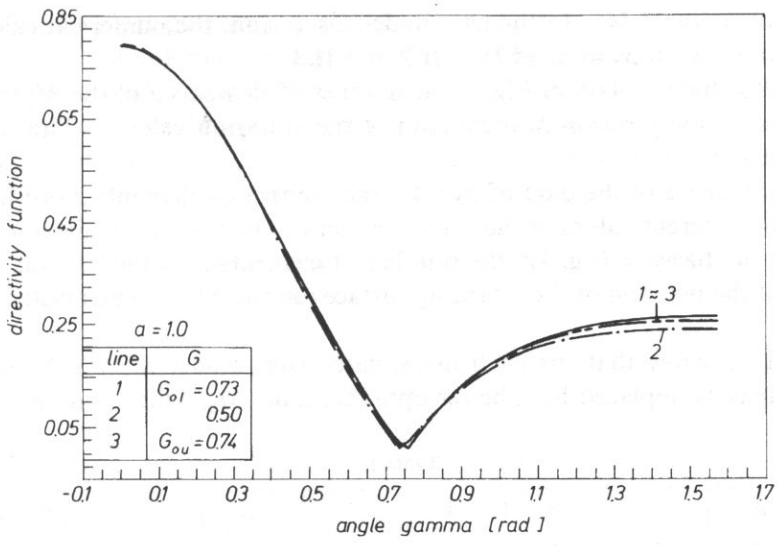

Fig. 11B. Directivity functions of the source, M_{ol}, M_r and M_{ou}; $a=1$, $\rho_c=.3$, $k=2.5$.

In Fig. 12, the discrete values of G_{ol} and G_{ou} as a function of "a" were presented. The variation of G_{ol} is more regular than that of G_{ou}.

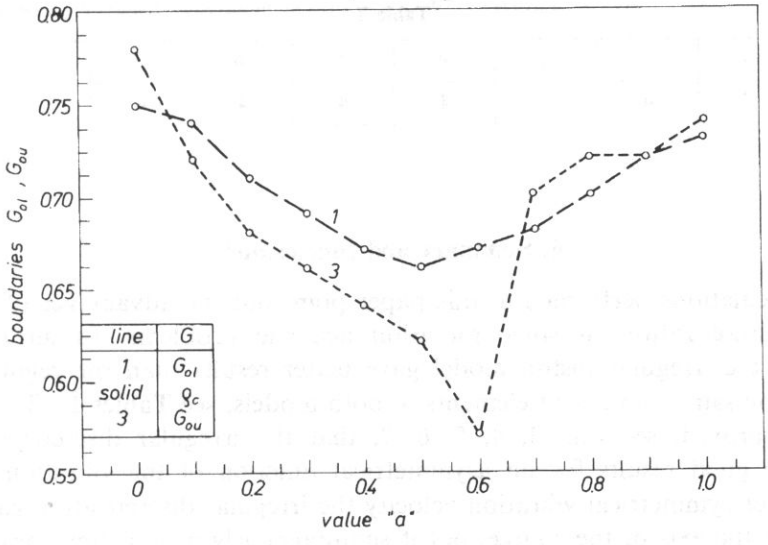

Fig. 12. Values of G_{ol} and G_{ou} as a function of a; $\rho_c=.3$, $k=2.5$.

The aim of the second part of calculations is to show that for the same number of elements M_{ol} gives better results than M_r. It was proved by giving the number of elements J of the model M_r whose directivity function is more similar to exact one

than the directivity of M_{ol}. In the case under discussion, the numerical calculations were done in three steps marked **II.1**, **II.2** and **II.3**.

II.1. On the base of data of Fig. 8, the number of elements J of the M_r was found as a function of the position of maximum of the vibration velocity. The results are given in Table 1.

II.2. On the base of the data of Fig. 10, the number of elements J of the M_r was found for the different values of the wave number k. The results are given in Table 2.

II.3. On the basis of Fig. 12, the number of elements J of the M_r was found as a function of the position of the vibrating surface ion the baffle. The results are given in Table 3.

Tables 1–3 show that for each investigated case model M_r which consists of J elements may be replaced by a better optimal model M_{ol} which contains less than J elements.

Table 1

ρ_c	.2	.3	.4	.5	.6	.7	.8
J	3	4	3	3	3	4	3

Table 2

k	2	3	4	5	6	7	8
J	4	4	3	3	3	3	3

Table 3

a	.2	.3	.4	.5	.6	.7	.8
J	4	4	4	4	4	4	4

6. Summary and conclusions

The calculations performed in this paper point out the advantages of applying irregular discretization to solve radiation acoustic problems. In all test cases considered the irregular piston model gave better results than the regular model assuming the same number of elements in both models, see Tables 1–3.

It was proved, see Fig. 3, 4, 5, 6, 7, that the irregular discretization gave particularly good results for an asymmetrical function of the vibration velocity. However, for symmetrical vibration velocity the irregular discretization gave worse results near the axis of the source, but it simultaneously gave better ones near the baffle, see Fig. 5. Thus the irregular discretization ought to be applied to the source with asymmetrical vibration velocity.

The main conclusion is that the irregular discretization ought to be applied to discretization of a source with arbitrary geometry and constant acoustic variables as well as to source with arbitrary geometry and arbitrary acoustic variables.

In the paper it was pointed out, see Fig. 8, 10, 12, that the least squares distance was a better measure of convergence/divergence between directivity functions of the model and exact one than the uniform distance. Optimalization of both measures gave quite similar optimal models. However, dependently on the vibration velocity or position of the vibrating surface in the baffle and the vibration frequency, the least squares distance which assured the optimal model was more regular than the uniform distance.

Other problem of irregular discretization of the plane sources are being investigated now. The results will be published.

References

[1] A. BJÖRCK, G. DAHLQUIST, *Numerical methods* (in Polish), PWN, Warszawa 1987.

[2] A. BRAŃSKI, *Acoustic modeling of the surface source — I; Piston model, discretizing error, axisymmetric problem.* Archives of Acoustics, **20**, 4, 321–326 (1995).

[3] A. BRAŃSKI, *Acoustical model of the plates* (in Polish), WSP, Rzeszów 1991.

[4] C.C. CHIEN, H. RAJIYAH, S.N. ATLURI, *An effective method for solving the hypersingular integral equations in 3-D acoustics.* J.A.S.A., **88**, 2, 918–935 (1990).

[5] M. TANAKA, *Some recent advances in boundary element methods,* Appl. Mech. Rev., **36**, 627–634 (1983).

[6] T.W. WU, A.F. SEYBERT, G.C. WAN, *On the numerial implementation of a Cauchy principal value integral to insure a unique solution for acoustic radiation and scattering,* J.A.S.A. **90**, 1, 554–560 (1991).

[7] W.I. ZANGWILL, *Nonlinear programming* (in Polish), WNT, Warszawa 1974.

ARCHIVES OF ACOUSTICS
20, 4, 347–359 (1995)

ACOUSTIC MODELLING OF SURFACE SOURCES
PART III. PISTON MODEL, ERROR OF THE MODEL, AXISYMMETRICAL PROBLEM

A. BRAŃSKI

Institute of Technology
Pedagogical College
35-310 Rzeszów, ul. Rejtana 16a

Two piston models of a plane axisymmetric source were compared. In the first of them, the constant vibration velocities of the elements were calculated as an integral mean value of the assumed vibration velocity. However, in the other, as arithmetic mean value of discrete values of vibration velocity. These models were compared for arbitrary discretization and for optimal one. For both models numerical experiments were carried out, first of all, as a function of the number of the discrete values of vibration velocity and the next as a function of nondimensional wave number. Numerical examples pointed out the parameters of such a source for which a "good" piston model may be built based on several discrete values of vibration velocity.

1. Introduction

During the several past years the boundary element method has been applied to various types of acoustic problems [4, 5, 6]. A considerable effort was made to develop the computational techniques in the analysis of radiation and diffraction problems. These problems, solved by the boundary element method, are closely linked to the modelling of the source. The problem of modelling itself (discretization and the methods of calculation of acoustic variables the elements) has no theoretical basis.

It seems that the first papers on modelling the acoustic surface sources problems are [1, 2, 3]; this paper is their continuation.

The first step in modelling a plane source consists is the discretization of its surface and of the vibration velocity. In the simplest model, the surface is replaced by planar elements on which constant vibration velocity is assumed. Then the plane elements of the model vibrate like pistons, and such a model of the source was called the piston model [1].

The piston model of the source with surface of an arbitrary shape and constant vibration velocity was considered in several papers, e.g. [4, 5, 6]. In such a case, only the surface of the source is discretized, and portions of the surface are replaced by planar elements. However, the vibration velocity of the planar elements remains constant.

The piston model of a source with a plane and variable vibration velocity on the surface was considered in papers [1, 2]. In the case of such a source, only the vibration velocity was discretized and it was replaced by constant values on the elements. In papers [1, 2] this constant value was as an integral mean value of the vibration velocity v^m.

The mean value is a rigorous one of an arithmetical mean value v^a of the values of function given in an infinite number of points (I-points) see Refs. [1, 2, 3]. From a practical point of view it means that in order to find the constant vibration velocity in one element of the model, it is necessary to measure the vibration velocity in an infinite number of i-points of the source (what is impossible) and next to calculate the arithmetical mean value.

The first problem of this paper is to define the minimal number of i-points necessary to calculate the v^a which differs from v^m by an assumed values. It also means that the model which has v^a on the elements differs by an assumed value from the model which has v^m on the elements. This difference was defined by analysing the divergence of the directivity functions of both models. Assuming v^m on the elements the model depends only on the discretization and not on the number of i-points. Then the divergence between the model and the source may be interpreted as the discretizing error [3], or the error of optimal piston model ($M_o^m E$) whose elements vibrate as v^m.

To find the influence of i-points on the divergence of the directivity function, an optimal piston model (M_o^m) [3] was considered. In this paper, the constant vibration velocity of the elements were calculated not as v^m but as the arithmetic mean value v^a. Thus, the error of arithmetic mean value ($v^a E$) will be added to the discretizing error. The sum of these errors was called the error of the piston model ($M^a E$); $M_o^m E + v^a E = M^a E$. The errors mentioned above were analyzed for different numbers of i-points as a function of shape vibration velocity, place of vibration surface in the baffle and dimensionless wave number.

The second problem of this paper is to find the optimal piston model in which the constant vibration velocity given on the elements depends on the number of i-points. This problem, for the constant number of elements and i-points on the element means finding the boundaries between the elements i.e. leads to optimal discretization. The divergence between the directivity function of such a model and that of the exact model depends on both the discretization and arithmetic mean vibration velocity. Thus, it is a measure of the error of optimal piston model ($M_o^a E$). Numerical calculations, assuming constant vibration velocity, concerning the second problem were made as a function of nondimensional wave number.

List of main symbols

M	piston model
$M_o(M_r)$	optimal (regular) piston model
$v^m, (v^a)$	integral (arithmetic) mean value vibration velocity

$M^m = M(v^m)$, $(M^a = M(v^a))$ piston model of which elements vibrate at $v^m(v^a)$

$v^a E$ error of arithmetic mean value vibration velocity

$M^m E$, $(M_o^m E)$ error of piston model (optimal piston model) of which elements vibrate at v^m

$M^a E$, $(M_o^a E)$ error of piston model (optimal piston model) of which elements vibrate at v^a.

2. Directivity function (DF) of axisymmetric source (AS)

The acoustic field of a circular driving surface placed in an infinite rigid baffle was considered. Assuming an axisymmetric vibrating velocity function, the axisymmetric acoustical field is obtained whose acoustic potential is given by Helmholtz – Rayleigh integral [3]. Directivity function of such an acoustic field normalized with the field of point source placed at the origin of coordinates is determined by formula [3].

$$Q_{0N}(\gamma) = \int_{\rho} v_{0N}(\rho)\, J_0(k\rho \sin\gamma)\, \rho \mathrm{d}\rho, \tag{2.1}$$

where

$$v_{0N}(\rho) = C_1 \sin(\pi\rho) \exp(-C_2\rho), \tag{2.2}$$

$v_{0N}(\rho)$ — asymmetric function of vibration velocity with regard to its zeros, C_1, C_2 — constants, they are so chosen that the function $v_{0N}(\rho)$ should fulfil assumed asymmetry, $J_0(x)$ — Bessel function of first kind and zero order, k — nondimensional wave number, ρ, ϕ, γ — spherical coordinates.

3. Directivity function of the model

3.1. Arithmetic mean value of vibration velocity (v^a)

For AS problem, the discrete data of vibration velocity given in i-points are described only by coordinates ρ_i. Arithmetic mean value of these data on j-element is defined by

$$v_j^a = \frac{1}{I} \sum_{i=1}^{I} v(\rho_i). \tag{3.1}$$

However, an integral mean value is

$$v_j^m = \frac{1}{L_j} \int_{G_{\rho 1}}^{G_{\rho 2}} v_{0n}(\rho)\, \mathrm{d}\rho, \tag{3.2}$$

where $L_j = G_{\rho 2} - G_{\rho 1}$.

The piston model of AS source is composed of sectors of the straight lines vibrating at either v^m or v^a. Directivity function of the model which consists of $j = 1, 2, \ldots, J$ elements is defined by Eq. (2.1). Substituting Eq. (3.1) or into Eq. (2.1) gives

$$Q_{0N}(\gamma)=\sum_{j=1}^{J} v_j \int_{\rho_j} J_0(k\rho \sin\gamma)\,\rho\,\delta\rho \tag{3.3}$$

where

$$v_j=\begin{cases} v_j^m \\ v_j^a \end{cases} \quad Q_{0N}(\gamma)=\begin{cases} Q_{0N}^m(\gamma) \\ Q_{0N}^a(\gamma) \end{cases}. \tag{3.4}$$

4. Modelling errors

As mentioned in the introduction, the modelling errors arise at the stage of discretization (discretization error — M^mE or M_o^mE) or at the stage of calculation of arithmetical mean value vibration velocity on the elements (error of mean value vibration velocity — v^aE). Thus, it was assumed, that if integral mean value v^m on the elements is calculated then the error v^aE is equal to zero.

The deviation between exact directivity function and the model is the result of modelling errors. There are a lot of measures of this deviation. In practice two of them are applied:

- least squares distance: $d_l(...)$
- uniform distance; $d_u(...)$

where $d_l(...)$, $d_u(...)$ are functions of the number of elements (J) and of the boundaries among the elements (G_1, G_2,...). In this paper, the analysis of modelling errors is based on the investigation of $d_l(...)$. A general definition of least squares distance of function $f(x)$ from $g(x)$ is given by formula [3].

$$d_l(f(x),g(x))=d_l(...)=\left\{\int_{x_1}^{x_2}[f(x)-g(x)]^2\,dx\right\}^{1/2}, \tag{4.1}$$

where x_1, x_2 — boundaries of integration.

In Ref. [3] it was pointed out that minimization of $d_l(...)$ belongs to optimalization problems. In the paper minimization of $d_l(...)$ is taken as a condition for obtaining an optimal piston model (M_o^m). The directivity of M_o^m assures the best convergence with the exact directivity in the least squares distance sence.

4.1. Discretizating error (M^mE)

Let the elements of the model vibrate at constant velocities which are calculated as v_j^m, Eq. (3.2); to simplify, the index "j" will be dropped out. If the directivity function of the model Q^m is compared to exact directivity function Q, then

$$M^mE=\rho(Q^m,Q), \tag{4.2}$$

where $Q^m=Q^m(J, G_1,...)$.

Because v^m does not depend on the number of i-points, then only discretization leads to M^mE.

The error M^mE may be reduced by

• more refined regular discretization; the number of j-elements (of the same shape and dimension) is increased [1],

• irregular discretization; the number of j-elements is constant but their shape and dimension are changed [2, 3].

Minimization of $d_t(Q^m,Q)$ leads to an optimal piston model M_o^m for which the discretizating error is marked as M_o^mE.

4.2. Error of mean value vibration velocity (v^aE)

Let elements of the model vibrate with the constant velocity calculated as v^a, Eq. (3.1). If the directivity function Q^a of such a model is compared to directivity Q^m (in both models the same discretization is assumed) then

$$v^aE=d_t(Q^a,Q^m) \tag{4.3}$$

where $Q^a=Q^a(J, G_1,...)$.

The error v^aE may be reduced by:

• increase the number of i-points on the element (which are regularly located on it). To investigate the effect of the number of i-points on the error v^aE and, consequently, on M^aE, is the main object of this paper.

• irregular location of i-points on the element assuming the constant number of these points. Here, this possibility will not be investigated.

Note that for constant discretization, i.e., for a constant number and size of the elements, $v^aE(i=\infty)=M^aE$.

4.3. Error of the piston model (M^aE)

Let elements of the model vibrate with a constant velocity v^a If the directivity function Q^a is compared to the exact one, then

$$M^aE=\rho(Q^a,Q). \tag{4.4}$$

It can be seen that the error M^aE depends on the discretization and on the number of i-points to be taken to calculate the constant vibration velocities of the elements.

It should be noted that each of the mentioned errors may be expressed by the other two

$$M^aE=v^aE+M^mE. \tag{4.5}$$

5. Numerical calculations

The error M^aE has already been discussed throughly in paper [3]. A model was found for which $d_t(J=2,G)$ takes the minimum. This model was called the optimal model (M_o^m).

In the first part of numerical calculations, based on M_o^m, two errors are evaluated, i.e. M^aE and v^aE of the model M^a. In order to find the influence of the number of i-points on the model, assuming constant G_o^m of the model M_o^m, the errors M^aE and v^aE of the model M^a were analyzed. The values of these errors are given for several i-points as a function of:

1 — asymmetry of vibration velocity; $\rho_c \in \langle .2,.8\rangle$, $a=0$, $k=2.5$ where ρ_c — place of the extremum of vibration velocity, a, b — inner, outer radius of driving AS surface ($b=a+1$).

2 — place of the driving surface in the baffle; $=3$, $a \in \langle .1, 1\rangle$, $k=2.5$,

3 — nondimensional wave number; $\rho_c=3$, $a=0$, $k \in \langle 1, 10\rangle$.

The results are presented in Figs. 1, 2 and 3 respectively. The Figures consist of three parts part (a) shows the picture of vibration velocity, (b) cross-section of vibration velocity and c error of the model M^aE, (v^aE).

Because of Eq. (4.5) the calculations concern only M^aE error. The error v^aE may be read from Figs. 1–3 as a difference of ordinates M^aE and M^mE. In Figs. 1–3 based on Ref. [3], M^mE is plotted by a solid line. However, error M^aE, for different number of i-points is plotted by dashed lines.

Regardless of the number of i-points assumed on one element, the following conclusions may be noted:

Fig. 1: for $\rho_c \cong 0$ the least error M^aE is obtained. Next, the better model can be obtained for $i=3$ rather than for $i=\infty$ ($\rho_c=0$ gives AS source whose maximum of vibration velocity is at z-axis,

Fig. 2: the error M^aE increases as an annular driving surface with a constant width retreats from the z-axis,

Fig. 3: the error v^aE decreases with the increasing nondimensional wave number k. To verify the last conclusion for a larger range of k, in Fig. 3 the value M^aE was given for $k=20$.

Numerical calculations show, that for $i=15$ the relative error

$$v^aE=\frac{|M^aE(i=15)-M^aE(i=\infty)|}{M^aE(i=\infty)}\cdot 100\% \tag{4.6}$$

is equal to 37.5% for $k=10$ and 34.2% for $k=20$.

Table 1. Boundary G_o^a of M_o^a versus the number of i-points and the shape of vibration velocity (ρ_c)

ρ_c \ "i"	3	5	7	9	11	13	15	31	∞
.0	.61	.57	.56	.56	.56	.56	.55	.55	.55
.2	.41	.44	.72	.67	.64	.62	.61	.57	.55
.3	.37	.41	.43	.85	.84	.83	.82	.78	.75
.5	.45	.35	.29	.24	.21	.19	.17	.11	.07
.7	.65	.54	.45	.41	.39	.37	.36	.32	.29
.8	.76	.68	.59	.53	.51	.49	.48	.45	.43

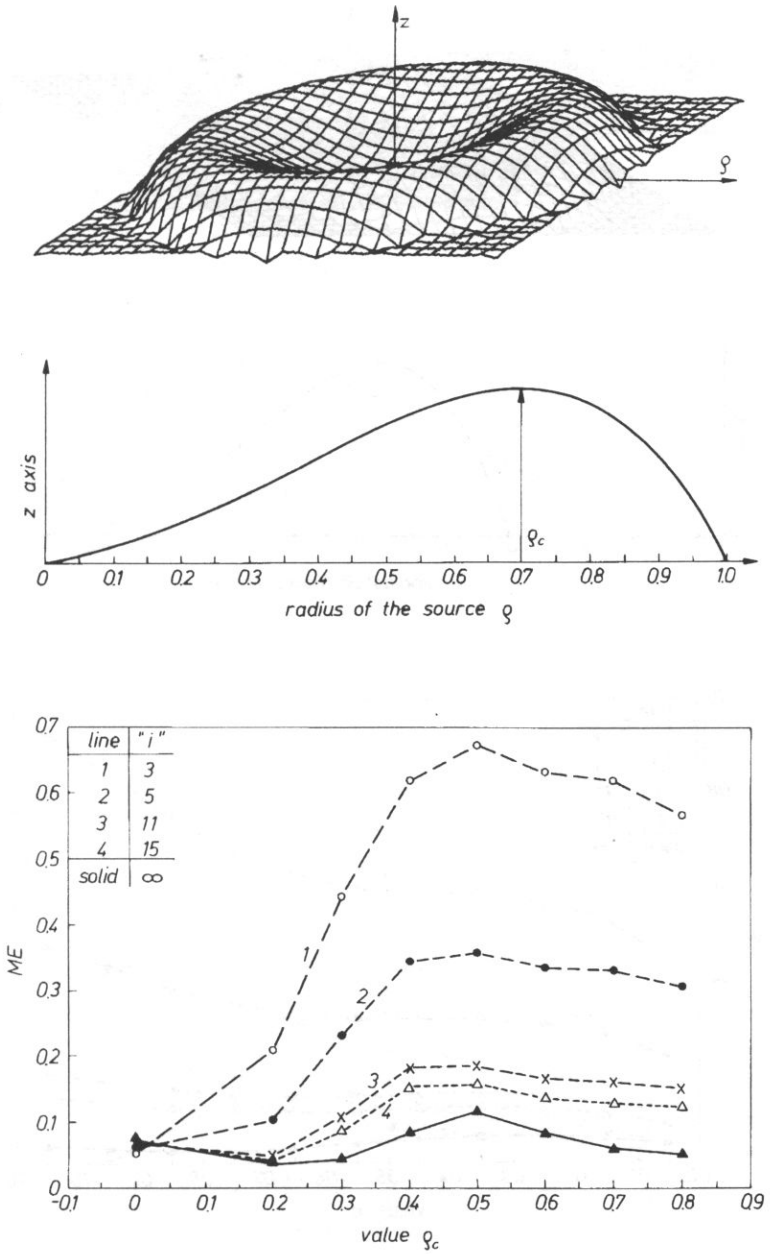

Fig. 1. (a) Picture of the driving surface, (b) Cross-section of the driving surface, (c) Model error (ME) versus the shape of vibration velocity (ρ_c).

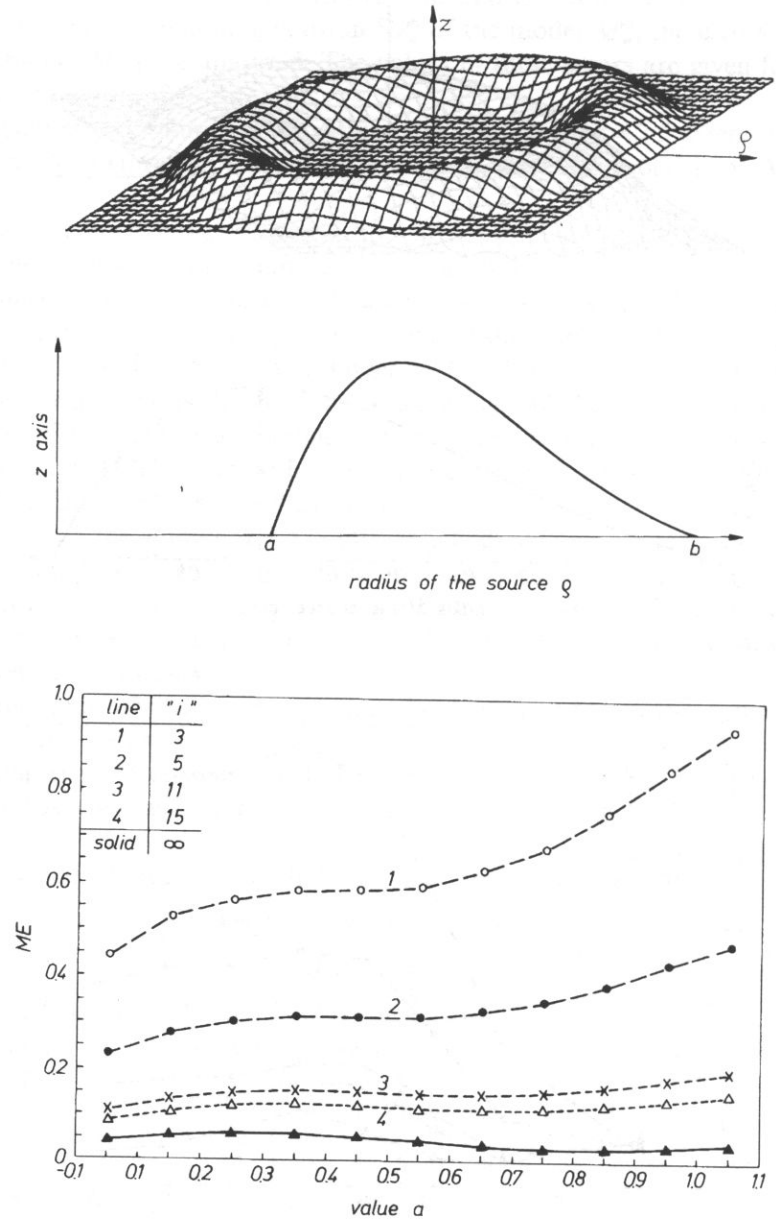

Fig. 2. (a) Picture of the driving surface, (b) Cross-section of the driving surface, (c) Model error (ME) versus a place (value „a") of the driving surface in the baffle.

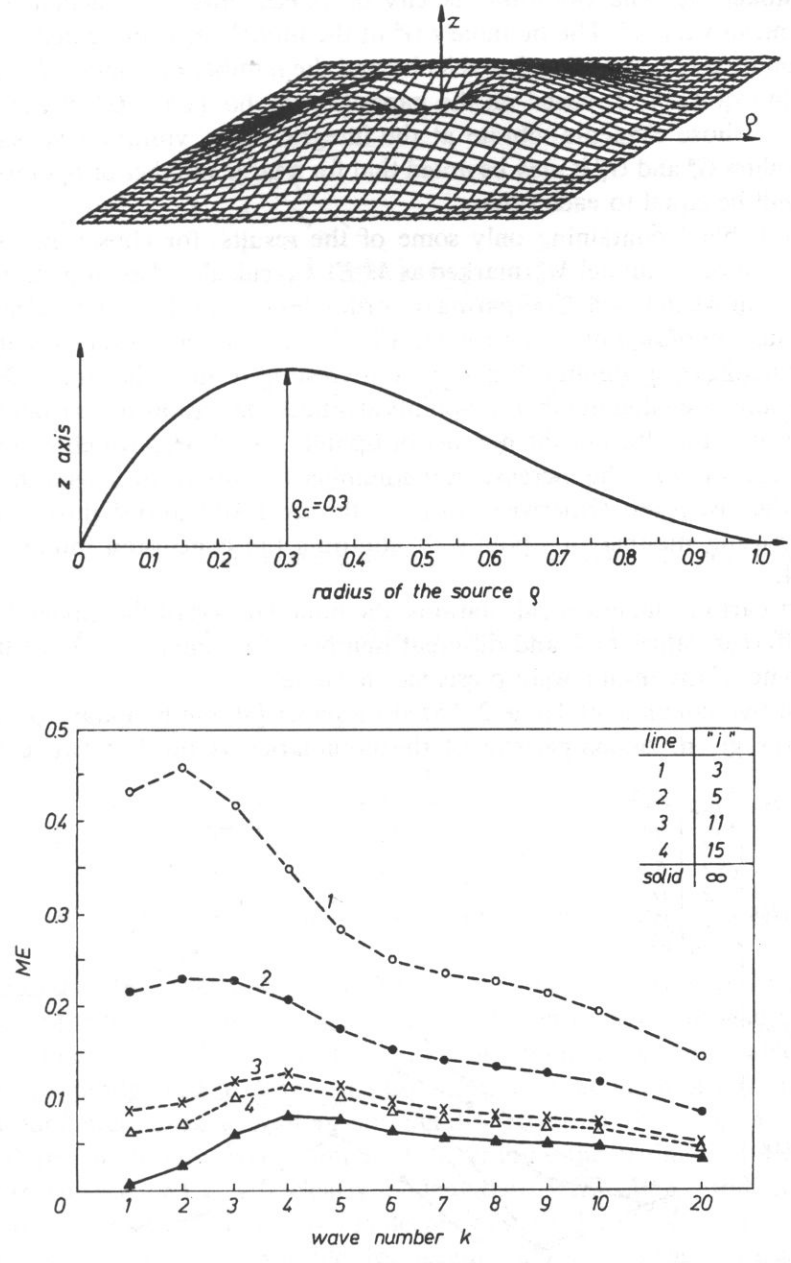

Fig. 3. (a) Picture of the driving surface, (b) Cross-section of the driving surface, (c) Model error (ME) versus the nondimensional wave number (k).

The second part of the numerical calculations is concerned with an optimal two-piston model M_o^a. The vibration velocity of its elements was calculated as an arithmetical mean value v^a. The boundary G^a of the model M_o^a is presented in Table 1 as a function of assymetry vibration velocity and the number of i-points, $k=2.5$. In the last column of Table 1, based on the paper [3], the boundary G_o^m of the model M_o^m was given whose elements vibrate at the integral mean vibration velocity v^m. Comparing values G_o^a and G_o^m it may be noted that for a large number of i-points these boundaries will be equal to each other.

Based on Table 1 containing only some of the results, for chosen number of i-points, the error of the model M_o^a (marked as M_o^aE) was calculated as a function of ρ_c. The results are shown in Fig. 4. Comparing the ordinates in Figs. 1 and 4 it is clear that, for the same number of i-points, the error M_o^a (Fig. 4) is considerably smaller than M^aE (Fig. 1). Furthermore, examining Fig. 4, it is interesting to note that for $\rho_c \cong 0$ the best results assures a smaller number of i-points identical conclusion arises from Fig. 1.

Figure 5 shows the effect of the number of i-points on the M_o^aE for chosen values ρ_c. This figure shows that the increase in the number of i-points decreases the error M_o^aE only in the case $\rho_c \neq 0$. Otherwise, for $\rho_c=0$ the error M_o^aE also slightly increases with the increasing number of i-points. It confirms the conclusion implied from Figs. 1 and 4.

In the last part of numerical calculations, the boundary G_o^a of the model M_o^a was found for different values of k and different number of i-points ($\rho_c=.3$, $a=0$ were assumed). Some of the results were presented in Table 2.

In the last two columns of Table 2, based on paper [3], the boundary G_o^m of the model M_o^m was given. A comparison of the boundaries at the last two columns

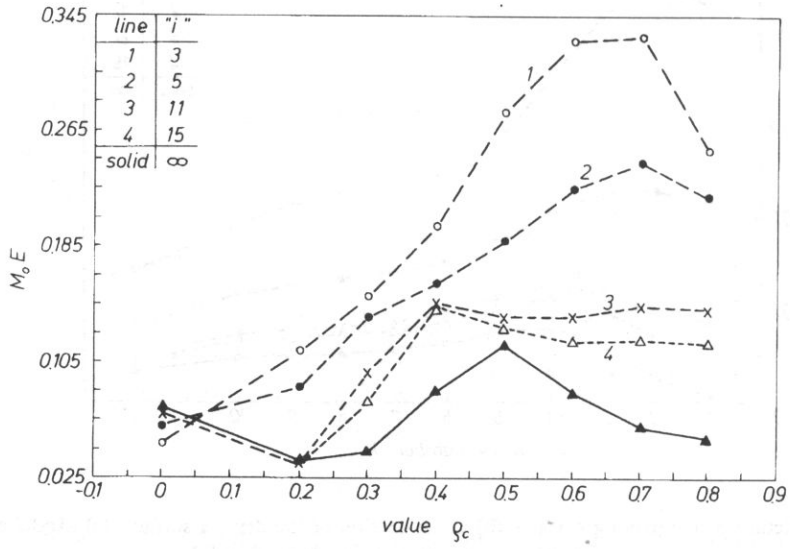

Fig. 4. Error of the optimal piston model (M_oE) versus the shape of vibration velocity (ρ_c)

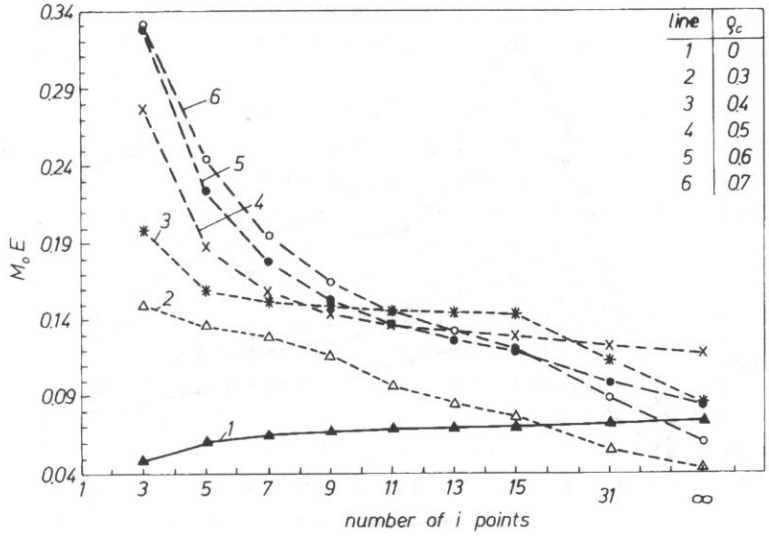

Fig. 5. Error of the optimal piston model (M_oE) versus the number of i-points

Table 2. Boundary G_o^a of M_o^a versus the number of i-points and the nondimensional wave number (k)

k \ "i"	3	5	7	9	11	13	15	31	∞
1	.44	.46	.47	.48	.86	.84	.82	.76	.71
2	.39	.41	.43	.44	.88	.86	.84	.79	.75
5	.41	.56	.63	.65	.68	.67	.67	.67	.67
9	.43	.49	.50	.52	.69	.69	.69	.69	.69
10	.43	.50	.53	.67	.68	.68	.68	.68	.68

indicates that, for lower values of k, the covergence between G_o^a and G_o^m is rather weak. However for higher values of k, several i-points on the element lead to $G_o^a = G_o^m$.

For boundaries G_o^a and chosen values of i-points, given in Table 2, the error $M_o^a(v_o^a E)$ is plotted in Fig. 6 as a function of k; note the jump of k from 10 to 20. To point out better advantages of an optimal discretization, the errors M^aE (depicted in Fig. 3) and M_o^a (Fig. 6) were compared. Examining the ordinates in the two figures, for particular k and i, it is clearly evident that $M_o^aE < M^aE$. Both M_o^aE and M^aE decrease if k increases, but only M_o^a decreases if $k<4$.

In the last numerical example, for several values of k, the error M_o^a, (v_o^a E) was investigated as a function of the number of i-points. Figure 7 shows the results; note the jump of i-points from 15 to 31 and from 31 to ∞. Examination of the data shows that the increase in the number of i-points ensures the decrease in the error M_o^aE but the decrease is little for a big number of i-points.

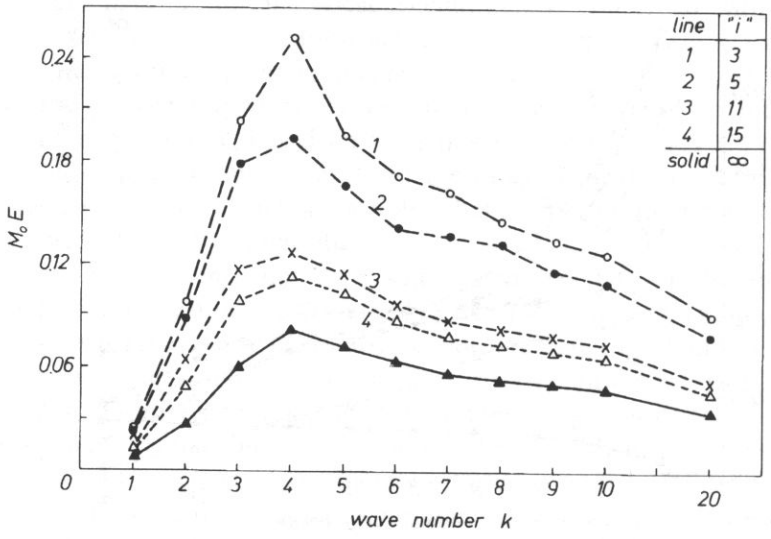

Fig. 6. Error of the optimal piston model (M_0E) versus the nondimensional wave number (k)

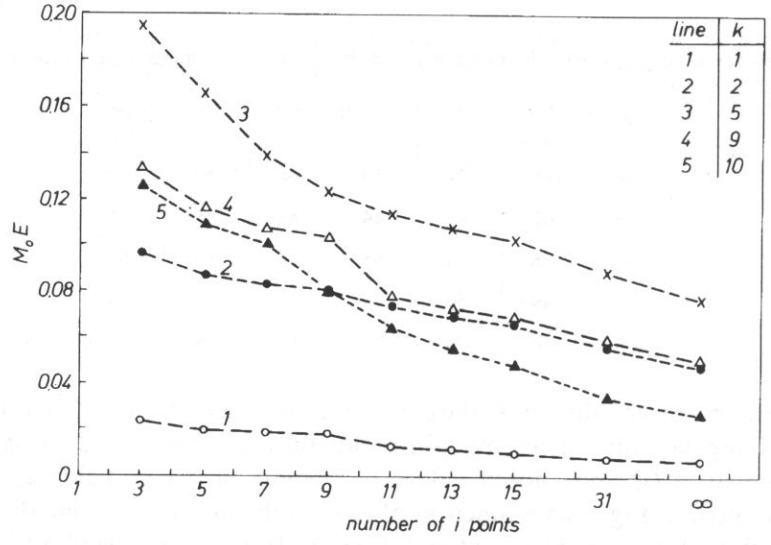

Fig. 7. Error of the optimal piston model (M_0E) versus the number of i-points

Conclusions

From the example performed in the first part of the numerical calculations it follows that, for arbitrary discretization, the error of vibration velocity v^aE decreases if the number of i-points increases (Figs. 1, 2, 3). This conclusion is not right if the

maximum of vibration velocity is in the axis of the source ($\rho_c = 0$). In this case, the smaller number of i-points on the element rather than greater one may be used to build a better model; Fig. 4.

In the second part of the numerical calculation, first of all the boundaries G_o^a of the model M_o^a were looked for. Considerations show that G_o^a depends on the number of i-points on the element, nondimensional wave number k and on the shape of the vibration velocity function. It was proved, quite similarly as in the first part, that $v_o^a E$ decreases if the number of i-points increases except the case when $\rho_c = 0$; Fig. 5.

Furthermore, in the third part of the numerical calculation, it was pointed out (Fig. 6) that, for low and high values of nondimensional wave number, several i-points on the element are necessary to build a good piston model.

The numerical examples show that, for axisymmetric vibration velocity of the plane source and for high wave number k, the good piston model may be build based on several (but not arbitrary) known values of vibration velocity in i-points. The last conclusion is confirmed by the fact that in all the investigated cases an optimal piston model assured better results than the regular one.

References

[1] A. BRAŃSKI, *Acoustical model of the plates*, (in Polish), WSP, Rzeszów 1991.

[2] A. BRAŃSKI, *Acoustical modelling of the surface sources, Part I. Piston model, discretizing error, axisymmetrical problem*, Archives of Acoustics, **20**, 4, 327–345 (1995).

[3] A. BRAŃSKI, *Acoustical modelling of the surface sources, Part II. Piston model, axisymmetrical function of vibration velocity, discretizing error, axisymmetrical problem*, Archives of Acoustics, **20**, 4, 311–326 (1995).

[4] Y. FURUE, *Calcualtion of sound diffraction by means of the integral equation*, The Second Joint Meeting of ASA and ASJ, (1988), private communication.

[5] W.L. MEYER, W.A. BELL, B.T. ZINN, *Boundary integral solutoin of three dimensional acoustic radiation problems*. J. Sound Vib., **59**, 2, 245–262 (1978).

[6] T. TERAI, *On calculation of sound fields around three dimensional object by integral equation methods*, J.S.V., **69**, 1, 71–100 (1980).

ARCHIVES OF ACOUSTICS
20, 4, 361–372 (1995)

RADIATION OF PIEZOELECTRIC RINGS INTO THE AIR THROUGH CYLINDRICAL WAVEGUIDES

W. PAJEWSKI, P. KIEŁCZYŃSKI and M. SZALEWSKI

Institute of Fundamental Technological Research
Polish Academy of Sciences
(00-049 Warszawa, Świętokrzyska 21)

In the paper the results of the investigations of the radiation of piezoelectric rings into the air through solid (e.g. glass, plexiglass, aluminium) cylinders are presented. The obtained radiation patterns approximate Bessel distribution. In the case of short cylinders the vibrations are more complicated, one obtains zero-order Bessel function with several zero-crossings. For long cylinders Bessel function is truncated, the quantity of sidelobes is reduced. The obtained results show that the configurations: piezoelectric ring–cylinder can be applied as ultrasonic transducers with narrow beam with limited diffraction in certain range. The additional advantage of this construction is the increase of vibration amplitude on the transducer axis, the disadvantage — small frequency bandwidth.

1. Introduction

Ultrasonic transducers with limited diffraction beams are an improvement in the field of object and environment recognition, in nondestructive testing and in medical imaging. They are competitive in relation to the focusing transducers. Complicated focus shift is necessary during the work of focusing transducers because the energy concentration occurs in the definite distance from the transducer. Increased depth of field can be obtained using arrays with dynamically focused transmission [11] or axicon transducers [3]. An acoustic beam with limited diffraction can be obtained using a transducer with Bessel distribution of vibrations on its surface. However such a beam has limited range and high sidelobes.

Large literature exists (e.g. [4, 11, 16]) concerning transducers with limited diffraction beams (Bessel beams or X waves) but still their theory is not complet. Durnin's theory [5] concerns in principle unlimited Bessel distribution of vibration. Its application to the ultrasonic waves requires to introduce truncated Bessel functions because apertures used in practice are finite. The important problem is also the way of sidelobes reduction [11]. It is necessary to analyze more precisely the near and far field and the influence of distribution disturbances in the form of additional functions.

The application of more general methods of calculations of radiation characteristics for transducers with nonuniform vibration distribution on the surface leads to the statement of differences in shapes of characteristics. These differences are caused by deviations from ideal Bessel distribution. To this end the transfer function method, developed by the authors, is very useful [8, 9].

The aim of this work is to apply the natural vibration distributions, which approximate Bessel distribution, to transducer constructions. It is known that the deformations occurring during the resonant vibrations of rings, membranes and cylinders can be described by combinations of Bessel functions. On the ground of the analysis of the theoretical works connecting the vibrations of rings and cylinders, e.g. [1, 13, 14], one can presume that certain modes of these vibrations can be used as a source of acoustic waves.

2. Ring radiation to a solid medium

2.1. Narrow ring ($R \gg \lambda$, $a_2 - a_1 < \lambda$)

A narrow ring with uniform amplitude of vibration in the axis direction gives an acoustic field with the pressure distribution described by zero-order Bessel function:

$$\frac{p}{p_0} = J_0\left(\frac{2\pi R}{\lambda}\sin\theta\right), \tag{2.1}$$

where: R — ring radius, λ — wavelength in the acoustic medium, θ — radiation directivity angle.

To satisfy the condition $R \gg \lambda$ for a solid medium is more difficult than for a gaseous medium. It requires to use the ring with large diameter or high frequency. Therefore the application of a ring to the generation of acoustic field with Bessel distribution is advantageous in megahertz frequency range. In this case the interference near field occurs in the form of two lobes, which in the certain distance transform in one central lobe and several sidelobes, in accordance with above mentioned formula.

2.2. Wide ring

For a wide ring the situation is more complicated. The uniform distribution of vibration amplitude on the surface leads to a complicated structure of acoustic field. This structure is more complicated than for the distributions described by Gauss function or truncated Bessel function.

In the literature one can find the approximation formulae for the calculation of acoustic field of a wide ring with uniform distribution of vibration amplitude. These formulae contain higher order Bessel functions [2]:

$$\frac{p}{p_0}=(a_2^2-a_1^2)^{-1}\left|a_2^1\frac{2J_1(x_2)}{x_2}-a_1^2\frac{2J_1(x_1)}{x_1}\right| \tag{2.2}$$

where: a_1 — inner radius of a ring, a_2 — outer radius of a ring, $x_1 = a_1 k\sin\theta$, $x_2=a_2 k\sin\theta$, $k=2\pi/\lambda$.

Besides the analytic formula one can use the transfer function method [8] for calculations of acoustic fields with optional parameters.

Figure 1 presents the acoustic field profile in the polystyrene at the distance 5 cm from the ring, calculated using transfer function method and the formula (2.2). The difference is not large, transfer function method gives more exact results. As can be seen the acoustic field distribution at this distance corresponds to Bessel function.

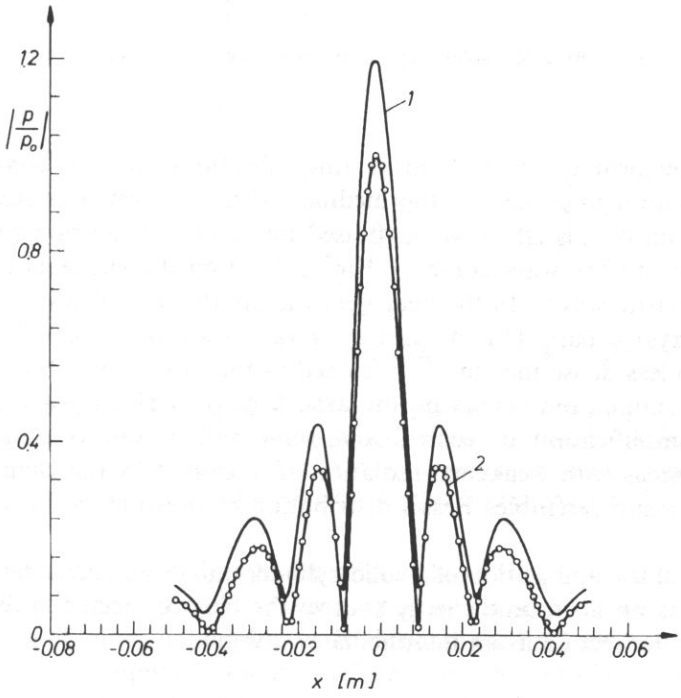

Fig. 1. Acoustic field in polystyrene at the distance 5 cm from the vibrating ring. 1) calculated using transfer function method, 2) calculated using analytical formula (2.2).

The application of piezoceramic ring for acoustic wave generation in gaseous media is not efficient owing to strong mismatching of the acoustic impedances. One can reduce impedance mismatching and increase ultrasonic energy transmission into the air using transducers consisting of one or some rings of piezoelectric ceramic embedded in plastic material [10]. The other method is to use an intermediate element in the form of a cylinder made of e.g. glass, plexiglass, aluminium. Such a cylinder

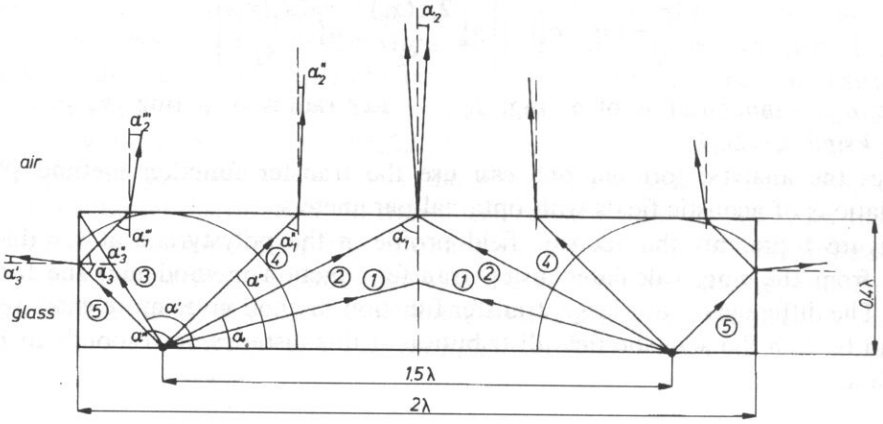

Fig. 2. Influence of an intermediate solid plate on the convergence of acoustic wave beam in the air.

permits to transform the amplitude of ring vibrations. It also concentrates the ultrasonic radiation into the air, the medium with very low acoustic impedance. For the depiction of this effect we have used the model of the ring with the width small in relation to the wavelength — Fig. 2, treating the elements of the ring as a source of acoustic waves. In the near field the interference of waves (presented in the form of rays) occurs. On the surface a ray going out from the more dense medium to the less dense medium is refracted in the direction of the configuration axis. The rays summation occurs on the axis. Finally after the wave transit of the cylinder the amplification of central and some side beams is obtained. Simultaneously the areas with weakened radiation arise caused by the change of the ray phase. Such a result resembles Bessel distribution of pressure in the vicinity of the cylinder surface.

In the case of the application of a solid cylinder one should consider two variants of its activity as an ultrasonic energy source: the first connected with its resonant vibrations and the second as an intermediate waveguide.

3. Resonant vibrations of cylinders with finite dimensions as a source of acoustic waves

The question of vibrations of cylinders with finite dimensions was the subject of many theoretical [6, 7, 15] and experimental [12, 17] works. However the problem has not been solved analytically in the general case because of the complicated boundary conditions. There are the solutions of the particular cases — the long rod or the thin plate. The other cases lead to the complicated equations which can be solved numerically. In these cases many modes exist. Only some modes have practical value and can be applied for ultrasonic energy radiation.

4. Vibrations of configurations: piezoelectric ring—cylinder

In ultrasonic transducers a metal cylinder is used as a constituent element with a piezoelectric plate or ring. The piezoelectric element excites resonant vibrations with large amplitude, which are the source of radiation. One could suppose that the strongest ultrasonic effects can be obtained in the case of resonant vibrations of the cylinder. However, as experiments indicate, the strongest ultrasonic effects are obtained in the case of resonant vibrations connected with the piezoelectric element — Fig. 3. In this case the cylinder is a waveguide which transmits the vibrations of the

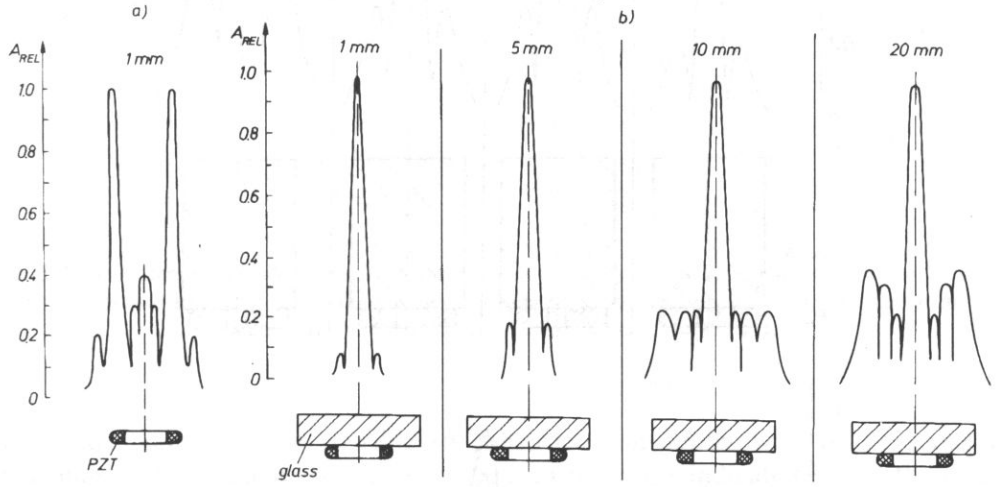

Fig. 3. Acoustic field of the ring radiating into the air. a) free ring ($\phi_{ext}=23$ mm, $\phi_{int}=14{,}5$ mm), distance 1 mm; b) ring connected with cylindrical waveguide ($\phi=40$ mm, $l=10$ mm), distances from the cylinder surface: 1 mm, 5 mm, 10 mm, 20 mm. $f=342$ kHz. Acoustic pressure measured on the transducer axis: a) 116 hPa, b) 500 hPa, 300 hPa, 180 hPa, 165 hPa, respectively.

piezoelectric element. According to the rules of wave transmission from one medium to the other one, for suitable relation of acoustic impedances one obtains the transformation of vibration amplitude. In this case the field generated in the cylinder and the vibration amplitude on its surface play an essential part. According to formula (2.1) or (2.2) the distribution of stress inside a cylinder with large diameter is described by Bessel function — formula (2.1) or by the sum of Bessel functions — formula (2.2) for a wide ring. The distribution of vibration amplitude on the cylinder surface corresponds to this stress distribution. The vibrations on the cylinder surface are the source of ultrasound in a gaseous medium. The pressure measured in the vicinity of vibrating cylinder surface has the profile which approximates the distribution described by Bessel function — Fig. 4. In this way it is possible to realize the transducer with Bessel distribution of vibration amplitude using a piezoelectric ring and a solid cylinder. The vibrations with such amplitude distribution can be applied for generation of nondiffracting acoustic beam in the air. Using different

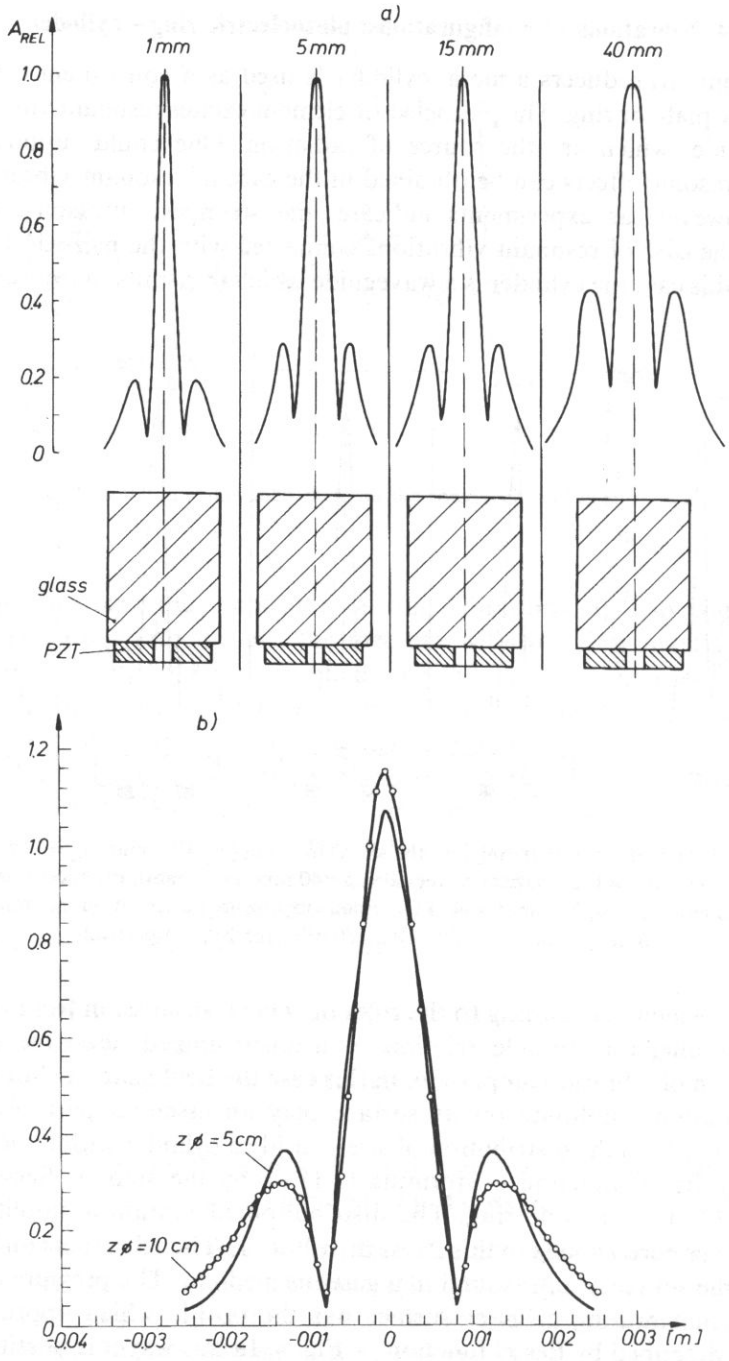

Fig. 4. Acoustic field generated in the air by vibrating piezoelectric ring ($\phi_{ext}=26$ mm, $\phi_{int}=5$ mm) with cylindrical waveguide ($\phi=30$ mm, $l=40$ mm) at different distances from the cylinder surface, $f=206$ kHz. a) measured using acoustic probe, b) calculated for truncated Bessel function distribution.

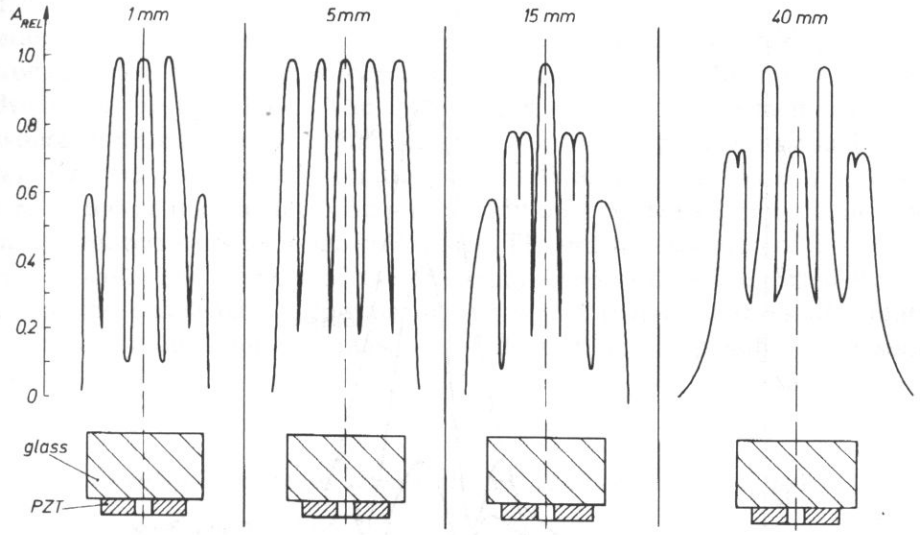

Fig. 5. Distribution of acoustic pressure in the air in the vicinity of cylindrical waveguide ($\phi = 35$ mm, $l = 20$ mm) excited to vibrations by the piezoelectric ring ($\phi_{ext} = 26$ mm, $\phi_{int} = 5$ mm), distances from the cylinder surface: 1 mm, 5 mm, 15 mm, 40 mm; $f = 195$ kHz.

waveguide materials it is possible to construct transducers with better acoustic matching to the medium. However as the measurements indicate (Fig. 5) there are vibration amplitude distributions on the waveguide surface different from zero-order Bessel function. This causes the deformation of the directivity patterns and the increase of the beam diffraction.

5. Influences of additional Bessel and Gauss functions on the directivity characteristics

Applying the transfer function method we have made a series of computer simulations for the examination of effects which occur when the distribution of vibration amplitude differs from Bessel function. The calculations have shown that the presence of additional functions in the vibration distribution on the cylinder surface has the unfavourable influence. It causes the beam broadening and the limitation of the nondiffracting beam range. The results indicate that the elimination of these disturbing functions is necessary. The search of ways of their limitation is important but difficult.

As an example the results of calculations are presented in Fig. 6 for Bessel distribution $J_0(\alpha r)$, Gauss distribution $\exp[-(r/b)^2]$ and the product $\exp[-(r/b)^2] \cdot J_0(\alpha r)$. The results indicate that the presence of Gauss function is

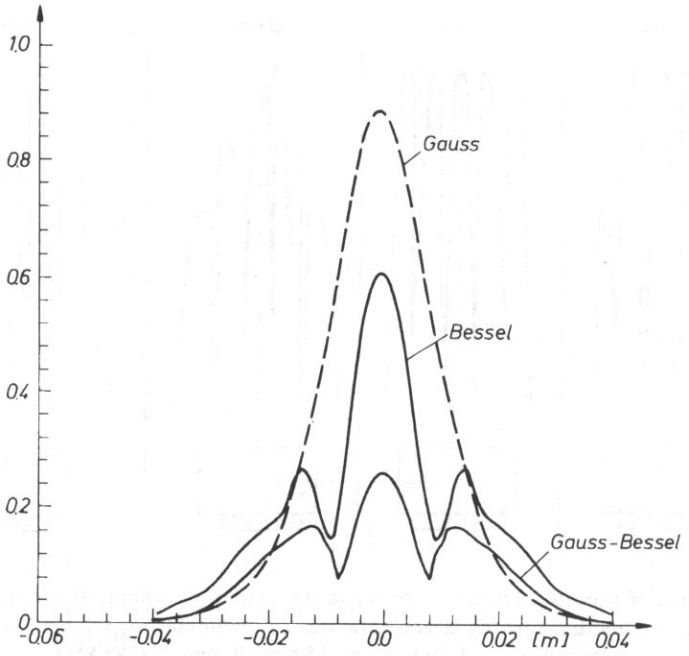

Fig. 6. Influence of the vibrations disturbing Bessel distribution on the radiation characteristics of the ring, $f = 334$ kHz, distance 30 cm.

unfavourable. The situation is similar for the sum or product of Bessel functions with different arguments. The characteristics of radiation are worse than for pure zero-order Bessel function. Thus the complication of the vibration distribution does not lead to the wanted radiation characteristic.

6. Problem of the frequency characteristic

Used methods of acoustic field generation with resonant piezoelectric transducers coupled to elastic elements (cylinder, plate, etc.) have the important shortcoming — narrow frequency band. The vibration amplitude distribution on the transducer surface changes with a change of frequency. This causes changes of the directivity pattern. Theoretical methods of acoustic field calculation permit to solve the problem for wide frequency band, however the practical realization of such systems with high efficiency is difficult. It leads to the complex systems with coupled vibrations or with strongly damped vibrations and even to the work of piezoelectric element beyond its resonance, what strongly limits the efficiency.

The width of frequency band of a transducer depends on the electromechanical coupling coefficient. Different modes have different electromechanical coupling

coefficients, then different frequency bandwidth. The introducing of additional vibrating elements (in the form of cylinder or plate) causes the decrease of electromechanical coupling coefficient. It leads finally to the reduction of frequency bandwidth of the transducer. The introduction of an elastic element causes the unfavourable distribution of elastic energy at the cost of piezoelectric and electric energy. One obtains wanted vibration distributions but the frequency band is reduced. It means that the introduction of additional elements is not advantageous for the transducers working in the pulse mode. The practical solution of this problem is very difficult. The keeping of the frequency bandwidth is connected with the change of the wavelength in the medium, it would require changes of vibration amplitude distribution on the transducer surface. It is not possible for resonant vibrations.

7. Results of the measurements of ring radiation through cylinders

The examples of the results of the measurements of radiation of systems: ring – cylinder are presented in Fig. 7 for different dimensions of cylinders. Bessel distribution with several zero-crossings is obtained for the short cylinders. The elongation of cylinders causes the reduction of Bessel functions terms, it leads to truncated Bessel function.

8. Analysis of the results and possibilities of their application in transducer constructions

When a ring radiates into the air through a cylinder the observed radiation distribution approximates Bessel distribution. The beam width approximates the width defined by Durnin's formula [5]. The beam range is shorter and depends on the difference between the vibration distribution and Bessel distribution. Strong sidelobes exist, the decay of the central lobe appears earlier.

The relations between the cylinder diameter, its length and the wavelength play apparently the essential part. In the case of short cylinders the vibrations are more complicated, one obtains zero-order Bessel function with several zero-crossings. For long cylinders Bessel function is truncated, the quantity of sidelobes is reduced.

The results of this work permit to establish the directions for realizations of the transducers with limited diffraction beam, which can replace a focused beam in certain range. The additional advantage is the increase of vibration amplitude on the transducer axis, the disadvantage — the narrow frequency band of the transducer.

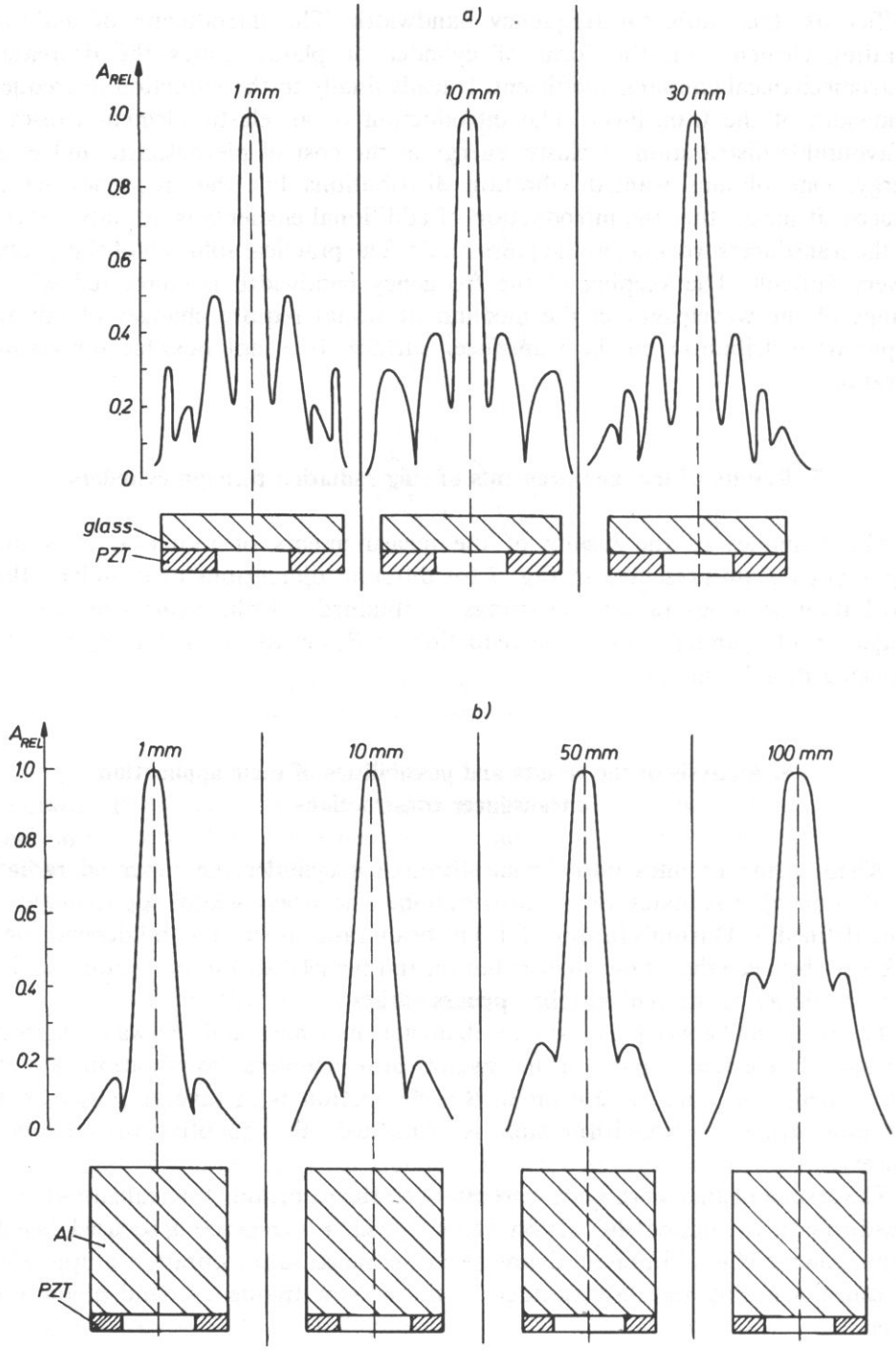
a)
A_{REL}
1.0
0.8
0.6
0.4
0.2
0
1 mm
10 mm
30 mm
glass
PZT
b)
A_{REL}
1.0
0.8
0.6
0.4
0.2
0
1 mm
10 mm
50 mm
100 mm
Al
PZT

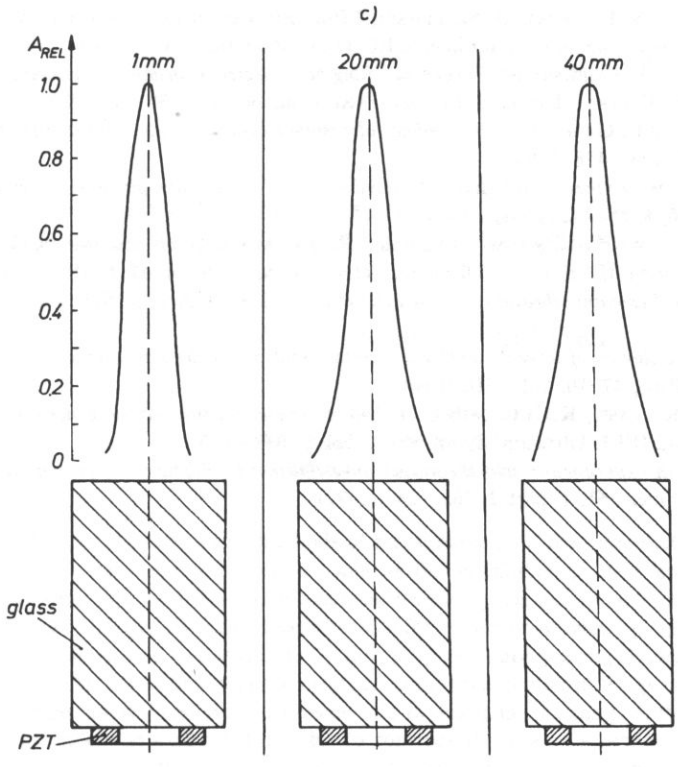

Fig. 7. Examples of acoustic fields in the air generated by PZT rings with different waveguides. a) glass waveguide, $l=10$ mm, $\phi=50$ mm; ring: $\phi_{ext}=50$ mm, $\phi_{int}=20$ mm; $f=252$ kHz, b) Al waveguide, $l=40$ mm, $\phi=38$ mm; ring: $\phi_{ext}=38$ mm, $\phi_{int}=20$ mm; $f=206$ kHz, c) glass waveguide, $l=65$ mm, $\phi=40$ mm; ring: $\phi_{ext}=30$ mm, $\phi_{int}=16$ mm; $f=194$ kHz.

References

[1] J.D. ACHENBACH, S.J. FANG, *Asymptotic analysis of the modes of wave propagation in a solid cylinder*, J. Acoust. Soc. Amer., 47, 5, part 2, 1290–1296 (1970).

[2] N.P. ALIESZIN, W.E. BIEŁYJ, A.Ch. WOPIŁKIN, A.K. WOSZCZANOW, J.N. JERMOŁOW, A.K. GURWICZ, *Methods of acoustic control of metals* (in Russian), Maszinostrojenie, Moskwa 1989.

[3] C.B. BURCKHARDT, H. HOFFMANN, P.A. GRANDCHAMP, *Ultrasonic axicon: a device for focusing over a large depth*, J. Acoust. Soc. Amer., **54**, 6, 1628–1630 (1973).

[4] J.A. CAMPBELL, S. SOLOWAY, *Generation of a nondiffracting beam with frequency-independent beamwidth*, J. Acoust. Soc. Amer., **88**, 5, 2467–2477 (1990).

[5] J. DURNIN, *Exact solutions for nondiffracting beams*, J. Opt. Soc. Amer., **4**, 4, 651–654 (1987).

[6] G.M.L. GLADWELL, D.K. VIJAY, *Natural frequencies of free finite-length circular cylinders*, J. Sound Vibration, **42**, 3, 387–397 (1975).

[7] J.R. HUTCHINSON, *Vibrations of solid cylinders*, J. Appl. Mechanics, **47**, 4, 901–907 (1980).

[8] P. KIEŁCZYŃSKI, W. PAJEWSKI, *Application of the transfer function method in calculations of the directivity patterns of ultrasonic transducers*, J. Appl. Phys., **70**, 12, 7257–7260 (1991).

[9] P. KIEŁCZYŃSKI, W. PAJEWSKI, M. SZALEWSKI, *Ultrasonic transducers with Bessel function distribution of vibrational amplitude on their surface*, IEEE Trans. Robotics Automation, **9**, 6, 732–739 (1993).

[10] P. KIEŁCZYŃSKI, W. PAJEWSKI, M. SZALEWSKI, *Ring piezoelectric transducers radiating ultrasonic energy into the air*, IEEE Trans. Ultrason. Ferroel. Freq. Control, **37**, 1, 38–43 (1990).

[11] J. LU, H. ZOU, J.F. GREENLEAF, *Biomedical ultrasound beam forming*, Ultrasound in Medicine and Biology, **20**, 5, 403–428 (1994).

[12] G.W. MCMAHON, *Experimental study of the vibration of solid, isotropic, elastic cylinders*, J. Acoust. Soc. Amer., **36**, 1, 85–92 (1964).

[13] P. KIEŁCZYŃSKI, W. PAJEWSKI, M. SZALEWSKI, *Ring vibrations in an acoustic medium as a source of ultrasonic radiation*, IEEE Trans. Ultrason. Ferroel. Freq. Control, **41**, 6, 789–795 (1994).

[14] S.N. RASBAND, *Resonant vibrations of free cylinders and disks*, J. Acoust. Soc. Amer., **57**, 4, 899–905 (1975).

[15] K.P. SOLDATOS, *Review of three dimensional dynamic analyses of circular cylinders and cylindrical shells*, Appl. Mech. Rev., **47**, 10, 501–516 (1994).

[16] K. YAMADA, K. TASEI, K. NAKAMURA, *Weighted conical transducer for generation of Bessel beam ultrasound*, 1992 IEEE Ultrason. Symp. Proc., vol. **1**, 613–618.

[17] J. ZEMANEK, *An experimental and theoretical investigation of elastic wave propagation in cylinder*. J. Acoust. Soc. Amer., **51**, 1, part 2, 265–283 (1972).

ARCHIVES OF ACOUSTICS
20, 4, 373–385 (1995)

METHODS OF MEASUREMENTS OF THE QUALITY FACTOR OF PIEZOELECTRIC RESONATORS WITH HIGH ELECTRICAL AND MECHANICAL LOSSES

W. PAJEWSKI and M. SZALEWSKI

Institute of Fundamental Technological Research
Polish Academy of Sciences
(00-049 Warszawa, Swiętokrzyska 21)

In the paper the analysis of methods of measurements of the piezoelectric resonators quality factors has been presented, as well as the possibility of their applications for resonators with high electrical and mechanical losses, e.g. ceramics and piezoelectric foils. The problem of the quality factor measurements for resonators excited by high electric field has been also discussed. To this end the authors propose to apply a ring-shaped piezoelectric transformer. This metod enables us to measure ceramic parameters in the quasi-linear range, to separate mechanical and electrical losses, and to determine the range of the linear work. The conducted analysis makes it possible to conclude the lack of a precise method of the quality factor and also the losses measurement for piezoelectric resonators with low quality factors, also in the case when nonlinear effects occur.

1. Introduction

Measurements of the mechanical and electrical quality factors of resonant vibrating elements give very important information about the piezoelectric material and resonator parameters. These measurements can be performed both in the linear and the quasilinear range of a resonator work. From measurements of the quality factor one can determine the electrical and mechanical losses of a piezoelectric material and the linearity of resonator's working range.

Methods of measurements of the mechanical or electrical quality factor of piezoelectric elements which are based on the resonator equivalent circuit are not very precise, because it is difficult to separate the mechanical part from the electrical part. In these methods one assumes that electrical losses are negligible at low voltage resonances and that the measured quality factor is connected with mechanical losses only. This assumption is not satisfied for measurements in high intensity electric fields [5], because electrical losses are proportional to the second power of the electric field intensity. In this case the measured factor of quality is connected with electrical losses as well as with mechanical losses of a vibrating resonator. Electrical losses are also considerable in resonators made of conducting piezoelectric materials [1].

The purpose of this work was to estimate the possibilities of application of the known methods of the quality factor measurements for investigations of piezoelectric resonators with high electrical and mechanical losses, also in the range of high electrical and mechanical fields. For the measurements in the case of high electric field excitation of a resonator, the authors propose to apply a ring-shaped piezoelectric transformer.

2. Measurements of the mechanical quality factor of resonators with moderate losses

The electromechanical equivalent circuit proposed by Van Dyke [16] is the basis for measurements of the mechanical and electrical quality factors. Using this circuit (Fig. 1) one can determine the input addmitance of a resonator, considering the mechanical losses.

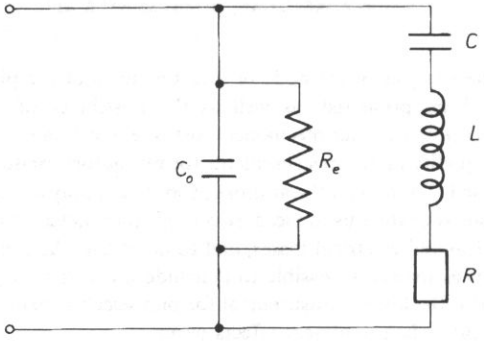

Fig. 1. Van Dyke's electromechanical equivalent circuit of a piezoelectric resonator.

$$Y=\frac{\omega^2RC^2}{(1-\omega^2CL)^2+\omega^2C^2R^2}-j\omega\left[C_0+\frac{C(1-\omega^2CL)}{(1-\omega^2CL)^2+\omega^2C^2R^2}\right]. \tag{2.1}$$

R — resistance corresponding to mechanical losses, L — motional inductance in the equivalent circuit, C — motional capacitance in the equivalent circuit, C_0 — shunt capacitance in the equivalent circuit. For the mechanical resonance $(1-\omega_s^2CL)=0$, and the equation (2.1) simplified to the form

$$Y=\frac{1}{R}-j\omega_sC_0, \tag{2.2}$$

$\omega_s=2\pi f_s$, f_s — series resonance frequency.
Taking into consideration the electrical losses one obtains

$$Y=\left(\frac{1}{R}+\frac{1}{R_e}\right)-j\omega_sC_0, \tag{2.3}$$

where R_e — resistance corresponding to electrical losses.

Both the electrical and mechanical losses depend on frequency, electrical field intensity and mechanical stress.

Equation (2.1) can be graphically presented as an admittance circle with characteristic points Fig. 2 corresponding to frequencies of: mechanical resonance f_s, parallel resonance f_p, resonance f_r, antiresonance f_a, and frequencies of minimal and maximal absolute admittance f_n and f_m. For small losses the circle diameter is equal to the real part of admittance.

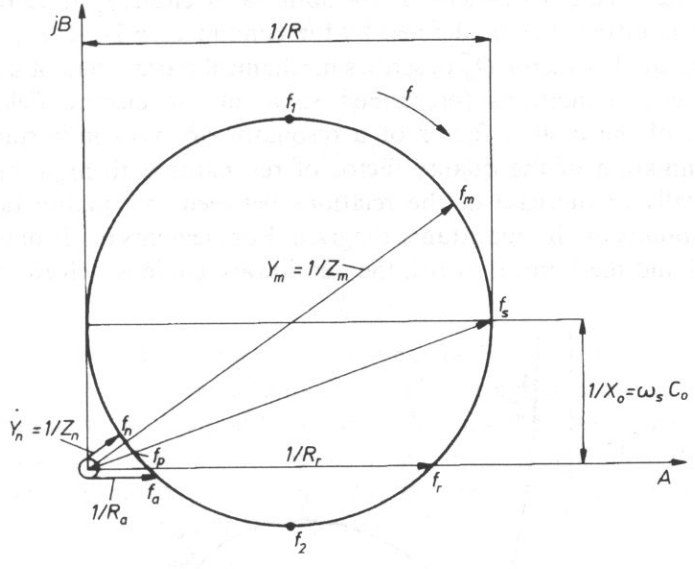

Fig. 2. Admittance circle of a piezoelectric resonator.

$$Y_{re}=\frac{1}{R}. \tag{2.4}$$

Van Dyke's equivalent circuit is very useful for measurements of the parameters of resonators with high quality factor. However, for the analysis of resonators working under variable conditions and, especially, in the nonlinear range, its application is limited. In this case Van Dyke's circuit can be used only as an indication for the determination of theoretical relations and the measurement of admittance as the function of frequency.

The mechanical quality factor is determined by means of lumped electric elements of the equivalent circuit:

$$Q_m^E=\frac{1}{\omega_s RC}, \tag{2.5}$$

and it can be determined using the admittance circle or the resonance curve

$$Q_m^E = \frac{f_s}{\Delta f}, \tag{2.6}$$

where Δf — difference of frequencies for the 3 dB — decrease of voltage.

$$Q_m^E = \frac{f_s}{f_2 - f_1}, \tag{2.7}$$

f_s, f_1, f_2 — characteristic frequencies on the admittance circle. f_1, f_2 correspond to the points on the admittance circle defined by the conductance $1/2R$ (Fig. 2).

Mechanical quality factor Q_m^E describes mechanical parameters of a resonator for prescribed electric conditions (prescribed value of the electric field). Therefore measurements of the quality factor of a resonator are very important. However, precise determination of the quality factor of resonator with high losses is complicated, especially in the case of the relations between the quality factor and the characteristic points on the admittance diagram. For elements made of materials with high electrical and mechanical losses, the admittance circle is deformed (cf. Fig. 3).

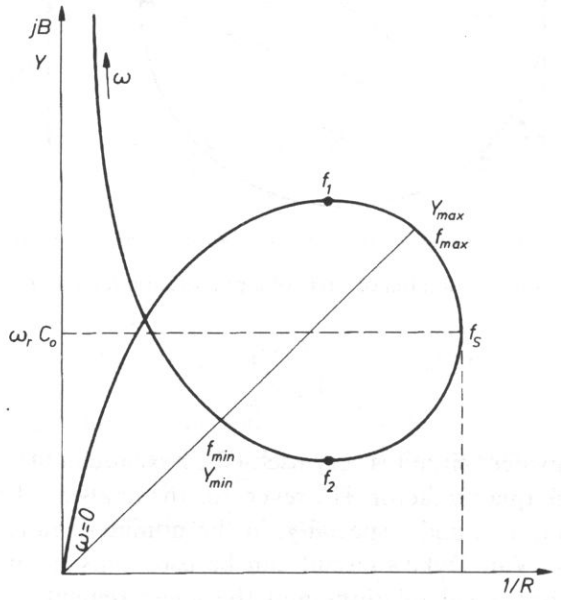

Fig. 3. Admittance diagram for a piezoelectric resonator with high losses.

3. Measurements of resonators with low quality factor

Measurements of the mechanical quality factor in the range of 10 – 100 is a difficult problem. Recently new piezoelectric materials are used, e.g. polymer foils (mainly PVDF) and composites with low mechanical and electrical quality

factors (far below 100). The commonly applied equations involving characteristic frequencies of the equivalent circuit for low losses case appear to be insufficient for the accurate determination of the quality factor. The equations in which frequencies $f_{\min}$, $f_{\max}$ are used (often denoted also by f_n, f_m), corresponding to the minimal and maximal absolute admittance corresponding f_1, f_2 and to the conductance $1/2R$, have been introduced [4, 9]

$$Q_m^E = \frac{f_{\min}^2 + f_{\max}^2}{f_{\min}^2 - f_{\max}^2}, \tag{3.1}$$

and

$$(Q_m^E)^2 = \frac{1}{4}\left[\left(\frac{f_1+f_2}{f_2-f_1}\right)^2 - 1\right], \tag{3.2}$$

or approximately

$$Q_m^E \cong \frac{1}{2}\left(\frac{f_1+f_2}{f_2-f_1}\right). \tag{3.3}$$

In these equations the electromechanical coupling coefficient is included not explicitly. For higher quality factors equations (3.1)–(3.3) are equivalent to the equation (2.7), since their characteristic points coincide. Besides the above mentioned equations, the following equations are also used in the case of independent determination of the electromechanical coupling coefficient k from the ratios of the measured fundamental and overtone resonant frequencies [10]:

$$Q_m^E = \frac{1}{k^2}\sqrt{\frac{Y_m}{Y_n}}, \tag{3.4}$$

$$Q_m^E = \frac{1}{k^2}\frac{\left(\frac{Y_m}{Y_n} - 1\right)}{\sqrt{\frac{Y_m}{Y_n}}}, \tag{3.5}$$

and [5]:

$$Q_m^E = \frac{1-k^2}{k^2}\left(\frac{Y_m}{Y_n}\frac{f_{\min}}{f_{\max}} - 1\right)\sqrt{\frac{Y_n}{Y_m}} \tag{3.6}$$

Y_m, Y_n — maximal and minimal value of the absolute admittance determined by means of the admittance diagram or the absolute admittance dependence on the frequency (Fig. 4).

In Table 1 the calculated values of the mechanical quality factor Q_m^E are presented. The values of Q_m^E were calculated for the electromechanical coupling coefficient $k = 0.3$ and for different ratios of admittances, using different formulae. It can be seen

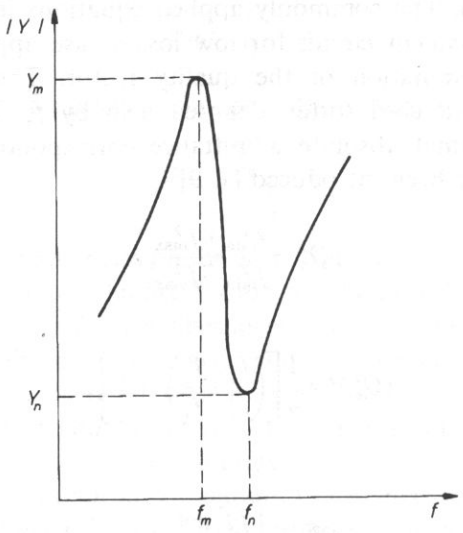

Fig. 4. Absolute admittance of a piezoelectric resonator as a function of frequency.

Table 1. Mechanical quality factors calculated by different formulae

$\sqrt{\frac{Y_m}{Y_n}}$	1.2	1.5	2	3	4	5	Formula
Q_m^E	13.3	16.7	22.2	33.3	44,4	55.5	(3.4)
	4.1	9.3	16.7	29.6	41.7	53.3	(3.5)
	5	10.2	17.4	30	42.4	54.1	(3.6)

in Table 1 that the differences are large for the small values of $(Y_m/Y_n)^{1/2}$ (it is also connected with high losses).

In the case of piezoelectric foil materials with high losses, Q_m^E can be determined from the slope of the straight line X_a/R_a (the ratio of the imaginary part of impedance to the real part of impedance near the resonance) [2]. The quality factor is calculated from the measurements of the impedance of the series circuit being a function of frequency near the mechanical resonance of a resonator. The dependence of X_a/R_a on the frequency is linear and the quality factor corresponds to the inclination of the straight line to the frequency axis,

$$\frac{X_a}{R_a} = -2Q_m^E \frac{\omega-\omega_0}{\omega_0}. \tag{3.7}$$

Here $2Q_m^E$ corresponds to the slope of the straight line $\frac{X_a}{R_a}(\omega)$, $\omega_0 = 2\pi f_0 = (\pi/t)(c^D/\rho)^{1/2}$, f_0 — thickness resonant frequency, t — resonator thickness, c^D — stiffened elastic constant, ρ — density.

As a result, one obtains the formula for the mechanical quality factor

$$Q_m^E = \frac{1}{2}\frac{X_a}{R_a}\frac{\omega_0}{\omega-\omega_0}. \tag{3.8}$$

This formula may be used also for the parallel circuit

$$Q_m^E = \frac{1}{2}\frac{B_a}{G_a}\frac{\omega_0}{\omega-\omega_0}; \tag{3.9}$$

B_a/G_a is the ratio of the imaginary part of admittance to the real part of admittance near the resonance.

In this case one calculates the ratio B_a/G_a from the admittance diagram by moving its centre along the conductance line and subtracting the value of the conductance connected with the electrical losses.

$$Q_m^E = \frac{1}{2}\frac{\omega_0 C_0 - \omega C}{\left(\frac{1}{R}-\frac{1}{R_e}\right)}\frac{\omega_0}{\omega-\omega_0}; \tag{3.10}$$

Notations C, C_0, R, R_e — cf. Fig. 1.

For the determination of the angle of inclination of the straight line B_a/G_a to the frequency axis it is sufficient to find the coordinates of one point in addition to the point ω_0, in the vicinity of the resonance. The results obtained from the calculations based on the formula (3.10) are very close to the results obtained by the formulae (3.4) and (3.6). The formulae (3.4) and (3.10) have been applied for the calculations of the quality factor of a barium-modified lead meta-niobate piezoelectric ceramic with small quality factor. Fot this purpose we have used the admittance diagrams obtained during investigations of this ceramic [11]. Figure 5 presents an example of such a diagram. The results of the calculations are presented in Table 2. In the same way we have also calculated the data from [2] for the piezoelectric foil PVF_2, $f_0 = 20.65$ MHz, $Q_B = 14.6$, $Q_f = 17.2$, $\frac{Q_f - Q_B}{Q_f} = 15\%$, where Q_B, Q_f are the quality factors calculated by means of the formula (3.10) and (3.4) respectively.

Table 2. Quality factors of plates of $Pb_{0.9}Ba_{0.1}Nb_2O_6$ ceramic determined from measurements and calculations using the formula (3.10) — Q_B and (3.4) — Q_f

f_0 [kHz]	2.25	3.3	2.8	3.05	2.32	4.7	5.3
Q_B	13.0	15.8	18.2	25.7	21.1	55.4	23.6
Q_f	13.4	16.5	18.6	30.5	23.2	71.0	25.2
$\frac{Q_f - Q_B}{Q_f}$ [%]	3.0	4.2	2.2	15.7	9.0	22.0	6.3

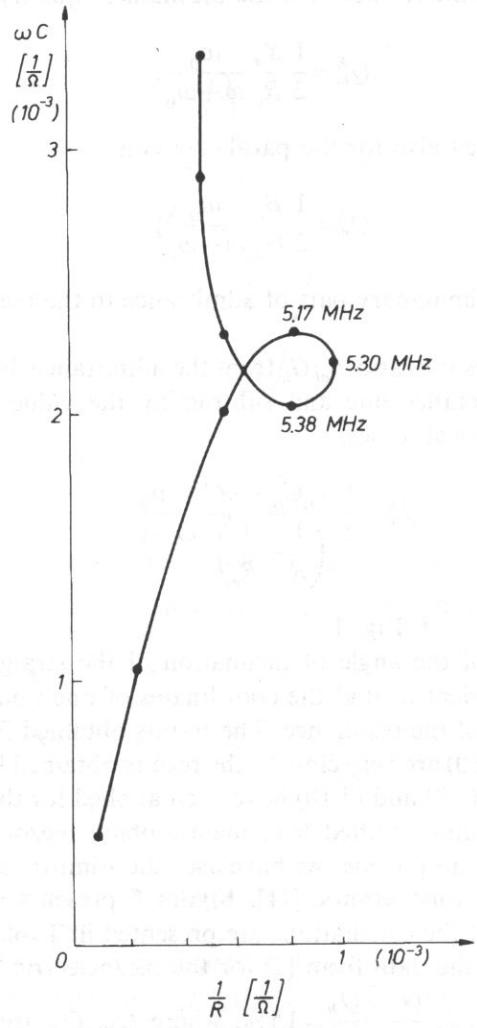

Fig. 5. Admittance diagram for a ceramic plate $Pb_{0.9}Ba_{0.1}Nb_2O_6$

It can be seen in Table 2 that the quality factor values calculated from the formula (3.10) are by 10% or less lower than the quality factors calculated from the formula (3.4) for $Q_m^E < 20$. Application of these quality factor values for the calculations of the electromechanical coupling coefficient (formulae (3.4)–(3.6)) leads to a considerable disagreement with the results obtained from the ratio of overtone frequencies [10, 11]. In this case one obtains considerably higher values of the coefficient k than the values following from the method described in [10]. These discrepancies result probably from the fact that the electric losses are not taken into consideration in the formulae (3.4)–(3.6). In all calculations the equivalent circuit and the admittance circle are

idealized, and the electric losses are not considered. The conventional formulae applied in the calculations are not sufficient in this case.

4. Measurements of the quality factor of a resonator in high electric fields

The formulae mentioned above cannot be used to calculate the quality factor for higher excitation voltages, when electrical losses increase and resonance curves deform. Their deformation is caused by nonlinear effects [3, 14]. When the amplitude of vibration increases more, changes of the resonance frequency and discontinuities of resonance curves appear — Fig. 6. In this case it is not possible to find the characteristic points on the admittance diagram. Discontinuities make it impossible to determine the quality factor. The resonance curve narrows apparently. It should be the proof of the increase of the quality factor. In fact, the quality factor decreases very

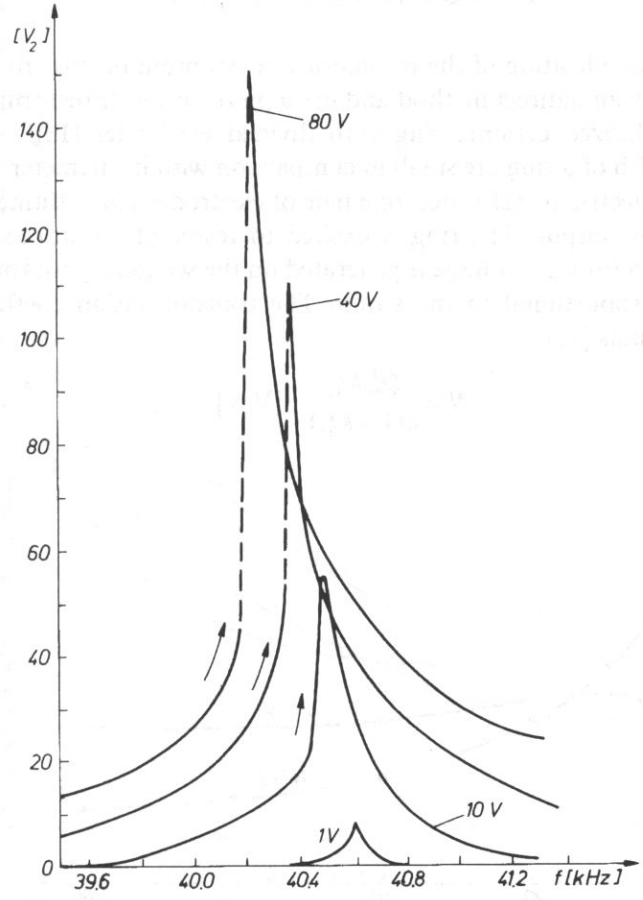

Fig. 6. Resonance curves of the PZT ring ($\phi_{ext}=30$ mm, $\phi_{int}=23$ mm, $d=3.6$ mm) for excitation voltages V_1. Transformer circuit, the secondary circuit is loaded by high resistance. V_1 values are written at the curves.

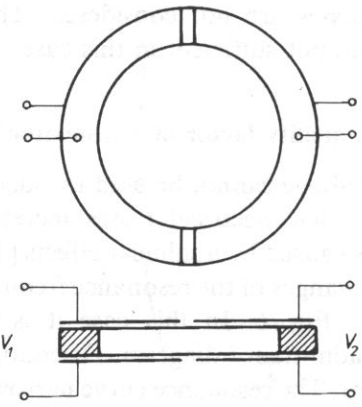

Fig. 7. Ring-shaped piezoelectric transformer

considerably. Strong heating of the resonator is a symptom of this effect [15]. In this case one can apply an indirect method and use a piezoelectric transformer in the form of an axially polarized ceramic ring with divided electrodes [13] — Fig. 7. The thickness and width of a ring are small in comparison with its diameter. Such a ring is a resonant piezoelectric transformer, one pair of electrodes constituting its input, the second pair — its output. The ring is excited to resonant vibrations by the input electrodes and as a result, a voltage is generated on the secondary (output) electrodes, its value being proportional to the strain. The transformation coefficient of such a transformer equals [12]

$$N=\frac{Q_m^E k_{31}^2}{\pi(1-k_{31}^2)} \quad [\mathrm{V/V}]$$

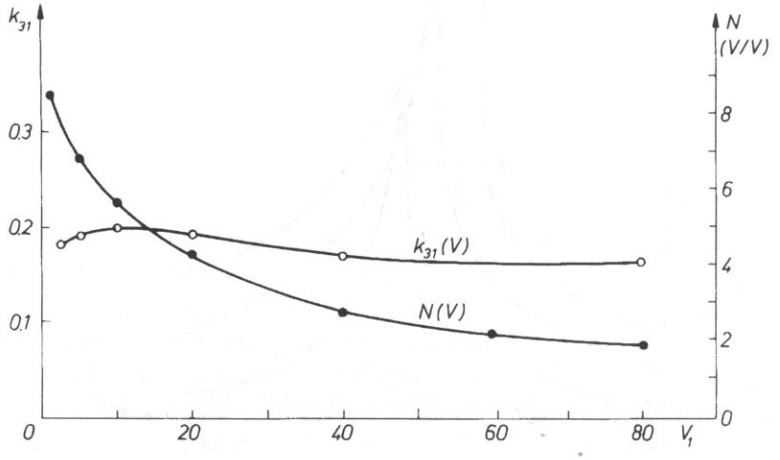

Fig. 8. Dependence of the electromechanical coupling coefficient k_{31} and the transformation coefficient N on the voltage exciting the ring transformer (PZT, $\phi_{ext}=30$ mm, $\phi_{int}=23$ mm, $d=3.6$ mm).

This formula can be used to calculate the quality factor for the measurement conditions. Then with a ring-shaped transformer it is possible to determine Q_m^E without the necessity of finding the characteristic points on the deformed admittance diagrams or resonance curves, it is very difficult or even impossible in certain cases.

The measurement of the transformation coefficient N is simple it is enough to measure the input and output voltages of the transformer. On the contrary, the measurement of the electromechanical coupling coefficient may be complicated. Experimental investigations of the transformer show that the electromechanical coupling coefficient does not change considerably with changes of the voltage exciting the transformer — Fig. 8. However, it is difficult to determine its value above the threshold of the discontinuity. The quality factor can be calculated in the quasilinear range by the determination of the k_{31} coefficient from the measurements of the

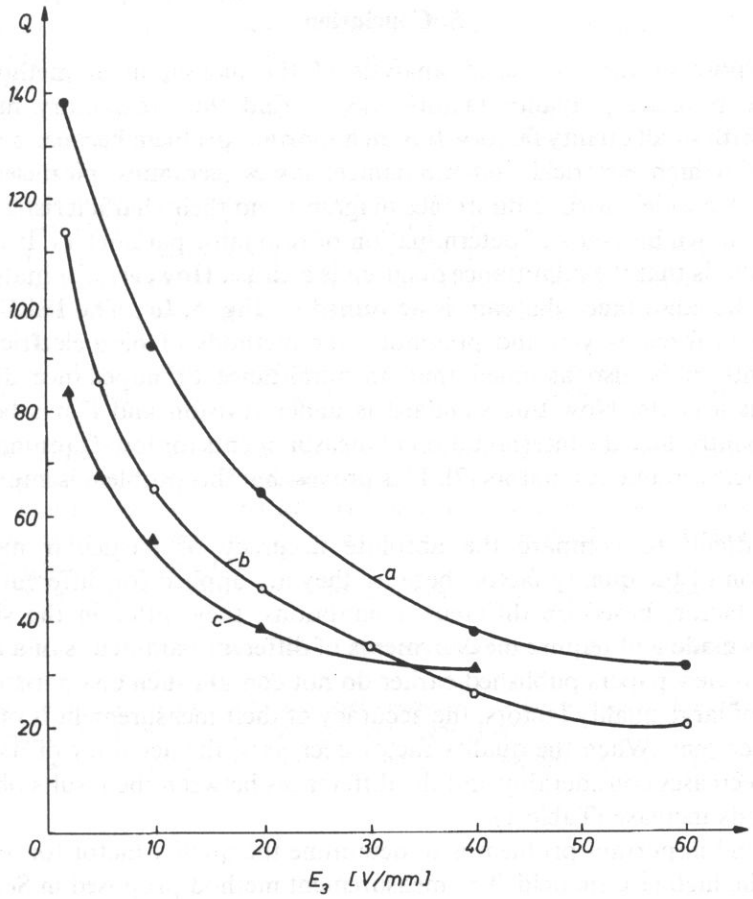

Fig. 9. Quality factor as a function of the electric field for the PZT ring with thickness 0.95 mm a) secondary electrodes shorted, b) secondary electrodes open, c) primary and secondary electrodes connected.

resonance and antiresonance [11] of a ring submerged in a viscous liquid. In this case discontinuities of resonance curves are eliminated. The real part of radiation impedance does not influence the resonance frequencies.

Figure 9 presents the quality factor as a function of the electric field for the $Pb/Zr_{0.45}\,Ti_{0.55}/O_3$ ring with the thickness 0.95 mm. The measurements have been conducted for three cases: a) the secondary electrodes shorted, b) the secondary electrodes open, c) the primary and secondary electrodes connected. The largest quality factor has been obtained for the shorted secondary electrodes, in this case the electrical losses in the secondary circuit are eliminated ($E=0$). For the connected electrodes and for the open secondary electrodes, the measured quality factor depends on the electrical and mechanical losses. The electrical losses can be calculated from the differences between the quality factors for the case b) and the case a) [13].

5. Conclusion

The purpose of the conducted analysis of the measurement methods of the piezoelectric resonators quality factors was to find the satisfactory method for resonators with small quality factors. It is an important problem because piezoelectric materials with high electrical and mechanical losses (ceramics, piezoelectric foils, composites) are widely used. Admittance diagrams and their characteristic points are used in the known methods of determination of resonator parameters. It is assumed in these methods that the admittance diagram is a circle. However, for materials with high losses the admittance diagram is deformed — Fig. 5. In "The IEEE Standard 177", being in force as yet, and presenting the methods of piezoelectric vibrators measurements, it is also assumed that an admittance or impedance diagram of a vibrator is a circle. Now this standard is under revision and it has been found necessary to introduce the interpretation of measurements for low-Q resonators, such as piezoelectric ceramic resonators [7]. This proves that this problem is important and live.

It is difficult to compare the absolute accuracy of particular methods of determination of the quality factor, because they are applied for different ranges of the quality factor, based on different assumptions, they differ in the simplifying assumptions made and require measurements of different parameters of a resonator. Also, some review papers published earlier do not contain such comparison, e.g. [8]. In the case of large quality factors, the accuracy of their measurement is of the order of several per cent. When the quality factor decreases, the accuracy of its measurement also decreases considerably and the differences between the results obtained by other methods increase (Table 1).

The second important problem is to determine the quality factor for a resonator excited by the high electric field. The measurement method proposed in Sect. 4 using a piezoelectric transformer in the form of a ceramic ring enables us to determine the ceramic parameters in the quasilinear range. It is possible to separate the electrical and mechanical losses and to determine the range of the linear work.

Finally, the authors conclude the lack of an accurate method of the quality factor measurement (and, consequently, of the losses) for piezoelectric resonators with low quality factors, and in the case when nonlinear effects occur.

References

[1] G. ARLT, *Resonance-antiresonance of conducting piezoelectric resonators*, J. Acoust. Soc. Amer., **37**, 1, 151–157 (1965).

[2] N.L. BUI, H.J. SHAW and L.T. ZITELLI, *Study of acoustic wave resonance in piezoelectric PVF_2 film*, IEEE Trans. **SU-24**, 5, 331–336 (1977).

[3] J.J. GAGNEPAIN, *Non-linear phenomena in bulk and surface acoustic wave resonators*, V Conference on Piezoelectronics, Warszawa 1980, pp. 10–17.

[4] R.M. GLAISTER, *Measurement of coupling coefficient and Q of low-Q piezoelectric ceramics*, Brit. J. Appl. Phys., **11**,8, 390–391 (1960).

[5] S. HIROSE, M. AOYAGI and Y. TOMIKAWA, *Dielectric loss in a piezoelectric ceramic transducer under high-power operation; Increase of dielectric loss and its influence on transducer efficiency*, Jap. J. Appl. Phys., part 1, **32**, 5B, 2418–2421 (1993).

[6] G.E. MARTIN, *Determination of equivalent-circuits constants of piezoelectric resonators of moderately low Q by absolute admittance measurements*, J. Acoust. Soc. Amer., **26**, 3, 413–420 (1954).

[7] T. MEEKER, *Publication and proposed revision of IEEE Standard 177–1966 "Standard definitions and methods of measurement for piezoelectric vibrators"*, IEEE Trans. **UFFC-40**, 1, 1–19 (1993).

[8] F.R. MONTERO DE ESPINOZA, J.L. SAN EMETERIO and P.T. SANZ, *Summary of the measurement methods of Q_m for piezoelectric materials*, Ferroelectrics, **128**, 1–4, 61–66 (1992).

[9] D. NOTERMAN, M. BRISSAUD, M. KLEIMANN and G. GRANGE, *Caractérisation de céramiques piézoélectriques à faible coefficient de surtension par une méthode d'identification*, Acustica, **66**, 1, 28–36 (1988).

[10] M. ONOE, H.F. TIERSTEN and A.H. MEITZLER, *Shift in the location of resonant frequencies caused by large electromechanical coupling in thickness-mode resonators*, J. Acoust. Soc. Amer., **35**, 1, 36–42 (1963).

[11] W. PAJEWSKI, *Piezoelectric properties of ceramic materials and their measurements* (in Polish), Elektroceramika, vol. 1, PWN, Warszawa 1981, pp. 191–233.

[12] W. PAJEWSKI and Vo DUY DAN, *Method of measurements of the electromechanical coupling coefficient k_{31} and piezoelectric constants d_{31}, g_{31} in nonlinear range* (in Polish), XXIII Open Seminar on Acoustics, Rzeszów 1986, pp. 139–142.

[13] W. PAJEWSKI and M. SZALEWSKI, *Piezoelectric ceramic in high fields* (in Polish), IFTR Reports 26/1992.

[14] S. TAKAHASHI and S. HIROSE, *Vibration-level characteristics of lead-zirconate-titanate ceramics*, Jap. J. Appl. Phys., part 1, **31**, 9B, 3055–3057 (1992).

[15] S. TAKAHASHI and S. HIROSE, *Vibration-level characteristics for iron-doped lead-zirconate-titanate ceramic*, Jap. J. Appl. Phys., part 1, **32**, 5B, 2422–2425 (1993).

[16] K.S. VAN DYKE, *The electrical network equivalent of a piezoelectric resonator*, Phys. Rev., **25**, 825 (1925).

ARCHIVES OF ACOUSTICS
20, 4, 387–400 (1995)

THE PROPAGATION OF ULTRASONIC WAVES IN CONDENSER OIL AT PRESENCE OF DC ELECTRIC FIELD

A. SKUMIEL AND M. ŁABOWSKI

Institute of Acoustics, Adam Mickiewicz University
(60-769 Poznań, ul. Matejki 48/49)

1. Introduction

A DC electric field externally applied to a dielectric liquid modifies the acoustic properties of the liquid.

Our earlier studies [1, 9] on the influence of an electric field on the propagation velocity of ultrasonic waves were based on the assumptions that the variations observed were due to changes in the free energy. Theoretical assessments for typical dielectric liquids and nearbreakdown field strengths show that the change in ultrasonic wave velocity should not exceed several mm/s and should occur in times comparable with the time determined by orientational relaxation of the polarization vector related with rotation of the dipolar molecules in the field.

Thus, the change in ultrasonic velocity observed on applying a DC electric field to an oil as a function of its viscosity and the structure and size of its molecules should occur in times of the order of microseconds. However, experiment fails to confirm the above assumptions [1, 9]. In fact, the change in ultrasonic velocity and the times involved are considerably in excess of those calculated theoretically. Hence, in the first part of our present paper, we invoke other theoretically admissible mechanisms to explain the changes in ultrasonic wave velocity in condenser oil in an external DC electric field.

In part 2 we report the influence of an electric field on the amplitude of the absorption coefficient of the wave in mineral non-polar and synthetic dipolar oils versus the electric field strength and temperature. We also propose different explanations for the variations observed. One of the causes of the experimentally observed behaviour of the dielectric liquids subjected to the action of a DC electric field due to the presence of gas bubbles.

2. The electric field surrounding a gas bubble

It will be remembered [2] that a dielectric liquid sample, even if purified repeatedly by physico-chemical methods, still contains an amount of small gas bubbles. The gaseous cavity the bubble is surrounded by a region of strong inhomogeneity of the

electric field [6] causing the free electric charges present in a real medium to be sucked away towards the surface of the sphere. If the resultant charge thus attached to the bubble is non-zero, the bubble will drift in the electric field in the direction of the electrode of opposite sign. The electric field distribution inside the bubble and in its neighbourhood is shown in Fig. 1. The region between the two planar parallel electrodes is filled with a liquid dielectric of relative electric permittivity ε_r containing a spherical bubble with an absolute electric permittivity approximately equal to that of vacuum.

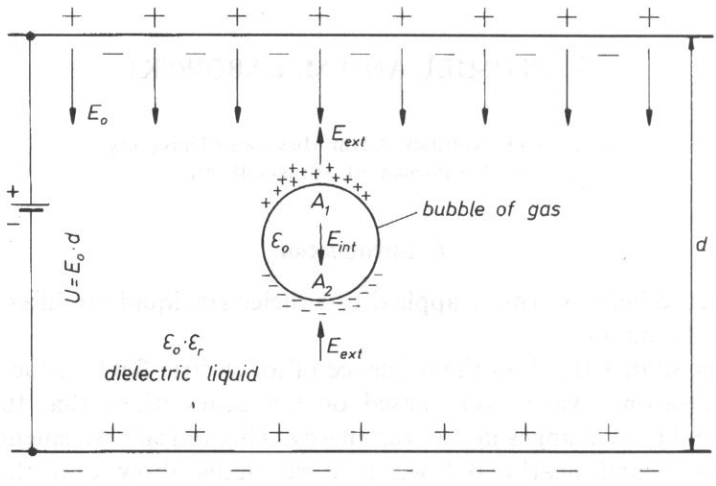

Fig. 1. Electric field distribution within and outside gas bubble in a dielectric liquid.

As the dielectric becomes polarized, electric charge is induced on the surface of the spherical cavity with the surface density distribution D_R given by

$$D_R = D_{\max} \cdot \cos\phi \,. \tag{2.1}$$

These polarization charges give rise to an electric field of their own independent of the initial field E_0.

The electric field strength E_{int} induced inside the bubble by the charges on its surface is in this case directed parallel to the original external field E_0.

As a result, the real field $E_{\text{int(re)}}$ inside the bubble will be

$$E_{\text{int(re)}} = E_0 + E_{\text{int}} \,, \tag{2.2}$$

whereas the resultant electric field strength $E_{\text{ext(re)}}$ outside the sphere in its neighbourhood will be given by

$$E_{\text{ext(re)}} = E_0 - E_{\text{ext}} \,. \tag{2.3}$$

The electric field strength induced within the sphere by the electric charges cosine-distributed on its surface can be shown to amount to

$$E_{\text{int}} = \frac{D_{\max}}{3\varepsilon_0}, \tag{2.4}$$

whence

$$D_{\max} = 3\varepsilon_0 E_{\text{int}}. \tag{2.5}$$

The electric flux $\Delta\Phi$ produced by the charge ΔQ accumulated on the spherical surface element ΔS in the neighbourhood of a point A_1 or A_2 is

$$\Delta\phi = \Delta Q = D_{\max} \cdot \Delta S = 3\varepsilon_0 \cdot E_{\text{int}} \Delta S. \tag{2.6}$$

The flux splits into two parts, the one inside the sphere, $\Delta\Phi_{\text{int}}$, and the other outside the sphere, $\Delta\Phi_{\text{ext}}$. The two can be defined as follows:

$$\Delta\Phi_{\text{int}} = \varepsilon_0 E_{\text{int}} \cdot \Delta S, \quad \Delta\Phi_{\text{ext}} = \varepsilon_0 E_{\text{ext}} \cdot \Delta S. \tag{2.7}$$

This enables us to determine the strength of the electric field E_{ext} induced outside the sphere in the point A_1 or A_2 by the polarization charges:

$$3\varepsilon_0 E_{\text{int}} \cdot \Delta S = \varepsilon_0 E_{\text{int}} \cdot \Delta S + \varepsilon_0 E_{\text{ext}} \cdot \Delta S, \tag{2.8}$$

i.e.,

$$E_{\text{ext}} = 2E_{\text{int}}. \tag{2.9}$$

Hence, we get from (2.3)

$$E_{\text{ext(re)}} = E_0 - 2E_{\text{int}}. \tag{2.10}$$

As we know [6], the normal components of the resultant field strength at the boundary between two dielectrics have to be inversely proportional to the electric permittivities:

$$\frac{E_{\text{ext(re)}}}{E_{\text{int(re)}}} = \frac{E_0 - 2E_{\text{int}}}{E_0 + E_{\text{int}}} = \frac{\varepsilon_0 \cdot 1}{\varepsilon_0 \varepsilon}, \tag{2.11}$$

whence

$$E_{\text{int}} = E_0 \frac{\varepsilon_r - 1}{1 - 2\varepsilon_r}. \tag{2.12}$$

With regard to the initial component of the field, E_0, we finally obtain the following expressions fot the real electric field existing inside and outisde the bubble:

$$E_{\text{int(re)}} = \frac{3\varepsilon_r}{1 + 2\varepsilon_r} E_0, \quad E_{\text{ext(re)}} = \frac{3}{1 + 2\varepsilon_r} E_0. \tag{2.13}$$

In the neighbourhood of the air bubble, the local electric field is weakened because the coefficient of relative permittivity of the liquid is $\varepsilon_r > 1$, whereas within the bubble it increases compared to the initial field.

For example, in the case of synthetic oil for which $\varepsilon_r = 4$ the field at the surface of the bubble falls to one third, and a considerable local field inhomogeneity arises in its neighbourhood. The respective field gradient attaches the free charge to the bubble and causes the latter to wander towards the neutralizing electrode.

The resultant electric field strength inside the bubble — which is much in excess of its macroscopic value — lowers the electric breakdown field value of the oil, an effect undesirable in the case of insulating systems.

In strong electric fields the breakdown value of the gas in the bubble obeys Paschen's law according to which the pre-breakdown voltage U_p is dependent on the diameter of the bubble d and the pressure p.

With a view to assess the electric breakdown value, the voltage across the diameter of the bubble along the lines of force of the field can be assumed to be given by $U \approx E_0 \cdot \varepsilon_r \cdot d$, where E_0 is the field strength in the oil, ε_r its relative electric permittivity, and d the diameter of the bubble. If U attains the pre-breakdown value U_p, electric discharge takes place inside the bubble. For an air bubble with $d = 0.1 - 1$ mm at 25°C and a pressure of $p = 1000$ hPa, the discharge voltage $U_p = 4.3 \cdot d^{0.63}$ [10].

Hence, the electric field strength E_p [kV/mm], at which ignition of incomplete discharges in an air bubble of diameter d [mm] takes place is found to be

$$E_p = \frac{4.3 \cdot d^{0.63}}{d \cdot \varepsilon_r}. \tag{2.14}$$

By Eq. (2.14) ignition in bubbles of diameter $d = 1$ mm immersed in mineral oil with $\varepsilon_r = 2.2$ should occur at $E_p = 2$ kV/mm, whereas in bubbles of diameter $d = 0.1$ mm — at $E_p = 4.6$ kV/mm.

In the mineral oil studied by us, where $d = 2 \cdot R_{cf} = 0.0916$ mm and $\varepsilon_r = 2.2$, the theoretical breakdown value amounted to $U_p = 0.95$ kV, whereas the electric field strength $E_p = 4.7$ kV/mm and was strongly in excess of that applied in our measurements. In practice, the formation and growth or vanishing of bubbles in oil can be due to a number of factors, such as temperature, moistness, the chemical composition of the oil, and the electric field strength.

An intense electric field can moreover destroy the molecular structure of the paraffine hydrocarbons by disrupting the bonds between the carbons and hydrogens, leading to the emergence of hydrogen and methane bubbles. On the other hand, molecules of aromatic hydrocarbons adsorb atoms of free hydrogen thus impeding the formation of hydrogen bubbles.

All this contributes to modify the acoustic properties of the medium under the action of an external electric field, both by affecting the propagation velocity of ultrasonic waves and their absorption coefficient in the medium. Apparently, these factors act in a way to remove the gas bubbles from the liquid [10].

Tests carried out by applying an AC field failed to affect the ultrasonic propagation velocity and signal amplitude.

3. Experimental

3.1. The method

The change in absorption coefficient of the ultrasonic wave on application of the DC field was recorded by the pulse method. A block diagram of our setup is shown in Fig. 2. In the course of our studies we measured the amplitude of the ultrasonic pulse of frequency 6 MHz before and after applying the DC electric field at right angles to the oil sample. The DC electric field ranged from 0 to 300 kV/m and the temperature from 0 to 40°C. The application of analog memory enabled us to record the ultrasonic pulse amplitude which, on traversing an analog-digital converter, was fed into the computer memory. Examples of the time-variations of the ultrasonic pulse amplitude recorded for the two oils investigated are given in Figs. 3a and 3b.

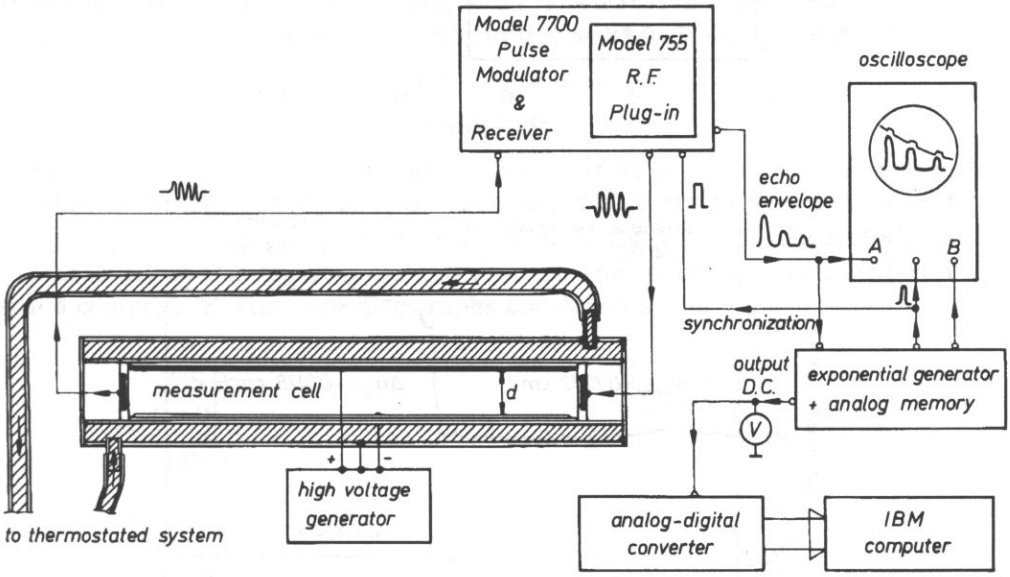

Fig. 2. Block diagram of our setup for determination of the amplitude absorption coefficient of an ultrasonic wave propagating in a dielectric liquid.

The procedure adopted by us involved calculating the mean value $\langle u_0 \rangle$ of the ultrasonic pulse amplitude over a period of 120 s preceding application of the external DC field as the mean value $\langle u_E \rangle$ during 120 s with the field switched on.

Let $\langle u_0 \rangle$ and $\langle u_E \rangle$ correspond, respectively, to the zero-field amplitude absorption coefficient $\langle \alpha_0 \rangle$ of the wave and $\langle u_E \rangle$ to its variation $\langle \Delta\alpha_E \rangle$ after once the electric field E_0 was applied. The field modifies the acoustic properties of the oil. Now $\langle u_0 \rangle$ and $\langle u_E \rangle$ can be expressed as follows:

$$\langle u_0 \rangle = U_A \exp^{-\langle \alpha_0 \rangle L} \quad \text{and} \quad \langle u_E \rangle = U_A \exp^{-\langle \alpha_E \rangle L}, \tag{3.1}$$

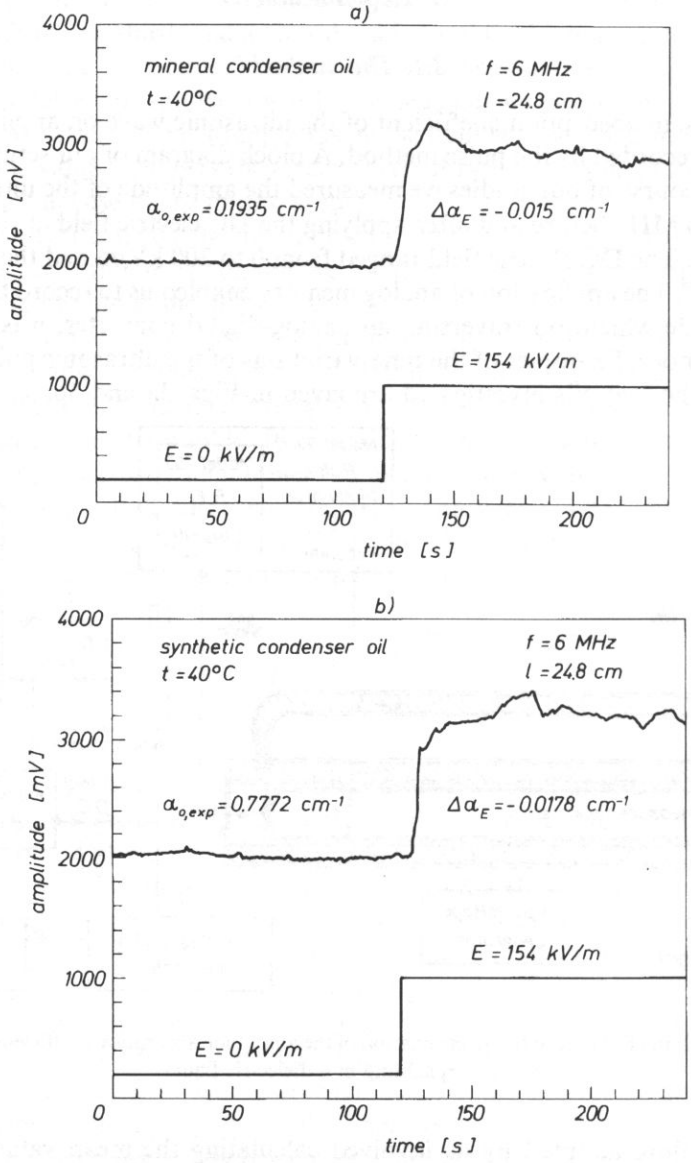

Fig. 3. The changes in ultrasonic pulse amplitude (6 MHz) prior to and after application of an external electric field E = 154 kV/m; a) in mineral condenser oil (MCO), b) in synthetic condenser oil (AKB).

where $l = 24.8$ cm is the axial distance between the measuring transducer and U_A the ultrasonic pulse amplitude obtained from the receiver transducer at $l = 0$.
Hence, we derive the following expression for $\Delta\langle\alpha_E\rangle$, the variation of mean amplitude absorption coefficient of the wave due to the external field, as measured directly in our experiment:

$$\Delta\langle\alpha_E\rangle=\langle\alpha_E\rangle-\langle\alpha_0\rangle=\frac{1}{l}\cdot\ln\left(\frac{\langle u_0\rangle}{\langle u_E\rangle}\right). \tag{3.2}$$

Thus, in order to determine $\Delta\langle\alpha_E\rangle$ we only have to measure the length l of the path traversed by the wave in the oil and the ratio of the pulse amplitudes prior to and after applying the field. The relative error incurred when measuring the change in amplitude absorption coefficient, $\Delta(\Delta\langle\alpha_E\rangle)/(\Delta\langle\alpha_E\rangle)$ calculated by the full differential method, is

$$\frac{\Delta(\Delta\langle\alpha_E\rangle)}{\Delta\langle\alpha_E\rangle}=\frac{\Delta u(\langle u_E\rangle+\langle u_0\rangle)}{\langle u_E\rangle^2\ln^2\left(\frac{\langle u_0\rangle}{\langle u_E\rangle}\right)}+\frac{\Delta l}{l}. \tag{3.3}$$

With the values $l=24.8$ cm, $\Delta l=0.01$ cm, $\Delta u=1$ mV, $\langle u_0\rangle=1$ V and $\langle u_E\rangle=2$ V, we arrive at a relative error of $\Delta(\Delta\alpha_E)/(\Delta\alpha_E)=0.2\%$, whereas the absolute error incurred in measuring the change in amplitude absorption coefficient $\Delta(\Delta\alpha_E)=0.000055\ \mathrm{cm}^{-1}$.

4. Results

Variations in the amplitude absorption coefficient of the ultrasonic pulse travelling in the sample exposed to different values of external field are shown in Fig. 4. Similarly Fig. 5 shows variations temperature T for different values of kV/m.

Moreover, we also repeated our experiments, using mineral oil saturated with air from a compressor. The respective graphs are shown in Fig. 6.

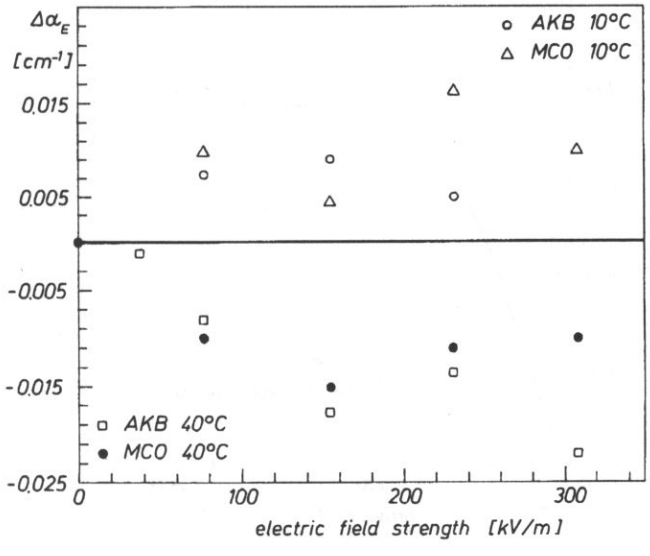

Fig. 4. Variations in amplitude absorption coefficient $\Delta\alpha_E$ of the ultrasonic wave in the oils versus the external electric field strength E.

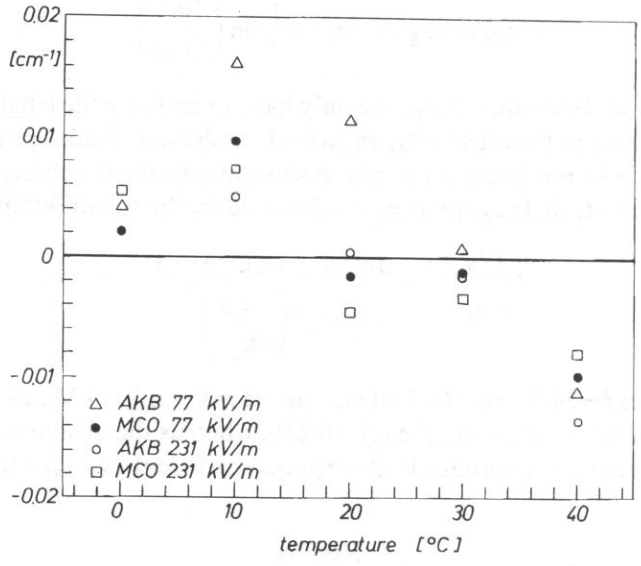

Fig. 5. The same as in Fig. 4 for the temperature of the oils.

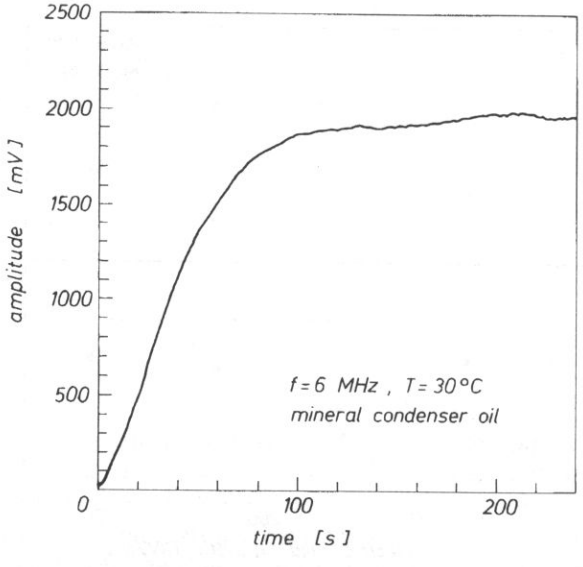

Fig. 6. Time-variation of the ultrasonic pulse amplitude 6 MHz, 30°C on traversal of a given path in the mineral oil after the production therein of a cloud of air bubbles.

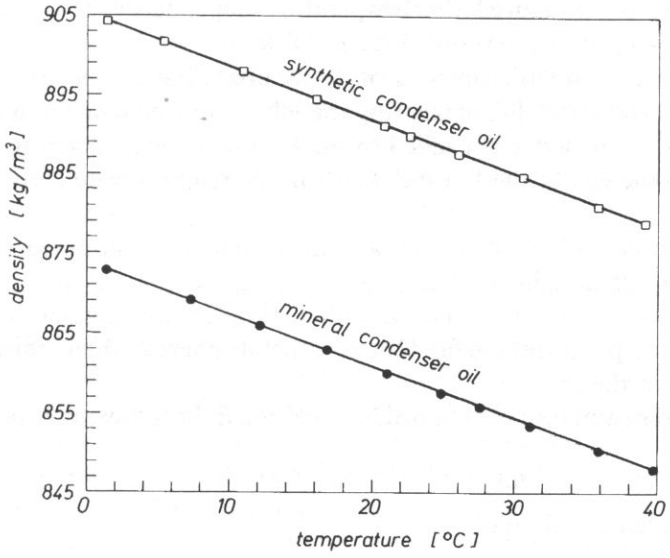

Fig. 7. The density $\rho(T)$ of the oils versus the temperature T.

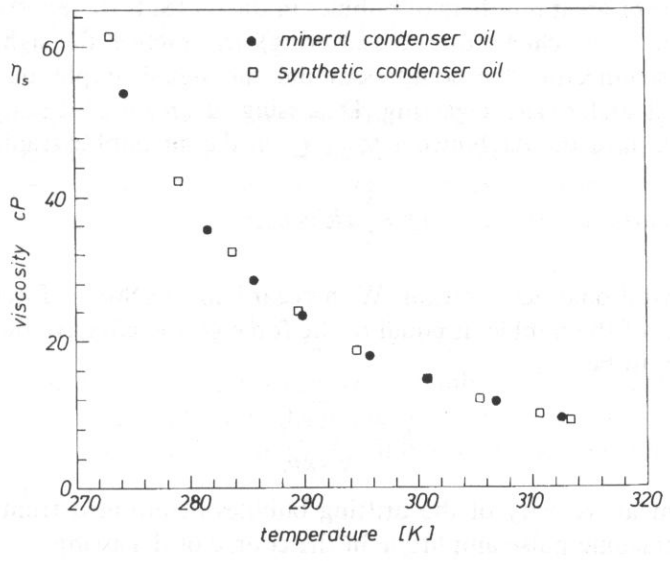

Fig. 8. The laminar viscosity $\eta_s(T)$ of the oils as a function of temperature.

Additionally, we measured the temperature dependence of the density ρ and laminar viscosity η_s on temperature Fig. 7 and 8.

We determined ρ with microprocessor device operating on the basis of the method proposed by KRATKY *et al.* [8], measuring the vibration frequency of a small, narrow tube in the form of the letter U excited by an AC magnetic field acting on a constant magnet fixed to the end of the U-tube. These measurements were carried out with an accuracy of 10^{-4}.

The correlation coefficient of the $\rho(T)$ measurements amounted to -0.9998 in mineral oil and -0.9999 in synthetic oil.

Laminary viscosity η_s was measured with a Höppler viscosimeter determining five times (for each temperature) the fall time of a metal sphere of diameter 15.57 mm and $\rho = 8140$ kg/m^3 in the oil.

To the experimental results obtained, we attributed the following exponential for η_s:

$$\eta_s(T) = 1.335 \cdot 10^7 \cdot \exp^{-0.0455 \cdot T}, \tag{4.1}$$

for mineral condenser oil, and

$$\eta_s(T) = 2.335 \cdot 10^7 \cdot \exp^{-0.0474 \cdot T}, \tag{4.2}$$

for synthetic oil, where the temperature is in Kelvin [K] and the viscosity is expressed in units of [cP].

5. Discussion of the results

The presence of great numbers of bubbles in the oil leads to very strong damping of the ultrasonic wave (chiefly due to scattering). In practice, the signal vanished.

Only on disconnecting the compressor did the signal amplitude begin to rise slowly as the oil underwent degassing. Degassing of an oil of density ρ_0 proceeds through the action of the Archimedes force Q on the air bubble (radius R):

$$Q = \frac{4}{3} \pi R^3 g \rho_0, \tag{5.1}$$

where g is gravitational acceleration. With regard to the Stokes force F which, at uniform motion of the bubble, is equal to the force Q, the effective radius R_{ef} of the bubble is found to be

$$R_{ef} = \sqrt{\frac{9 v \eta_s}{2 g \rho_0}}, \tag{5.2}$$

with v — the mean velocity of the drifting bubbles determined from the recorded variation in ultrasonic pulse amplitude in the course of degassing.

With the values occurring in the preceding example, $\rho_0 = 854.23$ kg/m^3, $\eta_s = 13.33 \cdot 10^{-3}$ Ns/m^2, $v = 294$ μm/s, we obtained for the effective radius of the bubble $R_{ef} = 45.8$ μm.

If incomplete discharge takes place in the bubble oxygen O_2 goes over into ozon O_3. Since ozon combines with the surrounding oil (especially at higher temperatures) the bubbles decrease in size [10]. Consequently, the ultrasonic amplitude absorption coefficient decreases. This process may well be responsible for the characteristic shape of the $\Delta\alpha_E(E, T)$ graphs of Figs. 4 and 5 obtained experimentally. In both cases the ultrasonic absorption specifically decreases at higher temperatures, at which diffusion of the gas out of the bubbles proceeds more intensely.

6. Ultrasonic wave propagation in a liquid with gas bubbles

Bubbles impede the propagation of ultrasonic waves, particularly so if the vibration eigenfrequency of the bubbles lies close to the frequency inducing their vibrations.

The whole process is fundamentally determined by the following factors:

- part of the acoustic energy is dissipated by the oscillating bubble which, as it were, becomes a spherical source emitting outwards in all directions,
- the temperature of the bubble rises as a result of its periodic oscillations induced by the ultrasonic wave and heat is transmitted to the surrounding medium, and
- losses in energy also come from the arisal of hydrodynamic microcurrents in the liquid medium surrounding the oscillating bubble.

The description of absorption and scattering of ultrasonic waves propagation in a liquid medium with gas bubble involves the following concepts:

- the effective active damping cross-section σ_e,
- the effective active absorption cross-section σ_a, and
- the effective active scattering cross-section σ_r.

These quantities are interrelated as follows:

$$\sigma_e = \sigma_a + \sigma_r. \tag{6.1}$$

Thus, the effective damping cross-section σ_e is meant to denote the area of the plane perpendicular to the direction of incidence of the ultrasonic wave for which the transmitted energy is equal to the sum of the energies absorbed and scattered by the bubbles. The active absorption cross-section σ_a and active scattering cross-section σ_r are defined as follows:

$$\sigma_a = \frac{Q_a}{I_p}, \qquad \sigma_r = \frac{Q_r}{I_p}, \tag{6.2}$$

where Q_a — is the energy flux absorbed by the bubbles, Q_r — is that scattered by the bubbles, and I_p — is the intensity of the incident wave.

In determining the values of these quantities use should be made of the following expressions [3]:

$$\sigma_e = \frac{4\pi r^2 \left(\frac{\delta}{\eta}\right)}{\left(\frac{f_0^2}{f^2} - 1\right)^2 + \delta^2}, \tag{6.3}$$

$$\sigma_a = \frac{4\pi r^2 \left(\frac{\delta}{\eta} - 1\right)}{\left(\frac{f_0^2}{f^2} - 1\right)^2 + \delta^2}, \tag{6.4}$$

$$\sigma_r = \frac{4\pi r^2}{\left(\frac{f_0^2}{f^2} - 1\right)^2 + \delta^2}, \tag{6.5}$$

with f_0 — the resonance frequency of the bubble, f — its oscillation frequency, r — its radius, δ — the damping coefficient of its oscillations in the liquid medium, and $\eta = 2\pi r/\lambda$ — the ratio of its circumference and ultrasonic wavelength.

For amplitudes small compared with the radius of the bubble, the resonance frequency of its oscillations is equal to

$$f_0 = \frac{1}{2\pi r_0} \sqrt{\frac{3\gamma\left(P + \frac{2\sigma_i}{r}\right)}{\rho}}, \tag{6.6}$$

with P — the pressure in the medium, $\gamma = C_p/C_v$ — the ratio of the specific heat at constant pressure and constant volume, σ_1 — the coefficient of surface tension on the gas-liquid boundary, and ρ — the density of the liquid medium.

For bubbles with a radius $r > 15$ μm the influence of the surface tension on the pressure inside the bubbles can be neglected, and Eq. (27) reduces to

$$f_0 = \frac{1}{2\pi r_0} \sqrt{\frac{3\gamma P}{\rho}}. \tag{6.7}$$

7. Acoustic degassing of liquids

A liquid containing gas bubbles becomes degassed under the action of an acoustic wave, especially if the wave is of high intensity.

The process of degassing runs in three stages, consisting of

(i) an increase in size of the small bubbles due to diffusion of the gas present in solution in the liquid;

(ii) coagulation of pairs and groups of small bubbles into bubbles of considerable size; this stage is dominated by the action of acoustic fluxes as well as Bjerkness and Brillouin forces; and, finally,

(iii) rapid flow of the now enlarged gas bubbles towards the surface of the liquid and their removal from the system.

The enhancement of the degassing process by the acoustic wave is due to the specific behaviour of the gas bubble, considered as an oscillator with one degree of freedom.

The analysis of the interaction between the bubble and the wave is greatly simplified if one assumes $r \ll \lambda$ (where λ is the acoustic wavelength in the liquid).

The periodical variations in pressure in the medium induced by the ultrasonic wave force the bubble to oscillate. Its radial oscillations obey the following linear differential equation [4]:

$$m\frac{\partial^2 v}{\partial t^2}+b\frac{\partial v}{\partial t}+kv=-P_A e^{i\omega t}, \tag{7.1}$$

where v denotes the deviation in volume of the bubble from its stationary value v_0, k is its elasticity coefficient, ω the angular frequency, P_A the pressure amplitude, t time, b dissipation coefficient, ant m generalized mass.

The general solution of Eq. (7.1) is

$$v(t)=\frac{-P_A e^{i(\omega t-\varphi)}}{\sqrt{m^2(\omega_0^2-\omega^2)^2+b^2\omega^2}}, \tag{7.2}$$

with φ the shift in phase between the inducing force and the oscillation, and $\omega_0=(k/m)^{0.5}$ the oscillation eigenfrequency of the bubble.

The deviation in volume from its stationary value becomes maximal at excitation by a wave of frequency close to that of the eigenfrequency of the bubble.

Under this condition, the rate at which diffusion of the gas into the bubbles proceeds is particularly high. They coalesce, they grow in size, thus considerably accelerating the process of degassing. In this process an important role belongs to the Bjerkness forces acting between two oscillating spheres (bubbles) acoustically excited to oscillate in a liquid medium.

If the oscillation frequencies of the two spheres are equal the force of interaction between them is [4, 5]:

$$F_B=\frac{4\pi\rho a^2 b^2 u_a u_b}{l^2}\cos\varphi, \tag{7.3}$$

with a, b their radii, l the distance between their centres, u_a and u_b the oscillation velocities of their surfaces, and ρ the density of the liquid.

Above, the shift in phase φ between the two bubbles is

$$\varphi=\operatorname{arctg}\frac{A-B}{1+AB}, \tag{7.4}$$

where the quantities A and B are

$$A=\frac{\delta_1\omega_{01}^2}{\omega_{01}^2-\omega^2}, \qquad B=\frac{\delta_2\omega_{02}^2}{\omega_{02}^2-\omega^2}. \tag{7.5}$$

with δ_1 and δ_2 denoting the respective oscillation damping coefficients and ω_{01}, ω_{02} the angular eigenfrequencies.

The oscillation velocities of the surfaces of two bubbles of radii a and b in a liquid of density ρ forced to oscillations under the action of an ultrasonic wave exerting a pressure P_A are, respectively,

$$u_a = \frac{P_A}{a\omega\rho\sqrt{\left(\frac{\omega_{10}^2}{\omega^2}-1\right)^2+\delta_1^2}}, \qquad u_b = \frac{P_A}{b\omega\rho\sqrt{\left(\frac{\omega_{20}^2}{\omega^2}-1\right)^2+\delta_2^2}}. \tag{7.6}$$

Obviously, at resonance i.e. for $\omega=\omega_0$ the pulsation velocity becomes maximal. On insertion of these expressions into (6.7) we arrive at the followig expression for the Bjerkness force acting between the two spheres:

$$F_B = \frac{4\pi ab\,P_A^2\cos\varphi}{\rho\omega^2 l^2\sqrt{\delta_1^2+\left(\frac{\omega_{01}^2}{\omega^2}-1\right)^2}\sqrt{\delta_2^2+\left(\frac{\omega_{02}^2}{\omega^2}-1\right)^2}}. \tag{7.7}$$

In the case of in-phase oscillations ($\varphi=0$) the two spheres experience a force of attraction, whereas if ($\varphi=\pi$) they mutually undergo repulsion.

In practice, in-phase oscillation take place if the oscillating bubbles are more or less of the same size greatly enhancing the process of degassing.

Thus ultrasonic investigation is seen to permit the measurements of the effective size of gas bubbles and the gas content in oils. The method should be of considerable interest with regard to applications in the Oil Industry.

Acknowledgements

This work was performed within the frame work of KBN nr 2PO3B 17908

References

[1] A. SKUMIEL and M. ŁABOWSKI, *Effect of an electric field on the ultrasonic wave velocity in oils*, Acustica, **74**, 109–119 (1991).

[2] I. ADAMCZEWSKI, *Ionization and conductivity of liquid dielectrics* (in Polish), PWN, Warszawa 1965.

[3] L.P. GAVRILOV, *Soderzane svogodnogo gaza v zidkostjah i metodyego izmerenja* [in:] Fiziceskiie osnovy ultrazvukovoi tehnologii (in Russian), [Ed.] L.D. Rozenberg, Iz. Sovetskaja Enciklopedia Moskva 1979.

[4] O.A. KAPUSTINA, *Degazacija zidkostiei* [in:] Fiziceskije osnovy ultrazvukovoi tehnologii (in Russian) [Ed.] L.D. Rozenberg, Izd. Sovetskaja Enciklopedia, Moscow 1979.

[5] L.P. GOLYAMINA [Ed.], *Ultrazvuk* (in Russian), Izd. Sovetskaja Enciklopedia, Moskva 1979.

[6] A. CHEŁKOWSKI, *Fizyka dielektryków* (in Polish), PWN, Warszawa 1979.

[7] A. SKUMIEL, *Acoustic wave propagation in mercury in constant external magnetic field*, Acta Physica Polonica, **A 83**, 173–185 (1993).

[8] J.O. KRATKY, H. LEOPOLD, and H. STABINGER, *Enzyme structure*, in: Methods in Enzymology vol. 27, Part D, Academic Press 1973, pp. 48–100.

[9] M. ŁABOWSKI, A. SKUMIEL and T. HORNOWSKI, Ultrasonic wave propagation velocity in nonconducting liquids in an external DC electric field, Acta Physica Polonica, **A 79**, 5, 683–693, 1991.

[10] W. LIDMANOWSKI, *Zarys teorii wyładowań w dielektrykach*, (in Polish), WNT, Warszawa 1988.

ARCHIVES OF ACOUSTICS
20, 4, 401–410 (1995)

THE ABSORPTION OF ULTRASONIC WAVES IN THE MIXTURES OF KNESER LIQUIDS

B.B.J. LINDE

Institute of Experimental Physics
University of Gdańsk
(80–952 Gdańsk, ul. Wita Stwosza 57)

Measurement of the absorption and velocity of ultrasonic waves in the mixtures of thiophene with m-. and p-xylenes were made by Eggers method of the frequencies between 0.3 and 5 MHz and temperature 293 K and carbon tetrachloride with o-, m- and p-xylenes by pulse method in the frequency range 20–30 MHz. The absorption decreased with increasing the quantity of xylenes, as is predicted by theory for gases and these results suggest that the absorption is probably due to the same phenomenon as in the gases. In measured frequency range is any dispersion region.

1. Introduction

For many years I have been carrying the acoustical investigation of pure heterocyclic liquids [16, 17]. These results and the investigation of other authors [3, 21, 24] show that the absorption of propagating ultrasonic wave rapidly goes down when the liquid medium (benzene, pyridine, thiophene, furane, thiazole etc.) contains the other cyclic or heterocyclic liquids (xylenes, picolines, lutidines etc.). First group of compounds has a great acoustical absorption and long relaxation time. For the second one the absorption is much lower and the relaxation times is about ten times shorter.

Recently many researches have been engaged in the problem of energy migration between the vibrational levels of different molecule of two gases, and ultrasonic wave [2]. It leads to faster deactivation of acoustically active internal degrees of freedom.

The results obtained from my acoustical research (the structure of vibrational levels and their activity in exchange of energy between translational-vibrational and vibrational-vibrational degrees of freedom as well as the results of gas mixture research) suggest the possibility of observation a transition between the vibrational levels of two different liquid molecules existing in the mixture of two liquids, and the propagating ultrasonic waves. This way we can observe changes in the deactivation process of acoustically active vibrational degrees of freedom. It is possible to notice shortening of the acoustical relaxation time caused by taking the energy from liquid

molecules, which have a longer relaxation time by the molecule having the shorter one. Certainly, such a migration of energy could be possible only between the vibrational levels of two molecules A and B for which energies will be similar $E_A \approx E_B$.

It was observed ealier that some substances, admixed even in small quantities, have a very marked effect on the absorption and dispersion of ultrasonic waves as well as in gases and liquids. General consideration of such an effect were made by EUCKEN and BECKER [10] for gases and PINKERTON [21], BAUER [3] and SETTE [24] for liquids at low frequency range.

2. Experimental methods and results

The acoustical measurements of velocity and attenuation coefficient were carried out by Eggers method which has been already described in earlier papers [9, 18] and pulse method for the frequency range from 20 to 30 MHz [29, 15]. The measurements were made at 293 K in the frequency range from 0.3 to 5 MHz for two mixture of thiophene with m- and p-xylenes and from 20 and 30 MHz for the mixtures of carbon tetrachloride (CCl_4) and o-, m- and p-xylenes. The accuracy for the velocity measurements was 0.1 percent and for the absorption 5 percent for the method of Eggers and 0.05% and 3 % for pulse method [15]. The temperature of the solutions was controlled to within 0.1 K with ultra-cryostat MK 70.

The absorption of ultrasonic waves in the mixtures are presented in Figs. 1, 2, 3, 4 and 5. In all the cases there were a very rapid decrease in α as the proportion of the less absorbing liquid was increased. Further increases in the proportion of the later had progressively less effect. The acoustical velocity in function of concentration has a linear dependence (Figs. 1, 2, 3, 4 and 5).

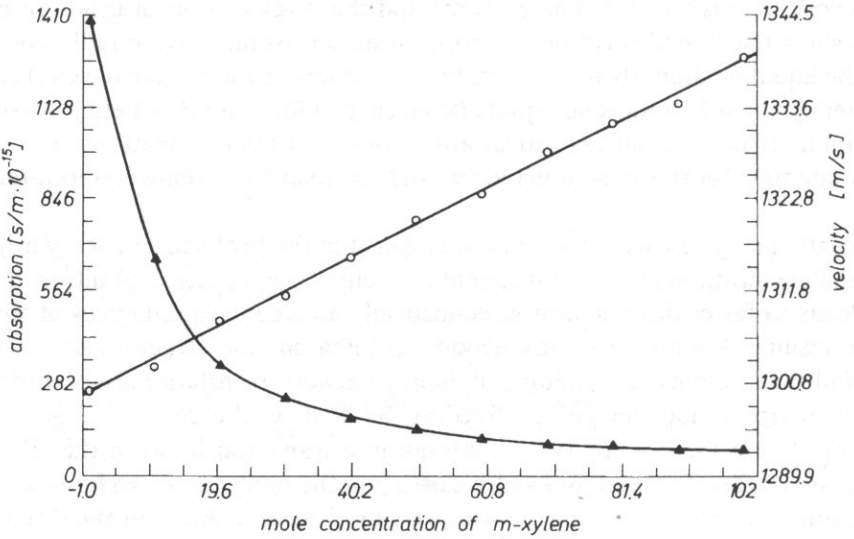

Fig. 1. Mixture of m-xylene/tiophene.

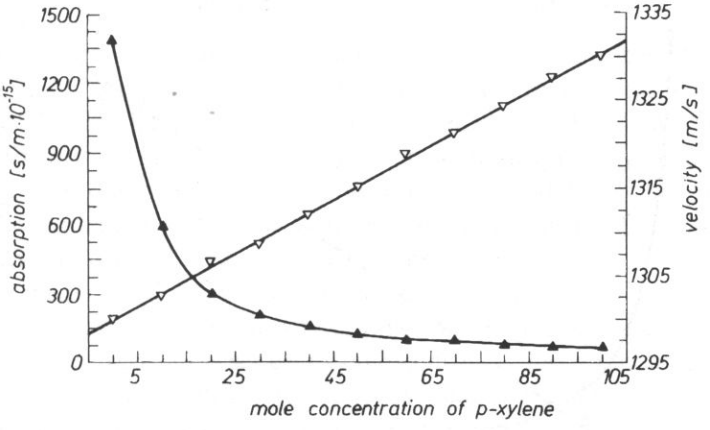

Fig. 2. Mixture of p-xylene/tiophene.

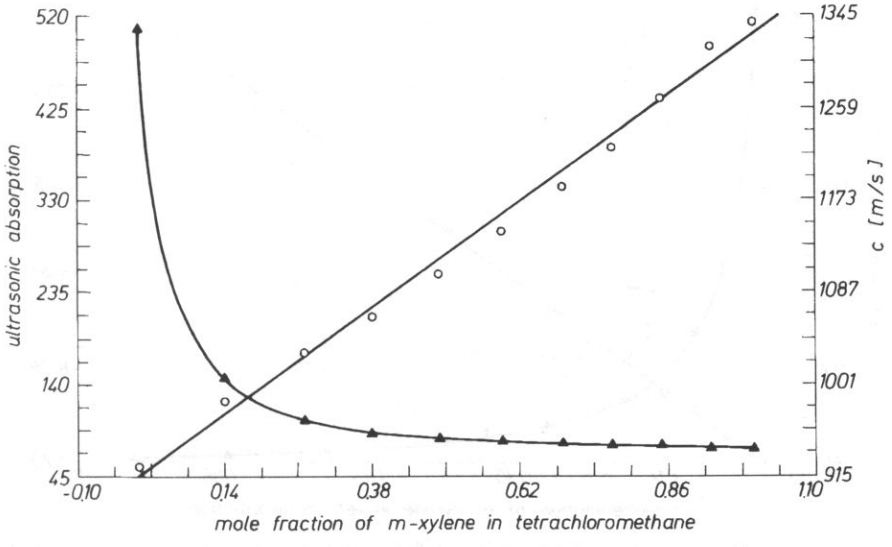

Fig. 3. The velocity and absorption versus concentration of m-xylene at the frequency of 30 MHz.

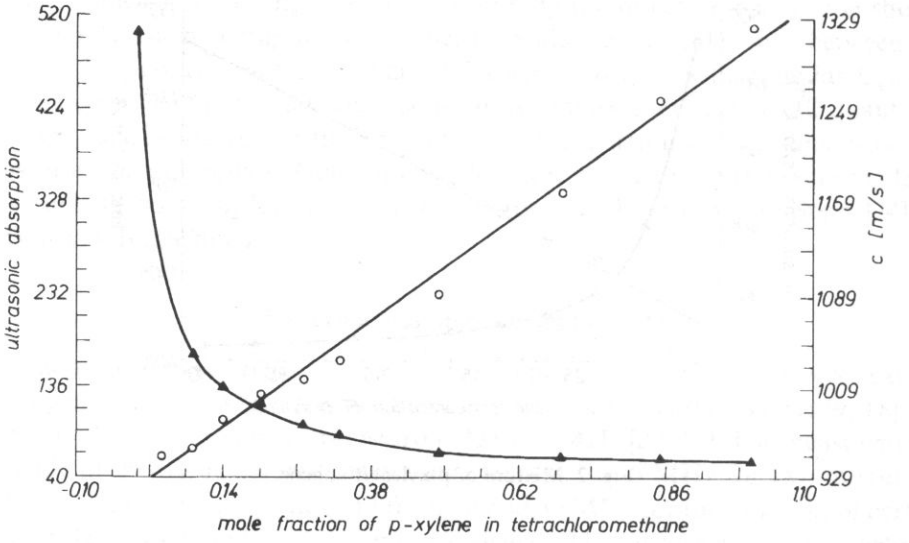

Fig. 4. The velocity and absorption versus mole fraction of p-xylene in tetrachloromethane at the frequency of 20 MHz.

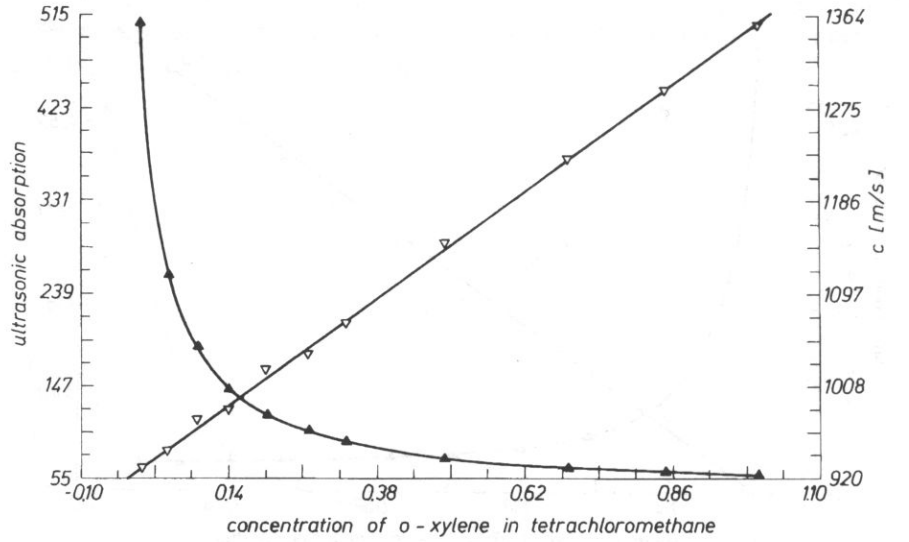

Fig. 5. The velocity and absorption versus mole fraction of o-xylene in tetrachloromethane at the frequency of 30 MHz.

3. Binary mixture of two Kneser liquids

It is already very well known that in case of gases small traces of impurities may have an extremely large effect on the absorption. A similar effect has been found in a number of liquids like carbon disulphide, benzene [11b], dichloromethane, [12] where the absorption falls very rapidly when a small quantity of a less absorbing liquid is added to one of high absorption. Pinkerton and Bauer has shown that this effect can be explained on a very simple relaxation picture. This basic ideas yield results which are in good agreement with experiment.

Let us consider the binary mixture: a mixture of liquids A (strongly absorbing) and B (other one) the equilibrium between the energies is associated with internal and external degrees of freedom is set up by collisions. „A" has a much smaller frequency than „B", so that an A molecule, once excited, has a much smaller chance of deexcitation than an excited B molecule. For simplicity in the analysis it will be assumed that only binary collision need be considered and that collision between

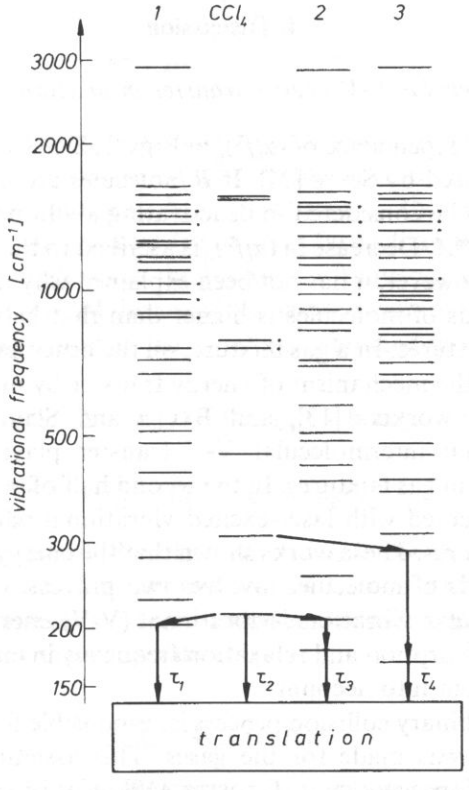

Fig. 6. Energy level diagram representing probably V-V and V-T relaxation process for vibrationally excited CCl_4 in the mixture with o- (2), m- (1), and p-xylenes (3), as represented by eqs. a, b, c. The dots indicate double degeneracy. The arrows between levels indicate near resonant intermolecular V-V transfer [27], the arrows down-direction V-T transfer. $\tau_{CCl_4,\ V\text{-}T} = 126$ ps, $\tau_{1,\ V\text{-}T}, \tau_{2,\ V\text{-}T}, \tau_{3,\ V\text{-}T} < 20$ ps. The frequencies beyond 2000 cm^{-1} can be negligible and they are not presented in this figure.

excited molecules may be neglected. A and A^* represent an unexcited and excited A molecule respectively, and similary for B and B^*. In this mixture an (A, A^*) collision is much less efficient than $a(B, B^*)$ collision because τ_B is much shorter than τ_A. In such a mixture it is possible to define four relaxation times as follows: τ_{AA} and τ_{BB} are the relaxation times for collisions between similar molecules of type A and B respectively τ_{AB} is that for collision of excited type A with deexcited B, and τ_{BA} that for colisions of excited B with deexcited A. Since the absorption in A is much greater than in B we can assume $\tau_{AA} > \tau_{AB}$ and write $\tau_{AB} = \tau_{BA} = \tau_{BB}$. The reason for this is that if molecule of type B possess a stronger mutual interaction, the interaction between A and B molecules may well be of the same order as between two molecules of B, and may expected to be much greater that the mutual interaction between molecules of type A. Thus, as the concentration of B molecules increases, the net efficiency of all collision tands rapidly to the value corresponding to the liquid B, so that the absorption falls sharply, and we can see it in the Figs. 1 to 5.

4. Discussion

4.1. V-T and intermolecular V-V energy transfer in mixture

The concentration dependence of $(\alpha/f^2)_0$ in Figs. 1, 2, 3, 4 and 5 might be explained with the theory proposed by SETTE [24]: If B molecules are mixed with A molecules, the binary collision to be considered in deactivating a vibrationally excited molecule A^*A, A^*B, B^*B and B^*A. Decrease in $(\alpha/f^2)_0$ is ascribed to the high efficiencies of A^*B and B^*A collisions. However, it has not been explained why the efficiency of collision between different kinds of molecules is higher than that between the same kinds of molecules in liquid mixtures. In a gas mixture, on the other hand, many workers have investigated in detail the mechanism of energy transfer by molecular collisions [1, 7, 28]. LAMBERT and co-workers [13], and BAUER and SCHOTTER [4] showed using ultrasonic method that intermolecular V-V transfer plays an important role in vibrational relaxation in gas mixtures. In the second half of seventieth, intermolecular V-V transfer was observed with laser-excited vibrational relaxation study in gas [6] and liquid [5, 14] mixtures. These works shown that the energy transfer by the colision between different kinds of molecules involves two process: vibrational-translational (V-T) and intermolecular vibrational-vibrational (V-V) energy transfers. The interpret the decrease in absorption and relaxation frequency in mixture system, these two processes must be taken into account.

It is assumed that binary collision process is responsible for the vibrational energy transfer in liquid, as was made for the gases. This assumption has been verified experimentally by MADIGISKY and LITOVITZ [10], CALAWAY and EWING [5], and theoretically by DAVIS and OPPENHEIM [8]. Let A the highly-absorbing liquid (thiophene or carbon tatrachloride) and B the low-absorbing (xylenes), that is the relaxation frequency of A is lower than that of B. The possible processes for V-T transfer are:

a) $$A^* + A \underset{k'_{AA}}{\overset{k_{AA}}{\rightleftharpoons}} A + A$$

b) $$A^* + B \underset{k'_{AB}}{\overset{k_{AB}}{\rightleftharpoons}} A + B$$

c) $$B^* + B \underset{k'_{BB}}{\overset{k_{BB}}{\rightleftharpoons}} B + B$$

d) $$B^* + A \underset{k'_{BA}}{\overset{k_{BA}}{\rightleftharpoons}} B + A$$

where k_{AA} is the forward rate constant in A^*A collision and the other symbols have a similar meaning. In these processes, each molecule is assumed to have two vibrational states, ground state and excited one, which includes all the vibrational modes responsible for the relaxation. The process for intermolecular V-V transfer is:

e) $$A^* + B \underset{k'_v}{\overset{k_v}{\rightleftharpoons}} A + B^*$$

If the vibrational quanta in the two molecules are not equal, the energy different is exchanged with translational energy. In pure liquid of A, the relaxation frequency is proportional to the rate constant k_{AA}. In mixtures, the increase in relaxation frequency of A indicates that process (b) or (e) is faster than (a). Process (c) and (d) are indirectly related through (e) to the relaxation frequency of A.

HERZFELD and LITOVITZ [11a] discussed the concentrations dependence of relaxation frequency of A using processes (a) — (e) and obtained the equation for small X:

$$f_r = \frac{1}{2\pi}\{k_{AA}(1-X) + k_{AB}X + [k_v k_{BA}X + k_v(k_{BB}-k_{BA})X^2]^* \qquad (4.1)$$

$$^*[k'_v + k_{BA} - (k'_v + k_{BA} - k_{BB})X]^{-1}\}$$

Here X is the mole fraction of B molecules, and f_r is the relaxation frequency for specific heat. A. MONKEVICZ [20] applied Eq. (4.1) to methane-water mixtures in vapour to get the rate constant k. The equation can also be applied to liquid mixtures as for the binary collision theory is valid.

5. CONCLUSION

The results of acoustical measurements of absorption coefficient as a function of mole fraction show that that transfer energy (the deexcitation of a molecule) is more probable between two different molecules than with molecules of the same species. It is possible that transfer of energy happens during the collision between the vibrationally excited molecule of thiophene and not excited of a xylene one. From the

table of vibrational degree of freedom [25], (Table 1) it is possible to conclude that here, may occur a rapid near resonant vibration-vibration transfer [26] between the lowest fundamental mode of thiophene (ν_1=452 cm^{-1}) and the made (ν_6=495 cm^{-1}) of p-xylene for thiophene — p-xylene mixture and between the made (ν_1=452 cm^{-1}) of thiophene and (ν_5=421 cm^{-1}) of m-xylene for thiophene — m-xylene mixture.

Table 1. Several main vibrational frequencies of thiophene, p- and m-xylenes [25]

p-xylene	Thiophene	m-xylene
(1) 170	(1) 452	(1) 205
(2) 290	(2) 567	(2) 230
(3) 313	(3) 606	(3) 279
(4) 386	(4) 690	(4) 404
(5) 405	(5) 712	(5) 421
(6) 495	(6) 749	(6) 484
(7) 489	(7) 834	(7) 517
(8) 645	(9) 868	(8) 538
(9) 671	(10) 905	(9) 679
(10) 702	(11) 1021	(10) 726
(11) 793	(12) 1032	(11) 770
(12) 810	(13) 1082	(12) 882
(13) 829	(14) 1253	(14) 910
(14) 936	(15) 1358	(15) 970

Table 2. Main vibrational frequencies of CCl_4 and several f_V for o-xylene [23]

CCl_4	o-xylene
(1) 218	(1) 179
(2) 314	(2) 211
(3) 459	(3) 257
(4) 762	(4) 406
(5) 768	(5) 434
(6) 790	(6) 486
(7) 797	(7) 506
(8) 1539	(8) 582
(9) 1550	(9) 700

From the acoustical results and spectroscopic data, Table 2. [23] and Fig. 6 it is possible to conclude that for the mixtures of CCl_4 and three isomers of xylenes the most probable transfer energy V-V could realise via $\nu_{1CCl} \rightarrow \nu_{2-oX}$; $\nu_{1CCl} \rightarrow \nu_{1-mX}$ and $\nu_{2CCl} \rightarrow \nu_{3-pX}$.

Intermolecular V-V transfer between higher modes would be negligible, since higher modes have smaller contribution to vibrational specific heat (it can be calculated theoretically from Einstein Planck formula [15]). The intermolecular V-V transferr in series from e.g. 495 cm^{-1} mode to the lowest mode of p-xylene (170 cm^{-1}) are expected to occur very quickly compared with the V-T transfer of the lowest modes of thiophene. Consequently, the vibrational energy of thiophene transferred to translational energy via two path: the V-T transfers (a), (b), and the intermolecular V-V transfer (e) followed by the V-T transfers (c), (d). The latter path would be much faster than the former one. Similar situation is for the second mixture of thiophene as well as for carbon tetrachloride and xylenes mixture.

In the other case, if there is no such a transfer, the relaxation time of this acoustical process will be longer (the relaxation time of CCl is 126 ps [22], and the thiophene's one even 500 ps [27], but the times of xylenes are less than 20 ps, [15]) and the absorption coefficient much higher, and there would not be so big influence of the impurities for the acoustical absorption.

Decrease in absorption — equivalent to relaxation frequency decreasing — shortening of the relaxation time — of highly-absorbing components is shown to be caused by the intermolecular V-V energy transfer. In binary mixtures than of highly-absorbing and low-absorbing fluids, in general, the decrease in absorption coefficient with the addition of low-absorbing liquids would be explained by intermolecular V-V energy transfer in the collision process between two different molecules. Similar results were obtained in the investigation of shortening of phosphorescence time in some binary mixtures [6]. From this research we can see that it is so important to have mixture of two cyclic or heterocyclic compounds or the other, but it is important to take the liquids with absorption caused mainly by Kneser effect.

For more clear interpretation it is necessary to provide acoustical investigation for higher frequency range for which the characteristic relaxation frequency will be in the range of measurement frequency.

Acknowledgement

Work supported by the University grant, BW 5200–5–0169–4.

References

[1] R.C. Amme and S. Legvold, *Vibrational transition and the intermolecular potential*, J. Chem. Phys., **33**, 1, 91–95 (1960).

[2] R.C. Amme, B. Jacobs and J.R. Oolson, *Vibrational relaxation in gaseous* SiF *by* Ar *and* Ne *at* 304 K, J. Acoust. Soc. Am., **89**, 6, (1991).

[3] E. Bauer, *A theory of ultrasonic absorption in unassociated liquids*, Proc. Phys. Soc., **A 62**, 3 No 351, 141–154 (1949).

[4] H. -J. Bauer and R. Schotter, *Collision transfer of vibrational energy from nitrogen and methane to carbon dioxide molecule*, J. Chem. Phys., **51**, 8, 3261–70 (1969).

[5] W.F. Calaway and G.E. Ewing, *Vibrational relaxation of small molecules in the liquid phase: liquid nitrogen doped with* O_2, CO, and CH_4, J. Chem. Phys., **63**, 7, 2842–53 (1975).

[6] H.L. Chen and C.B. Moore, *Vibration energy transfer in hydrogen chloride mixture*, J. Chem. Phys., **54**, 9, 4080–84 (1971).

[7] T.I. Cottrell and J.C. Mc Couberey, *Molecular energy transfer in gases*, Butterworths, London 1961.

[8] P.K. Davis and I. Oppenheim, *Vibrational relaxation in liquids*, J. Chem. Phys., **57**, 1, 505–517 (1972).

[9] F. Eggers and Th. Funck, *Ultrasonic measurements with millilitre liquid samples in the* 0.5–100 *Mhz range*, Rev. Sci. Instrum., **44**, 8, 969–977 (1973).

[10] A. Eucken and R. Becker, *Die Stossanregung intramolecularer Schwingungen in Gasen und Gasmischungen auf Grund von Schalldispersionsmessungen I. Versuchsmethodik und Ausvertung bei exakten Messungen der Schallgeschwindichkeit im Ultraschallgebiet*, Z. Physik. Chem., **B27**, 219, (1934).

[11] a) K.F. HERZFELD and T.A. LITOVITZ, *Absorption and dispersion of ultrasonic waves*, Academic Press, New York 1959 a) p. 212
b) K.F. HERZFELD and T.A. LITOVITZ, *Absorption and dispersion of ultrasonic waves*, Academic Press, New York, London 1959 b) p. 136.
[12] J.L. HUNTER, D. DOSSA, J. HAUS and D. SETTE, *Relaxation experiments in binary mixtures of Kneser liquids*, J. Chem. Phys., **60**, 11, 4605–4611 (1974).
[13] J.D. LAMBERT, D.G. PARKS-SMITH and J.L. STRETTON, *Multiple vibrational relaxation in polyatomic gases and mixtures*, Trans. Faraday Soc., **66**, 2720–2731 (1970).
[14] A. LAUBEREAU and W. KAISER, *Vibrational dynamics of liquids and solids investigated by picosecond light pulses*, Rev. Mod. Phys., **50**, 3, 607–65 (1978).
[15] B. LINDE, PhD Thesis, Gdańsk 1979.
[16] B. LINDE, *Acoustical relaxation in heterocyclic liquids*, Archives of Acoustics, 7, 2, 163–170 (1982).
[17] B. LINDE, M. KOSMOL and A. ŚLIWIŃSKI, *Determination of the influence of liquid molecule structure on acoustic absorption quantity*, Archives of Acoustics, **11**, 4, 353–383 (1986).
[18] B. LINDE, E. ROSENFELD, *A test of Eggers method application for some pure organic liquids investigation*, Proc. of the XXXVI OSA, 106–11, Białowieża 1988.
[19] W.M. MADIGOSKY, and T.A. LITOVITZ, *Mean free path and ultrasonic vibrational relaxation in liquids and dense gases*, J. Chem. Phys., **34**, 489–97 (1961).
[20] A.A. MONKIEWICZ, *Changes in the vibrational Napier relaxation time of methane-water mixtures*, JASA, **42**, 1, 258–266 1967.
[21] J.M.M. PINKERTON, *The absorption of ultrasonic waves in liquids and its relation molecular constitution*, Proc. Phys. Soc., **B62**, 2, 350, 129–141 (1949).
[22] K.G. PLASS, *Relaxation in organischen Flüssigkeiten bei, 1 GHz*, Acoustica, **19**, 4, 236–42 (1967/68).
[23] B. SCHRADER, W. MEIER, *DMS Raman/IR, Atlas of organic compounds*, Verlag Chemie GmbH, Weinheim 1974.
[24] D. SETTE, *On the ultrasonic absorption in binary mixtures of unassociated liquids*, J. Chem. Phys., **18**, 12, 1592–1594 (1950).
[25] L.M. SVIERDLOV, M.A. KOVNER and E.P. KRAINOV, *Kolebatelnye spektry mnogoatomnych molekul*, Nauka, Moskva 1970.
[26] K. TAKAGI, and K. NEGISHI, *Measurements of high frequency ultrasonic velocity and absorption in liquid thiphene with high-resolution Bragg reflection method*, Japan. J. Appl. Phys., **15**, 6, 1029–35 (1976).
[27] K. TAKAGI, P.K. CHOI and K. NEGISHI, *Effect of near-resonant energy transfer on vibrational relaxation in liquid dichloromethane-benzene mixture*, J. Chem. Phys., **74**, 2, 1438–41 (1981).
[28] L.M. VALLEY, and S. LEGVOLD, *Sound dispersion in ethane-ethylene mixtures and in haloethane gases*, J. Chem. Phys., **36**, 2, 481–485 (1962).
[29] J. WEHR, *Pomiary prędkości i tłumienia fal ultradźwiękowych*, (in Polish) PWN, Warszawa 1972.

ARCHIVES OF ACOUSTICS
20, 4, 411–418 (1995)

C H R O N I C L E

Professor Antoni Śliwiński
— JUBILEE

The Scientific Symposium was held on 15-th of February 1994 at Gdańsk University on the occasion of 65-th birthday of Professor Antoni Śliwiński. The Symposium was organized by the Institute of Experimental Physics (University of Gdańsk) and the Gdańsk Sections of the Polish Acoustical Society and Polish Physical Society.

The followers and friends of Professor Śliwiński took part in the Symposium and they represented not only the Gdańsk community but other regions such as Gliwice, Kraków, Poznań, Rzeszów, Szczecin, Warszawa and Wrocław. During the opening ceremony Professor Jerzy Ranachowski (Institute of Fundamental Technological Research of Polish Academy of Sciences) summarized the scientific achievement and the professional career of the honoured guest. Congratulation letters were read on the occasion. Professor J. Burnewicz, pro-rector of Gdańsk University and Professor E. Kozaczka, a representative of the Commander of the Naval Academy awarded Professor Śliwiński medals from both Universities. Professor Śliwiński received many congratulations, wishes, thanks and flowers from the well-wishers.

Speeches were made. Professor L. Filipczyński (Institute of Fundamental Technological Research of Polish Academy of Sciencess) mentioned his first contacts with Professor Śliwiński. Professor F. Kaczmarek, who has been his collegue since the student time spoke about beginning of their early academic career at Poznań University. Professor E. Hojan (Poznań University) reminded those gathered Professor Śliwiński's contribution is designing the room acoustics during the reconstruction of the Great Opera Theatre in Warsaw under Professors M. Kwiek and E. Karaśkiewicz supervision. Professor Szustakowski read a congratulation letter, written by the Commander of the Technical Military Academy, with thanks for the cooperation in the field of acoustooptics. Directors Dr K. Knapiński (Institute of Experimental Physics, University of Gdańsk) and Professor J. Dera (Institute of Oceanology, Polish Academy of Sciences) expressed their thanks for the enormous amount of efforts given to the teaching and research activities in both places. The respectives of the Polish Acoustic Society Professor A. Opilski and Dr T. Pustelny

(Gliwice Section), Dr A. Drzymała (Rzeszów Section), Professors E. Hojan and M. Łabowski (Poznań Section) congratulated and wished the further success. Then Professor Śliwiński expressed his career in limeric composed by his family.

The participants had the opportunity to listen to the following papers during the Symposium:

1. Acoustic sensor of gasses — Professor A. Opilski (Institute of Physics, Silesian Technical University, Gliwice).
2. Dynamic properties of liquids in ultrasonic fields — Professor R. Płowiec, (Institute of Fundamental Technological Research of Polish Academy of Sciencess).
3. Investigation of the influence of the constant magnetic field on the propagation of ultrasonic field in the conductive media — Professor M. Łabowski (Institute of Acoustic, University of Poznań).
4. Detection of tissue elastic properties by MRJ method. — Professor Cz. Lewa (Institute of Experimental Physics, University of Gdańsk).

Finally the informal part of the Symposium took place, patronated by the local „Solidarity" Trade Union, with its warm atmosphere, a glass of wine and the song „Sto lat" (that could be expressed as a wish of „One hundred years").

We would like to highlight to the attention some facts of Professor Śliwiński's career.

He was born on 15-th of November 1928 in Jarocin (near Poznań). In 1942 he completed grammar school in Gliniak (near Mińsk Mazowiecki). In 1947, after graduating from the State Secondary School for Adults in Bydgoszcz, he started his studies in the Department of Mathematics and Natural Science, Physics Division, at Poznań University and graduated with a master of philosophy in physics in 1952. In the meantime (1950) he undertook the post at Poznań University, and nearly from the begining he had been under Professor Marek Kwiek supervision (until Kwiek's tragic death). Promoted by Professor Kwiek he prepared his Ph.D. thesis on the phenomenon of ultrasonic wave propagation in the media being near the critical point, where the fluctuation of the state parameters occured and completed the thesis in 1960. Still with Poznań University he became the associate professor after the presentation of the thesis concern with the light diffraction by ultrasonic waves propagating in the transition media. In 1970 he joined the newly founded Gdańsk University where he has been working until now. Beside his scientific, research and teaching activites he appeard to be excellent manager that is why he has been acting as the Head of the Acoustic Group, the Dean of the Mathematics-Physics-Chemistry Faculty, vice-rector of Gdańsk University. He has been the initiator of the research work and a leader of the big group of scientists from the very beginning of his activity at Gdańsk University. In 1973 he helped to initiate founding for the Environmental Laboratory of the Acoustics and Spectroscopy, the unit that had been devoted to the environment protection of Gdańsk region, with special attention to acoustics problems among them noise pollution.

Professor Śliwiński scientific outputs is mainly concern with the wide aspects of acoustics:

1. Acoustooptics: investigations of light diffraction by ultrasonic waves, non-linear effects occuring during diffraction of the strong laser light by ultrasonic wave, application of interferometric techniques to the examination of ultrasonic fields and transducers.

2. Molecular investigations and ultrasonic spectroscopy: examinations of the organic substances including polymers and liquid crystals, viscoelastic media.

3. Room acoustics: examinations of noise and vibration, material noise.

4. Hydroacoustics: acoustic examianation of the Baltic Sea, surface water pollution.

5. Photoacoustic spectroscopy.

Professor Śliwiński promoted 27 ph.d. thesis, five people among his coworkers become the associated professors and three of them full professors. Number of Ph.D. thesis and dissertation for associate professor degree were reviewed by him as well in Poland as abroad. Either as a referee or reviewer he gave his acess to the nomination procedure for full professors.

Professor Śliwiński wrote as an author or co-author more than 200 papers known to the internal audience. He is a member of Physics, Acoustics and Marine Investigation Committees of the Polish Academy of Sciencess and Several Research Councils. Awarded a fellowship he became a member in the international societies such as European Physics Society, Audio-Engineering Society and Polish ones: Polish Acoustic Society (being a President for the last two tenures), Polish Physical Society, Gdańsk Scientific Society and Gdańsk Academic Society. Moreover he took part in the editorial boards of the following journals: Ultrasonic, Acoustic Letters, Archives of Acoustics, Oceanologia, Acustica, Akusticheskij Zhurnal, Optoelectronics Review. During 1981–1987 Professor Śliwiński represented Poland in the International Comission on Acoustics (of Internal Union of Pure and Applied Physics). He was honoured and awarded a number times. The international audience had many opportunities to listen to his lectures during the conferences, meetings or seminars.

On the other hand Professor Śliwiński is known as an organizer of many scientific meetings: five of them on acoustooptics, i.e. „Spring School on Acoustooptics and Applications", „Prospects in Modern Acoustics, Education and Development and the Open Seminars on Acoustics.

He closely collaborates with foreign academic centers such as Universities in Leuven, Halle, Bremen, Triest and PTB from Braunschweig.

Professor Śliwiński has been building his own acousto-optic school, that is regarded as very strong scientific center and that is why the Spring School on Acoustooptics has become so popular as well in Poland as abroad.

Bogumił Bolesław Juliusz Linde
Anna Markiewicz

98TH AES CONVENTION — 25—28.02.1995 — PARIS
POLISH AES SECTION REPORT

Audio Engineering Society Conventions became traditional world meetings of all scientist, engineers, industry managers, producers, dealers and even fanciers interested in the domain of sound and vision systems, equipments, facilities, components, hard – and software computer elements etc. Such meetings take place twice a year: Spring Convention in Europe (denoted with consecutive even numbers), and Fall Convention in the USA (denoted with odd ones).

The latest European Conventions: the 94th in Berlin, the 96th in Amsterdam, and the 98th one in Paris, reported herewith, were marked with parcitipation of several newly organized AES Sections from countries of former Eastern socialist block of states. Among the members of those Sections, the most numerous participation was of the Polish Section. Since the Berlin Convention, the Polish AES Section has organized, for the third time already, inexpensive coach expeditions for their members, mostly student-members, to participate in Conventions. Such participation is highly valubale, especially for young adepts of acoustics, sound engineering and related topics who otherwise would be unable to cover all costs of participation, accomodation, transport etc. In appreciation of those numerous participations and of other initiatives, as well as assessing the whole scientific activity of the Polish Section, the Vice-President for Europe AES Region, Mr Dan Popescu, during the special Convention meeting in Paris, highly estimated its achievements in 1994, calling the Polish Section „the best of all Europe Sections".

Among Polish participants of the 98th AES Convention, held in Paris, at Palais de Congrès, were numerous authors and coauthors who read their papers and took part in discussions during the debates within the scientifical Convention program. The debates were grouped in the sixteen sessions: Audio Data Reduction I & II (A & C), Architectural Acoustics I & II(B & D), Electronic Music and Musical Instrument Acoustics (E), Sound Reinforcement I & II (F & H), Audio Electronics (G), Audio Signal Processing I & II (I & K), Transducers I & II (J & L), Measurement (M), Psychoacoustics I & II (N & P), Networks and Interfacing (O).

All the eighty five Convention papers were supported by a preprint. The Polish presentation included the following ones (in brackets — preprint no. and in parentheses — session no.): A. Czyżewski, B. Kostek, S. Zieliński, *New Approach to the Synthesis of Organ Pipe Sound* [3957] (E2); B. Żółtogórski, *Inverse Radiation Problem — Capabilities and Limitations*, [3981] (J1); D. Ruser, H. Ruser, *An Elementary High Resolution Microphone System for Localization of Sound Source in Air*, [4002] (M1); M. Niewiarowicz, *Directional Properties of Sound Sources During Transients*, [4004] (M3); B. Kostek, *Statistical versus Artificial Intelligence Based Processing of Subjective Tast Results* [4018] (P3); M. Kin, J. Renowski, *The Influence of Spectrum on Perception of Differential Pitch Sensitivity for Short Waves*, [4020] (P5).

Moreover, Polish AES Section members, in particular the young student-members, have taken an active participation in the, so called, workshop sessions.

Those were devoted to the following technical aspects: Preservation of and Access to Audio and Video Carriers; New Digital Media Developments; Wave Front Sculpture for Sound Reinforcement; Premastering for the New CD Formats; The Interaction of the Visual and Auditory Senses: „How Does One Measure It"; Current Trends of Research in Musical Instruments Acoustics; Musical and Non-Musical Application; Digital Audio Broadcasting.

Apart from the scientific activities, the participants got an enormous quantity of information concerning the most recent audio systems and equipments presented during a large exhibition, accompanying traditionally the Convention. The exhibition was held inside the Convention site, at the Palais de Congrès, on three levels, however, being easy acessible to all participants. More than three hundred enterprises, from all over the world, displayed their best products in richly outffitted demonstration stands, giving a visitor a unique possibility to keep track of the development trends in the whole domain of audio engineering. Broadly disseminated leaflets, prospects, technical data lists, system descriptions, records, even manuals, etc. will provide valuable information and reference source for participants at their professional practice.

Immediate press assessments, which appeared still before closing of the Conventions debates, have stated that the greatest interest of industry representatives concentrated on problems connected with the digital sound processing and the reinforcement systems. The latter ones were often entitled as room acoustics or building acoustics problems, however, only sound reinforcement techniques were treated thereby, withouth any reference to proper desing, measurement and acoustical correction or adaptation of rooms. At any rate, those were discussed during session debates devoted to Architectural Acoustics.

Generally, the scientific part of the Paris Convention was not so largely filled as e.g. the 94^{th} one, held in Berlin. The number of papers was almost halved in comparison to Berlin record. However, may be, it was intended by Paris Convention Committee, which probably dismissed a part of the submitted papers in order not to exaggerate the numbers of parallel sessions, necessary otherwise. So, the more important is the number of Polish Section presentations, which amounted 7% of the total number of papers.

It may be interesting to compare the share of authors' contributions from particular countries. The most numerous were twelve papers from the U.S.A. Next in number were papers from Germany and from the United Kingdom, ten papers from each country. Nine papers were presented by French authors. Eight ones by Dutch authors. Poland and Russia presented six papers each. Danish authors presented four papers. Finnland and Hong-Kong presented three papers each. Two papers came from authors from Greece, Ireland, Portugal and Switzerland. One paper was presented by authors from Australia, Austria, Italy, Japan, Spain and Sweden. Thus, it was a really international contribution to audio engineering scientific progress.

Such yearly repeated contact with the international progress in the audio engineering domain is, without a doubt, a very useful event for the Polish AES

Section members and for their entire scientific and professional surrounding. Thus, a continuation of similar contacts in the future seems to be highly desirable. In this context, it has to be added here, that the 100th AES Convention, the jubilee one, will be held in Copenhagen, at Bella Center, on May 11–14, next year, 1996.

Marianna Sankiewicz
(Chairman of the Polish AES Section)

Information about CIB W–51 Acoustics Meeting in Warsaw, 25–27 May 1994

The Information Council for Building Research Studies and Documentation is an international organization concerned with studies, research and documentation in the building industry. It unites 70 countries. It has over 500 collective and individual members.

Over 70 International Committees and Working Groups operate within CIB. One of them is the W–51 Acoustics Committee. The Committee is headed by Prof. A. Cops and Prof. G. Vermeir from the Catholic University in Leuven.

The W–51 Acoustics Committee consists of the representatives of Research Centers, dealing with building acoustics, requiring more in -depth theoretical and experimental examination, are discussed during these meeatings. Discussions are held on the chosen scientific issues, study and measurement methods, and the results of studies obtained in the last several years in the various Institutes are analyzed.

Scientific presentations are prepared for the Committee meetings and these are later presented and discussed at the seminar. Later on these papers are prepared — according to the publisher's requirements — for publication in Applied Acoustics.

A collective publication is prepared from each seminar, which includes the written and presented papers. This publication includes the papers presented at the meeting of the CIB W–51 Acoustics Committee on May 25–27, 1994 in Warsaw.

The seminar in Warsaw was devoted to two very significant groups of topics, namely:

I. Experimental study and modeling of sound insulation in construction building joints in buildings.

II. Sound absorption, shape and indicator of reference curve, measurement and desing.

A total of 21 papers were announced 11 — in Section I, 10 — in Section II; 18 papers were presented. From which 16 were delivered in the form of xerox-copied publications the remaining 2 due to research being in progress, were only presented, and will be published at a later date in Applied Acoustics. Three papers were not sent in their authors were also absent.

A list of the presented papers, according to the program of the meeting, is given.

Participation in the CIB W−51 Acoustics Committee meeting undoubtedly allowed its participants to confront the progress of studies conducted on similar topics in the various countries, as well as facilitated better planning in the area of building acoustics studies to be carrier out in the forthcoming years.

Prof. André Cops
Laboratory for Acoustic and Thermal Physics
Catholic University of Leuven, Belgium

Prof. Gerrit Vermeir
Laboratory for Building Physics
Catholic University of Leuven, Belgium

Prof. Jerzy Sadowski
Zakład Akustyki Instytutu Techniki
Bdowlanej.

Presented papers

Theme 1 — JUNCTION DAMPING: modeling, experiments

1. Bosmans I., Mees., Vermeir G. (Belgium),
   Structure-borne sound transmission between thin orthotropic plates: analytical solution.
2. Craik R. (England), Osipow A. (Russia),
   The use of elestic interlayers at joints to reduce structure-borne sound transmission.
3. Villot M., Jean P. (France),
   Structure-borne sound transmission through a pillar-beam-floor system. Case of bulidings constructed on top of covered railways.
4. Pedersen D.B. (Denmark),
   Estimation of vibration attenuation through junctions of building structures.
5. Gerretsen E. (The Netherlands),
   Junction transmission with double-leaf building elements.

Theme 2 — JUNCTION DAMPING: examples, applications

1. Nightingale T. (Canada),
   Application of the CEN draft building acoustics prediction model to a lightweight double leaf construction.
2. Martin H.J., Moorlach M.F.C. (The Netherlands),
   Sound transmission and junction damping in sheet steel dwellings.
3. Szudrowicz B., Iżewska A. (Poland),
   Simplified evaluation of flanking transmission based on the mean mass and mean area of flanking elements.

4. Pietrzyk A., Kropp W., Kihlman T. (Sweden), *Numerical simulation of low frequency air-borne sound transmission in buildings.*

Theme 3 — SOUND ABSORBTION: reference artefacts, measurement, design

1. Vorländer M. (Germany),
   Reverbation room measurements and preparations of round robin tests on the sound absorption coefficient of reference artefacts.
2. Kristiansen U.R., Vigran T.E. (Norway),
   On the design resonant absorbers.
3. Chyla A., Czyżewski K., Nurzyński J. (Poland),
   Reverberation time: comparison of measurement results obtained in the laboratory using different methods and instrumentation.
4. Mirowska M. (Poland),
   Sound absorption of spatial acoustics absorbers, laboratory measurements, repeatibility, reproducibility.

Theme 4 — SOUND ABSORPTION MEASUREMENT: simulation, experiments, in-situ mesurement

1. Mees P., Vermeir G. (Belgium),
   Numercal simulation of sound absorption in reverbation rooms.
2. Cops A., Vanhaecht J., Leppens K. (Belgium),
   Sound absorbtion in a reverberation room: causes of discrepancies on measurement results.
3. Mommertz E. (Gremany),
   Angle-dependent in situ measurements of the complex reflection coefficient using a subtraction technique.
4. Madalik L. (Estonia),
   Measurements and computer simulation of sound field of the St. Charles' Church in Tallin.

2nd International Congress on Acoustical and Vibratory Surveillance Methods and Diagnostic Techniques

Clamart (Paris), France 10-12 October 1995

Organised by: Société Française des Mécaniciens (S.F.M.),
Société Française d'Acoustique (S.F.A.), and International Measurement Conference (IMEKO)

The Congress is hosted by a research centre (D.E.R.) of Electricité de France (E.D.F.)

TECHNICAL PROGRAM

The domain of the Congress covers all scientific and technical matters which contribute to the development of surveillance and diagnostic using acoustical and vibratory information

The program is divided into six topics areas:

- physical modelling
- signal processing
- vibration mechanics
- acoustics
- innovative techniques
- case histories and systems

Inter-noise '96. The 25th International Conference on Noise Control
July 30th through to August 2nd 1996
The Adelphi Hotel and Conference Centre, Liverpool, England

The conference is promoted by the Institute of Acoustics and organised under the superversion of. The International Institute of Noise Control Engineering. The theme for '96 is „Noise, the next 25 years — scientists engineers and legislators in partnership". The objective of the event is to promote all aspects of technical and administrative control of excessive noise in order to provide a safer and more acceptable environment for all. Conferences are organised annually alternating between US and other international venues, the '94 conference was in Yokohama, Japan and the '95 event is in Newport Beach, California, USA. Attendance is usually around 1.000 drawn from industry, government and academia from around the world.

Further information is available from Cathy Mackenzie at Institute of Acoustics, Agriculture House, 5 Holywell Hill, St Albans AL1 1EU, UK — Telephone 01727 848195, Fax 01727 850553.